University of Pardubice

Faculty of Chemical Technology

Department of Physical Chemistry

Mgr. Mariia Lemishka

Binuclear transition metal ion centers in zeolites:

Their preparation, characterization, and catalytic properties

Ph.D. thesis

Supervisor: Mgr. Jiří Dědeček, CSc., DSc.

Supervisor-consultant: Doc. Mgr. Edyta Anna Tabor, Ph.D.

Supervisor-consultant: Doc. Ing. Zdeněk Sobalík, CSc.

J. Heyrovský Institute of Physical Chemistry of the CAS, v. v. i.

2024

Declaration

On this date, I declare that I have developed this work independently. This work is original and was performed under the supervision of Mgr. Jiří Dědeček, CSc., DSc. I have cited all the information sources used and all relevant literature.

I have been made aware of the fact that my work is subject to the rights and obligations arising from Act No. 121/2000 Sb., On Copyright, on the Rights Related to Copyright, and on the Amendments to Certain Acts (Copyright Act), as amended. I am especially aware of the fact that the University of Pardubice has the right to conclude a license agreement for the use of this thesis as a school work under Section 60, Subsection 1 of the Copyright Act and that if this thesis is used by me or there is a license to use it granted to another entity, the University of Pardubice is entitled to request a reasonable fee from me to cover the costs incurred for the creation of the work, depending on the circumstances, up to their actual amount. I acknowledge that, in accordance with Section 47b of Act No. 111/1998 Sb., On Higher Education Institutions and on the Amendments to Other Acts (Act on Higher Education Institutions), as amended, and the Directive of the University of Pardubice No. 7/2019 Rules for Submission, Publication, and Layout of Theses, as amended, the thesis will be published through the Digital Library of the University of Pardubice.

I also declare that neither this Ph.D. thesis nor its significant part has been submitted to obtain any other academic degree, diploma, or qualification.

Prohlášení

V tuto chvíli prohlašuji, že jsem tuto práci vypracovala samostatně, jedná se o původní práci, kterou jsem vypracovala pod vedením Mgr. Jiřího Dědečka, CSc., DSc. Všechny použité informační zdroje a relevantní literaturu jsem uvedla.

Byla jsem seznámena s tím, že se na mou práci vztahují práva a povinnosti vyplývající ze zákona č. 121/2000 Sb, o právu autorském, o právech souvisejících s právem autorským a o změně některých zákonů (autorský zákon), ve znění pozdějších předpisů, zejména se skutečností, že Univerzita Pardubice má právo na uzavření licenční smlouvy o užití této práce jako školního díla podle § 60 odst. 1 autorského zákona a že v případě užití této práce mnou nebo udělením licence k užití, jejího poskytnutí jinému subjektu, je Univerzita Pardubice oprávněna požadovat přiměřenou odměnu na úhradu nákladů vynaložených na vytvoření práce, a to podle okolností až do jejich skutečné výše. Beru na vědomí, že v souladu s § 47b zákona č. 111/1998 Sb. o vysokých školách a o změně a doplnění dalších zákonů (zákon o vysokých školách), ve znění pozdějších předpisů, a směrnicí Univerzity Pardubice č. 7/2019 Pravidla pro zadávání, zveřejňování a úpravu závěrečných prací, ve znění pozdějších předpisů, bude práce zveřejněna prostřednictvím Digitální knihovny Univerzity Pardubice.

Dále prohlašuji, že tato doktorská práce ani její podstatná část nebyla předložena za účelem získání jiného akademického titulu, diplomu nebo kvalifikace.

V Pardubicích dne 18.6.2024 Mgr. Mariia Lemishka

The experimental work presented in this Ph.D. thesis was conducted at the J. Heyrovský Institute of Physical Chemistry of the Czech Academy of Sciences, Department of Structure and Dynamics in Catalysis, between 2016 and 2024. This dissertation – a commentary on six papers published in peer-reviewed internationally renowned scientific journals was written with the permission of all co-authors.

Acknowledgments

First of all, I would like to express my sincere gratitude to my supervisor, Mgr. Jiří Dědeček, CSc., DSc., for his valuable advice, support, guidance, and patience, and for all the opportunities offered to me at the beginning of my research career. A big thanks to Doc. Mgr. Edyta Tabor, Ph.D, for her knowledge, incredible motivation, and belief in me. I am also very grateful to Doc. Ing. Zdeněk Sobalík CSc., for our fruitful discussions. I would like to thank Kinga Mlekodaj, Ph.D., for giving me wise advice from the first day of my study. Many thanks to RNDr. Štěpán Sklenák, Ph.D., DSc., for providing the DFT calculations used in my thesis. I would like to thank Prof. Ing. Roman Bulánek, Ph.D., for his supervision and help at the University of Pardubice. I am also thankful so much to Mgr. Veronika Pashkova, Ph.D., for the opportunity to work at the J. Heyrovský Institute of Physical Chemistry and to be in the Czech Republic. I would like to express my sincere gratitude to my colleague and friend, Mgr. Sofiia Tvorynska, Ph.D., for her valuable advice and support. I would like to thank all my colleagues, especially from the J. Heyrovský Institute of Physical Chemistry of the Czech Academy of Sciences, the University of Pardubice (Faculty of Chemical Technology), and the Ivan Franko National University of Lviv, who were involved in my research activities.

My gratitude extends to my little son Daniel and my husband Bohdan for their trust in me and unwavering love. I am also thankful for the support and encouragement from my parents Vasyl and Oksana, my sister Vasylyna, Bohdan's family, my extended family, and close friends.

Many thanks and appreciation to the organization EURAXESS.CZ in Prague for assisting my family and me in obtaining residence permits. I would also like to thank the Armed Forces of Ukraine for their invaluable work, which helped me stay strong during my Ph.D. studies.

Finally, I would like to acknowledge the following funding sources, which supported my research activities: i) 15-13876S. Zeolites with (semi)monomodal aluminum distribution in the framework. The Czech Science Foundation (GACR); ii) 17-00742S. Binuclear metal ion structures in zeolites. GACR; iii) 17-09188Y. Innovative approaches for zeolite synthesis. GACR. iv) 19-02901S. Innovative approaches for methane recovery – Enzyme-inspired zeolitic catalysts. GACR.

Contents

Abstract

Transition metal ion (TMI)-exchanged zeolites have shown excellent activity and selectivity in the oxidation of methane (CH_4) to methanol (CH_3OH) at room temperature. Therefore, a detailed understanding of the structure-activity-stability relationship for their use in the reaction is required. In this thesis, newly developed (reported for the first time) TMI-based Fe(II)-, Co(II)-, Ni(II)-, and Mn(II)-ferrierite (FER) along with Fe(II)-mordenite (MOR) zeolite catalysts are presented for molecular oxygen (O_2) and nitrous oxide (N_2O) splitting for the selective oxidation of CH_4 towards CH_3OH. In addition, experimental and theoretical methods were applied to investigate the O_2 and N_2O activation over the presented metallozeolites. This research has confirmed the formation of highly reactive species called alpha oxygen (α-O) and their reactivity in CH_4 oxidation. The theoretical study of O_2 activation was also extended to Fe(II)-beta (*BEA) and Fe(II)-Linde Type A (LTA) zeolites.

The first part of this thesis focuses on explaining the methodology, which was based on a combination of several techniques, such as in-situ Fourier-transform infrared spectroscopy (FTIR), X-ray absorption near-edge structure, Mössbauer, ultraviolet-visible spectroscopy, mass spectrometry, FTIR analysis in the gas phase, and density functional theory calculations used to study the formation, stabilization, evolution, and reactivity of α-O from O_2 cleavage over Fe-FER, and following treatment with CH_4.

In the study, special attention was dedicated to analyzing the stabilization, siting, and location of bare divalent cations of Fe, Co, Ni, and Mn in the extra-framework cationic positions in the FER matrix. In addition, the unique type of active (binuclear) centers was investigated in the TMI-based FERs, which is the crucial point for subsequent treatment with O_2 or N_2O and CH_4. Also, the potential of zeolites (MOR, *BEA, and LTA) other than the FER matrix was evaluated in order to find an arrangement suitable for the formation of an optimal distance between two divalent metal (M(II)) ions (binuclear center formation), which could cooperate in O_2 dissociation. Additionally, the aluminum (Al) distribution was studied in MOR zeolite.

The following sections are devoted to the investigation of the potential for O_2 activation and the following CH_4 selective oxidation over Co(II), Ni(II), and Mn(II) in the FER matrix. The formation of α-O, obtained by N_2O decomposition and its activity toward CH_4 to CH_3OH oxidation, was studied over the binuclear centers of Fe(II), Co(II), and Ni(II)-FERs. Finally, the influence of zeolite topology on the catalytic performance in catalytic reduction (CR_{N2O}) and selective catalytic reduction (SCR_{N2O}) reactions over Fe(II)-FER and Fe(II)-MOR with similar Fe(II) loadings was investigated.

Abstrakt

Zeolity vyměněnými ionty přechodných kovů (TMI) vykazují vynikající aktivitu a selektivitu při selektivní oxidaci metanu (CH_4) na metanol (CH_3OH) již při pokojové teplotě. Pro jejich použití v této reakci je však třeba podrobně prozkoumat vztah mezi strukturou, aktivitou a stabilitou. V této práci jsou prezentovány (poprvé uvedeny) nově vyvinuté zeolitové katalyzátory na bázi přechodových iontů Fe(II)-, Co(II)-, Ni(II)- a Mn(II)-ferrieritu (FER) a Fe(II)-mordenitu (MOR) pro štěpení molekulárního kyslíku (O_2) a oxidu dusného (N_2O) pro následnou selektivní oxidaci CH_4 na CH_3OH. Kromě toho byla za použití experimentálních a teoretických metod zkoumána aktivace O_2 a N_2O na prezentovaných metalozeolitech. Tento výzkum potvrdil vznik vysoce reaktivních forem tzv. alfa kyslíku (α-O) a jejich reaktivitu při oxidaci CH_4. Teoretické studium aktivace O_2 bylo rozšířeno o zeolity Fe(II)-beta (*BEA) a Fe(II)-Linde typ A (LTA).

První část této práce se zaměřuje na vysvětlení metodiky, která založené na kombinaci různých technik, jako je in-situ infračervená spektroskopie s Fourierovou transformací (FTIR), rentgenová absorpční spektroskopie, Mössbauerova spektroskopie, ultrafialová a viditelná spektroskopie, reakční testy s využitím hmotnostní spektrometrie a FTIR spektroskopie pro analýzu plynné fáze a DFT výpočtů, které se používají ke studiu vzniku, stabilizace, vývoje a reaktivity α-O při štěpení O_2 na Fe-FER a po jeho interakci s CH_4.

Zvláštní pozornost byla v této studii věnována analýze stabilizace, umístění a poloze “holých“ (bare) dvojmocných kationtů Fe(II), Co(II), Ni(II) a Mn(II) v mimomřížkových kationtových pozicích v matrici ferrieritu. Dále byl zkoumán jedinečný typ aktivních (binukleárních) center ve FER na bázi iontů přechodných kovů, který je jedinečný při reakci s O_2 nebo N_2O a CH_4. Rovněž byl vedle FER vyhodnocen potenciál dalších zeolitů (MOR, *BEA a LTA) s cílem nalézt uspořádání vhodné pro vytvoření optimální vzdálenosti mezi dvěma dvojmocnými ionty kovu (M(II)) pro tvorbu binukleárních center, které by mohly spolupracovat při disociaci O_2. Kromě toho bylo studováno i rozložení hliníku (Al) v mordenitu, jako klíčového parametru pro stabilizaci binukleárního centra.

Následující části jsou věnovány zkoumání potenciálu aktivace O_2 a následné selektivní oxidaci CH_4 na Co(II), Ni(II) a Mn(II) v matrici FER. Tvorba α-O získaného rozkladem N_2O a jeho aktivita vůči oxidaci CH_4 na CH_3OH byla studována na binukleárních centrech Fe(II)-, Co(II)-, a Ni(II)-FER. Za účelem analýzy vlivu topologie zeolitu na výkon katalyzátoru v reakcích katalytické redukce a selektivní katalytické redukce oxidů dusíku byly použity katalyzátory Fe(II)-FER a Fe(II)-MOR s podobným obsahem Fe(II).

Keywords

Alpha oxygen, Ferrierite, Heterogeneous Catalysis, Infrared spectroscopy, Methane, Methanol, Molecular oxygen, Mordenite, Selective oxidation of methane to methanol, Transition metal ion sites, Zeolite.

Klíčová slova

Alfa kyslík, Centra na bázi přechodných kovových iontů, Ferrierit, Heterogenní katalýza, Infračervená spektroskopie, Kyslík, Metan, Metanol, Mordenit, Selektivní oxidace metanu na metanol, Zeolity.

List of abbreviations and symbols

α	alpha
α-O	alpha oxygen
β	beta
γ	gamma
AlO_4^-	aluminate tetrahedra
^{27}Al (3Q) MAS-NMR	aluminum triple quantum magic angle – spinning nuclear magnetic resonance
*BEA	beta zeolite
CHA	chabazite
CR	catalytic reduction
DFT	density functional theory
DR	diffuse reflection
1D	one-dimensional
2D	two-dimensional
3D	three-dimensional
FER	ferrierite
FAU	faujasite
FTIR	Fourier-transform infrared
IS	isomer shift
L	ligand
LTA	Linde type A zeolite
LTL	Linde Type L zeolite
M(II)	divalent metal cation
MAZ	Mazzite zeolite
M/Al	divalent metal-to-aluminum molar ratio
MFI	Mobil-type five zeolite
MOR	mordenite
MX	metal-halogen
m/z	mass to charge ratio
4-MR	four-membered ring
6-MR	six-membered ring
8-MR	eight-membered ring
10-MR	ten-membered ring

12-MR	twelve-membered ring
pMMO	monooxygenase enzymes contain the copper active site
QS	quadrupole splitting
RT	room temperature
SCR	selective catalytic reduction
Si/Al	silicon to aluminum molar ratio
^{29}Si MAS-NMR	silicon magic angle–spinning nuclear magnetic resonance
SiO_4	silicate tetrahedra
Si-OH-Al	Brønsted acid sites
sMMO	monooxygenase enzymes contain a di-iron bridged center
TMI	transition metal ion
TMI/Al	transition metal ion to aluminum molar ratio
T–O–T	skeletal antisymmetric mode in FTIR spectral region (1350 – 850 cm^{-1})
UV-Vis	Ultraviolet-visible
XANES	X-ray absorption near edge structure
XRD	X-ray diffraction
XRF	X-ray fluorescence

I Introduction

1.1 Transition metal ion extra-framework sites in the metallozeolites and aluminum distribution

Zeolites represent one of the most important groups of heterogeneous industrial catalysts, being widely applied in hydrocarbon processing (acid – base catalysis), selective hydrocarbon oxidation, and the abatement of nitrogen oxides (NO_x) (redox catalysis).[1, 2] The outstanding catalytic properties of zeolite catalysts result from a unique combination of their chemical composition and structure. Zeolites are crystalline microporous aluminosilicates built from silicate (SiO_4) and aluminate (AlO_4^-) tetrahedra that share corners to form a regular channel/ cavity system.[3] The variety of pore architectures results in different pore sizes, different dimensionalities of the channel system, from one- to three-dimensional (1D to 3D), and the presence of cages and other structural features, which are reflected in the inner surfaces of zeolites (250 – 1000 m^2/g).[4, 5]

The isomorphous substitution of aluminum (Al) in the SiO_4 framework induces a negative framework charge, which can be balanced by two types of extra-framework cationic species – the protons involved in Brønsted acid sites (Si-OH-Al) represent active sites in acid-catalyzed reactions, and bare cations and metal-oxo cationic species serve as the active sites in redox-catalyzed processes.[6, 7] Thus, zeolite catalysts combine a shape selectivity function (concerning substrates, products, and transition states) with 'well-defined' but tunable, active sites dispersed across the large, internal zeolite surface. Moreover, zeolite catalysts are mechanically, thermally, and chemically stable, and their manufacture on an industrial scale has been well demonstrated.[8]

Zeolites can be divided into two main categories depending on the amounts of silicon (Si) and Al atoms in the framework.[9] The Si-rich zeolites, which are characterized as materials with a Si/Al molar ratio > 5, include the pentasil zeolite family, which is a SiO_4 structure composed of pentagonal arrangements of atoms, as observed in ferrierite (FER), mordenite (MOR), Mobil-type five (MFI), and beta (*BEA) zeolites.[10] By contrast, because Al-rich zeolites are considered to have a matrix with Si/Al < 5, the most common zeolites in this category are Lynde type A (LTA)[11] or chabazite (CHA)[12] frameworks. Recently, attention has been focused on the Al-rich form of the *BEA zeolite.[13, 14]

The organization of Al atoms in the zeolites (also known as the Al distribution) represents a key factor in the stabilization of catalytically active centers (both protons and transition metal ion (TMI) centers) through Al atom concentrations, locations, and distances in the zeolite matrix.[15-17] From studies on Al distributions in zeolites, Al-O-Al sequences do not exist, according

to Loewenstein's rule on zeolites.[18] In a pioneering study, Dedecek et al. described a new and important parameter for catalysis – mutual Al atom arrangements in Si-rich zeolites.[9] They developed a method for the complete analysis of the vicinity and location of Al atoms, and their distribution between Al pairs and single Al atoms. This was based on a well-verified methodology employing triple quantum ^{27}Al(3Q) and ^{29}Si magic angle-spinning nuclear magnetic resonance (MAS-NMR) spectroscopy and the UV-Vis spectroscopy of bare Co(II) ions in dehydrated Co-zeolites. It was experimentally proven that, in Si-rich FER, MFI, and MOR zeolites, Al atoms can be organized as exclusively Al pairs (Al-O-(Si-O)$_2$-Al) or single Al atoms. By contrast, in Al-rich *BEA zeolites, except for single Al atoms and Al pairs, Al-O-Si-O-Al sequences, and closed, unpaired Al atoms (Al-O-(Si-O)$_3$-Al) can be observed (Fig. 1).[10] In Al-rich LTA zeolites, the Al-O-Si-O-Al sequences predominate.[11]

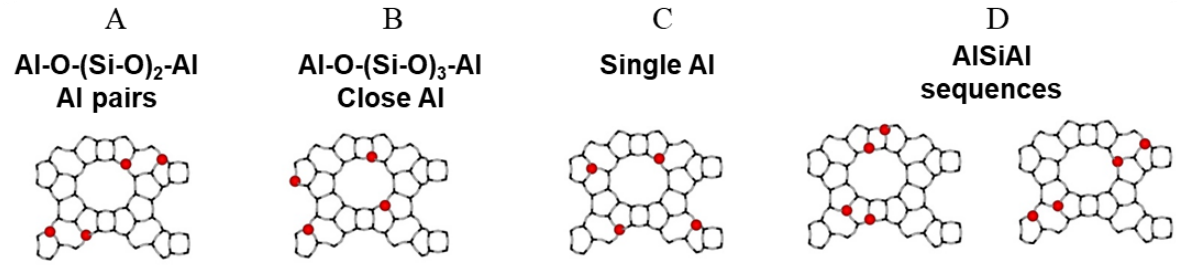

Fig. 1. As an example, schematic representations of: (A) Al pairs; (B) close unpaired Al atoms; (C) single Al atoms; and (D) Al-O-Si-O-Al sequences, observed in *BEA structures. Al atoms are shown in red.

The organization of the Al atoms in zeolites plays a crucial role in the stabilization of various types of ion/oxo species in metallozeolites. It has been confirmed that the introduction of TMIs to zeolites has led to the formation of several types of counter-metal (M)-ion/oxo species (as schematically depicted in Fig. 2).[19] Here, bare cations (balancing the negative zeolite charge) have coordinated to four O atoms in the framework and to cation-oxo species, bi(poly) nuclear cation-oxo species, metal-ion(oxo) clusters, and metal-oxide species.[20, 21]

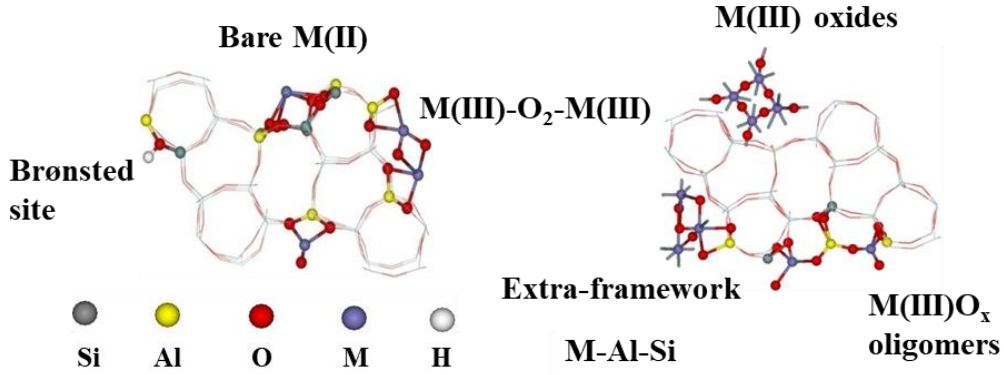

Fig. 2. Schematic depiction of the possible types of TMI centers formed in metallozeolites. Adapted from Sazama et al.[19]

The formation of various types of cation species in zeolites depends on the type of zeolite structure, the preparation procedure used to introduce the metal (ion exchange or impregnation methods are the most applicable),[22, 23] and the type and concentration of cations used. It has been shown that metallozeolite cations balance the negative charge of the zeolite and are located in rings containing two Al atoms called cationic positions or cationic sites. However, the study reported here was focused on an analysis of the formation, cooperation, and redox behavior of the bare cations located in cationic positions in FER, MOR, *BEA, and LTA zeolites.

For the first time in the MOR topology, Wichterlova et al.[24] spectroscopically (via Ultraviolet-visible (UV-Vis) diffuse reflection (DR) and Fourier-transform infrared (FTIR) spectroscopy) confirmed the existence of three cationic positions of bare Co(II) ions (indicated by alpha (α), beta (β) and gamma (γ) in Fig. 3) that differed in their symmetry and location in the zeolite matrix. They also identified the spectroscopic features of the cations in individual sites. The divalent cations sitting in the α cationic positions of MOR zeolites are located above the center of six-membered rings (6-MRs) and are coordinated to four oxygen (O) atoms from the same ring. These are located on the wall of the main channel and are readily accessible. The β cationic sites in MOR zeolites are distinguished as the most populated fraction of all the cationic positions. The divalent cations balanced in this position are coordinated to four O atoms of the eight-membered ring (8-MR) in zeolite and exhibit a planar geometry. In the γ cationic positions, divalent cations are stabilized in a closed coordination sphere with pseudo-octahedral coordination. It has been determined that this position is a less-occupied site.

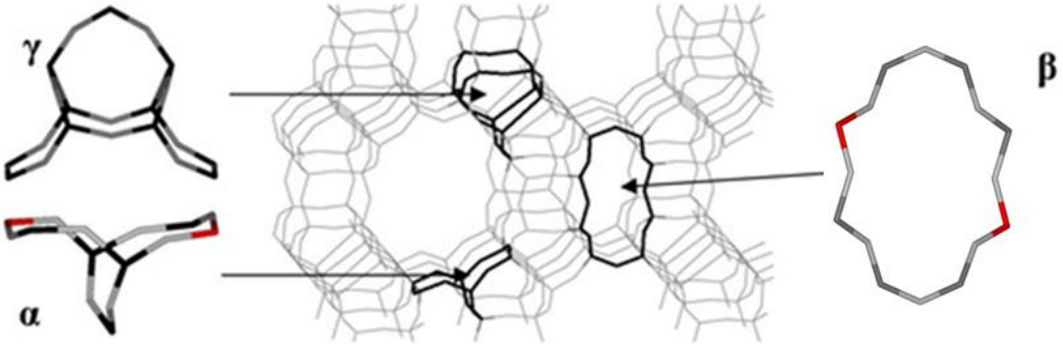

Fig. 3. Local framework structures of the α, β, and γ sites in MOR zeolites. Al atoms shown in red, Si atoms in black, and O atoms in gray.

A few years later, Dalconi et al.[25] confirmed the presence of the same three cationic positions in FER zeolites using a spectroscopic method and X-ray diffraction. It should be noted that, for metallozeolites with high metal loadings, except for divalent cations located in cationic positions, various ion/oxo metal species, including oxides, can be formed.

1.2 Zeolite topologies discussed in the thesis and their catalytic properties

The 3D FER zeolite structure, with a two-dimensional (2D) channel system consisting of ten-membered ring (10-MR) and 8-MR channels,[4] and due to its high stability under thermal, hydrothermal and chemical treatments, is known as having excellent heterogeneous catalyst properties for isomerization, carbonylation, and cracking. TMI-containing FER zeolites exhibit remarkable catalytic performance in redox catalysis, such as N_2O abatement, selective catalytic reduction (SCR_{N2O}), hydrocarbon oxidation, and oxidative dehydrogenation.[26, 33] In these processes, a metal center that can easily perform redox cycles plays a crucial role. It has been suggested that these features have TMI cations located in cationic positions. In FER zeolites, the presence of the three types of cationic sites (α, β, and γ) (Fig. 4)[26-28] have been confirmed through a series of computational, spectroscopic, and diffraction experiments. The symmetry and location of these three cationic positions in FER zeolites are similar to those described from above cationic positions in MOR zeolites (Section 1.1)

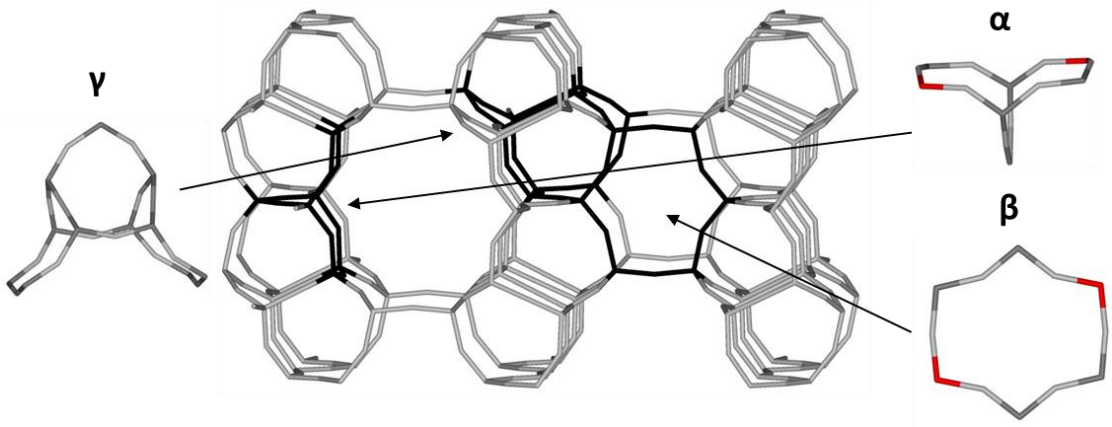

Fig. 4. Local framework structures of the α, β, and γ sites in FER zeolites. Al atoms shown in red, Si atoms in black, and O atoms in gray.

Using UV-Vis spectroscopy, Kaucky et al.[29] monitored the population of particular cationic positions (α, β, and γ) in high-Si (Si/Al 8.6) FER zeolites, using Co cations as the probe molecules. The study revealed that the FER framework contained 66% Al in the form of Al pairs, while the remaining 34% of the Al existed as isolated atoms. In addition, they showed that 6-MRs with Al pairs in the β cationic site formed the predominant fraction, which accounted for 50% of all the framework Al atoms. The remaining Al-pair sequences were located in the α site, which accounted for 10% of all the framework Al atoms.

Recently, the investigation of the cationic positions in FER zeolites has been expanded through DFT calculations, which have predicted the existence of two β cationic positions – β-1 and β-2 – in Fe-FER zeolites.[30] In both β positions, the Fe(II) ion is located in the plane of a 6-MR, coordinated to four oxygen atoms in the ring, with the O-Fe-O angle being 176° (β-1) and

172° (β-2) (Fig. 5A and B). The DFT calculations also confirmed that, in the α cationic position, the Fe(II) was located above the center of the 6-MR, with two Al atoms and coordinated to four oxygen atoms in the same ring (Fig. 5C). By combining the results from Mössbauer with ^{27}Al 3Q MAS-NMR and DFT calculations, it was revealed that the incorporation of M(II) ions was most effective in β-2, less effective in β-1, and least effective in the α site. The tendency of M(II) ions to reside in cationic sites follows the trend α < β-1 < β-2.[26]

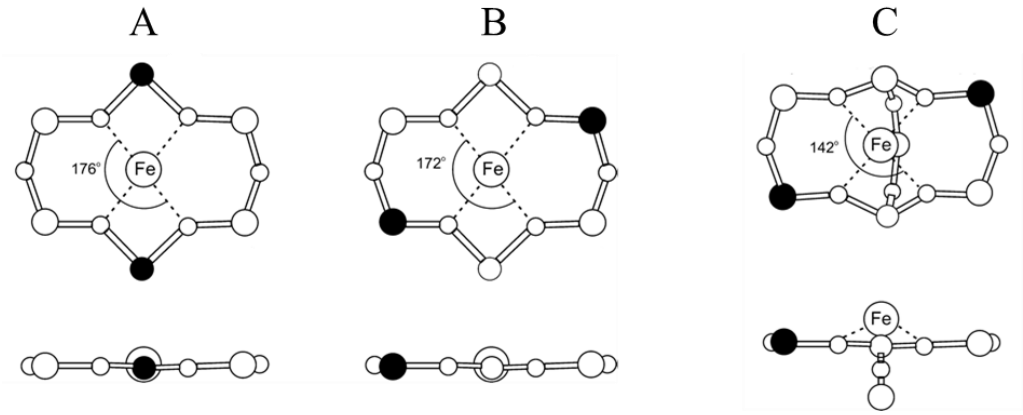

Fig. 5. Local configuration of 6-MRs of a FER zeolite with the Fe(II) cation in the: (A) β-1 position; (B) β-2 position; and (C) α site. The top/bottom panels show the top/side views of the 6-MRs.

Another industry-important zeolite is the MOR zeolite, which is used in refining and petrochemical catalytic processes.[31] The TMI-based MOR is known as a catalyst in environmentally friendly processes, such as N_2O decomposition,[32] SCR,[32] oxidative dehydrogenation,[33] and catalytic reduction (CR).[34] The MOR is a large-pored pentasil-ring zeolite, with Al in the framework and a 1D channel system formed by a twelve-membered ring (12-MR) channels and side pockets that are accessible through 8-MRs.[4] However, in terms of the Al distribution, this MOR zeolite structure has not been studied in detail. The determination of the organization of Al atoms in commercially available MOR zeolites could significantly influence the preparation of MOR zeolite catalysts with the desired cationic sites.

The other matrix that has been studied is that of the *BEA zeolite, which has been demonstrated as industrially important in several reactions, including cracking,[35] hydrocracking,[36] alkylation,[37] acylation,[38] isomerization,[39] and biomass conversion.[17] The *BEA zeolite matrix is used in redox catalysis for the SCR of NO_x.[40] The *BEA zeolite topology consists of two or three polymorphs (A, B, and C) gathered from a four-membered ring (4-MR), a five-membered ring (5-MR), and 6-MR forming an intersecting 3D channel structure with 12-MRs.[13, 41] The framework of the *BEA zeolite has 3D intersecting channels of 6.6 Å × 6.7 Å size, providing advantageously easy diffusion, even of voluminous organic molecules.[42]

The results of FTIR and UV-Vis spectroscopy studies of TMI-*BEA zeolites have confirmed the presence of the three cationic sites (α, β, and γ) (Fig. 6) for the A and B polymorphs

and for Si-rich and Al-rich *BEA matrices.[43, 44] The β site in a 6-MR containing two Al atoms (Al pair) is the most populated cationic site for hosting divalent cations.[45]

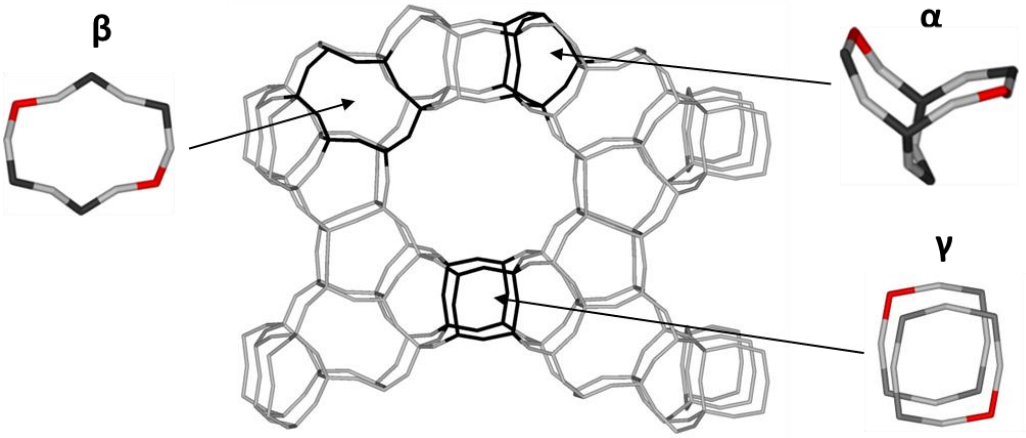

Fig. 6. Cationic sites of bare, divalent TMIs in *BEA Polymorph A and B zeolites. Al atoms shown in red, Si atoms in black, and O atoms in gray.

The LTA zeolite (Si/Al 1), classified as Al-rich, is one of the most widely studied and used zeolite materials in industry, employed in adsorbing gas and gas purification.[11, 46] The 3D LTA zeolite has a cubic structure composed of secondary building units – eight alpha cages (super cages) and eight beta cages (sodalite), as shown in Fig. 7.[47, 48] Compared with MOR, FER, and *BEA zeolites, the LTA zeolite does not contain a channel system. Instead, it is built from cavities connected by 8-MRs. The super cages are interconnected through an open window in the 8-MR, while the sodalite cages are coupled by 4-MRs and attached to the super cages through 6-MRs. It has been suggested that the TMI cations are located in cationic positions in TMI-LTA zeolites, situated inside the sodalite cage in the 6- or 8-MRs.[47, 48] However, from an energetic point of view, the most likely site for the accommodation of bare M(II) cations is the 6-MR on the surface of the sodalite cage. A recently reported thermodynamic study of TMI Mn(II)-, Co(II)-, Cu(II)-, and Zn(II)-exchanged LTA zeolites has shown that the interaction between the framework and the different cations plays a crucial role in their stability.[49]

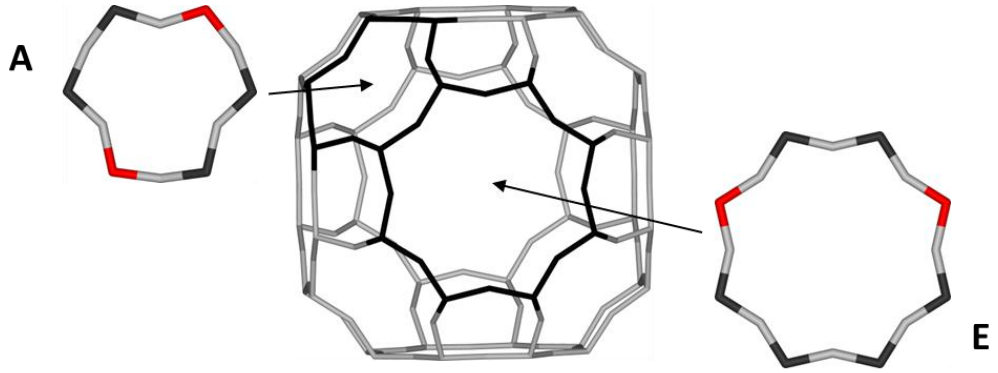

Fig. 7. A and E – most common cationic positions of bare divalent TMI in LTA zeolite matrix. Al atoms shown in red, Si atoms in black, and O atoms in gray.

1.3 Methane: Its properties and utilization

From an economic and environmental perspective, there has been a great deal of interest in the chemical utilization of CH_4,[50] which is a potent greenhouse gas.[51] However, CH_4, being a main component of natural gas, represents the cheapest and most abundant source of hydrocarbons.[52] The chemical features of CH_4, such as its low electron and proton affinity, weak acidity, low polarizability, high carbon-hydrogen (C-H) bond strength (439 kJ/mol), and high ionization energy, make it highly resistant to chemical transformation. Nevertheless, it has been shown that the transformation of CH_4 to valuable products requires the presence of catalysts. The role of the catalyst in the process of the formation of oxygenated from CH_4 is the activation of the oxidant.[50] The most promising way to transform CH_4 is via its direct oxidation to methanol (CH_3OH), which is a significant and valuable commodity//platform chemical in the chemical industry and a potential energy carrier.[53]

Since the beginning of the 20th century, the selective oxidation of CH_4 to CH_3OH has been performed using both homogeneous and heterogeneous catalysts.[54, 55] In a homogeneous way, Shilov et al.[56] reported that when CH_4 was heated to 100°C in a sealed ampoule containing platinum tetrachloride ($PtCl_4$) and deuterium oxide (D_2O)/acetic acid (CH_3COOD) mixture, H/deuterium (D) exchange was observed to occur, indicating that CH_4 activation could occur under mild conditions. However, it has not been possible to bring the Shilov et al. system close to commercial levels, due to the loss of the catalyst such that it cannot be reused. An important breakthrough in CH_4 conversion came in 1998, with the use of a ligand-modified Pt system in fuming sulfuric acid (H_2SO_4) that oxidized CH_4 to CH_3OH, giving an overall selectivity of 81%.[57]

In a heterogeneous way, CH_4 has been oxidized to CH_3OH over TMI oxides, such as molybdenum oxide (MoO_3), vanadium oxide (V_2O_5), and Fe(III)/silica (SiO_2).[58, 59] In the 1980s, heterogeneous Mo materials were among the most active catalysts used for CH_3OH production.[59] In 2008, impressive CH_4 conversion and CH_3OH selectivity values (13.2% and 78.8%, respectively) were reported over Fe(III)/SiO_2.[58] From 1990 to the present, metal-containing zeolites (e.g., Zn-ZSM-5) have been reported for the catalytic, selective partial oxidation of CH_4 to CH_3OH with O_2 under flow conditions.[60, 61] The study demonstrated that CH_3OH could be formed selectively under the proper conditions. The selectivity of CH_3OH reported by Lyons et al.[61] was 64% at 4.6% conversion, while Walsh et al.[60] reported 20.6% selectivity at 5.5% conversion.

The low-temperature selective oxidation of CH_4 to CH_3OH over metallozeolites has been suggested as a promising way of CH_4 utilization. Thus, in the literature, four mechanisms for C-H bond activation in CH_4 have been suggested (Fig. 8).[62] In the first mechanism – oxidative addition

– a low-valent metal reductively splits the C-H bond by donating two electrons to the C-H σ* antibonding orbital. In the mechanism of second – electrophilic activation, a C-H – bonding orbital donates to a vacant metal d orbital, and this weakens and polarizes the C-H bond so that the CH_4 can be deprotonated. In the third – sigma-bond metathesis – binding to the metal halogens (MX) fragment plays a similar role in activating the C-H bond. In the final mechanism, highly electrophilic reactive metal-O species with low-lying, unoccupied molecular orbitals are localized on a metal-O fragment. These are activated as acceptor orbitals for H-atom abstraction, even from the stable C-H bonding levels of CH_4.

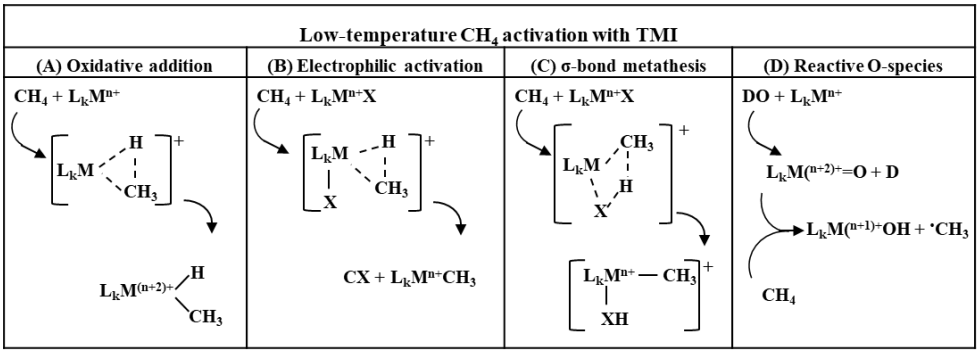

Fig. 8. Schematic showing the four mechanisms of C-H bond activation in CH_4: (A) oxidative addition; (B) electrophilic activation; (C) sigma-bond metathesis; and (D) oxidation with a reactive metal-O species. L – ligand; M – metal; X – halogen; D – deuterium; H – hydrogen; C – carbon; O – oxygen.[62]

The reactive-O-species strategy is employed by nature and metallozeolites to activate strong C-H bonds. The formation of isolated, highly reactive-O-species is a result of the activation of an oxidant over the TMIs in zeolites. Subsequently, various oxidants can be employed (e.g., N_2O, NO, H_2O_2, O_3, and H_2O) for CH_4 oxidation. However, these oxidants cannot be compared with the freely available atmospheric molecular oxygen. The following sections (1.4 and 1.5) provide detailed descriptions of the oxidation properties of metallozeolites in the selective oxidation of CH_4 using N_2O and O_2 as oxidants.

1.4 Selective oxidation of CH_4 over TMI-containing zeolites

The stabilization of TMI species within the zeolite matrix offers the potential for a range of applications, including catalysts for processes such as the selective oxidation of CH_4 to CH_3OH, the selective reduction of NOx in exhaust gases, and the direct decomposition of NO and N_2O.[63-66] Over recent years, zeolites containing TMIs have been proposed as a chemical looping approach for selective CH_4 oxidation to CH_3OH.[67] In this process, CH_4 is oxidized by small molecules, such as O_2 and N_2O, that have been previously activated over TMI-containing zeolites. However, in comparison to N_2O, molecular O_2, due to its easy availability and eco-friendly properties, represents the most desirable oxidant from both environmental and economic points of

view.[66, 68] The CH_3OH produced from CH_4 oxidation has the dual potential of serving as both an energy carrier and a key chemical raw material for obtaining value-added products (e.g., formaldehyde or dimethyl ether). The current investigation into CH_4 oxidation over metallozeolites is reported below through experimental and theoretical approaches.

The majority of the current research focusing on CH_4 oxidation over metallozeolites has been directed toward the behavior of Fe and Cu cations embedded in various zeolite topologies, including ZSM-5, mazzite (MAZ), MFI, MOR, FER, *BEA, faujasite (FAU), and ZSM-13.[69-72] Since the first report by Panov et al.[73] in 1990 on the formation of highly reactive oxygen species (α-O) upon CH_4 oxidation with N_2O over Fe-ZSM-5 (stabilization of the Fe(II)/α-O sites) [see Eqs. (1) and (2)], numerous investigations have been conducted.[58, 74-77]

$$Fe(II) + N_2O \rightarrow N_2 + [Fe(III)\text{-}O^-]^{2+} \quad (1)$$

$$[Fe(III)\text{-}O^-]^{2+} + CH_4 \rightarrow Fe(II) + CH_3OH \quad (2)$$

Other studies have confirmed the oxidation of CH_4 to CH_3OH by N_2O over Fe-exchanged into various zeolite topologies (ZSM-5, MOR, MFI, CHA, and *BEA).[69] In addition, recently, it has been shown that previously O_2-treated Cu species in zeolites (e.g., MFI, MOR, MAZ, FER, CHA, FAU, *BEA, Linde Type L (LTL)) oxidize CH_4 to CH_3OH.[68, 70, 78-80] It should be noted that the main feature of α-O stabilized on metallozeolites is its ability to selectively oxidize CH_4 to CH_3OH or benzene to phenol.[75] In 2005, Groothaert et al.[81] first reported the selective oxidation of CH_4 to CH_3OH by O_2 over Cu-MOR zeolites. Later, in 2009, Woertink et al.[82] determined the geometric and electronic structure of Cu species in CH_4 transformation present in Cu-MOR by DFT calculation. In addition, Co-, Ni-, and Mn-based zeolites have been used for selective CH_4 oxidation.[98, 99] However, the information available on their application is limited. Furthermore, it has been shown that the reaction pathways of CH_4 oxidation over metallozeolites strongly depend on the type of active TMI species present in the zeolite. It should also be noted that data from the literature indicate that CH_4 oxidation over metallozeolites, regardless of the type of oxidant (O_2 or N_2O) requires the use of effluent to remove the oxidation products bonded on the surface of the TMI-zeolite-based catalysts. Table 1 contains the results, including the reaction temperature and catalytic performance obtained from the oxidation of CH_4 to CH_3OH over Fe-, Cu-, Co-, and Ni-modified zeolites. Nevertheless, the selective oxidation of CH_4 over zeolite-based catalysts still suffers from several issues that need addressing in order to be able to develop more active and selective catalysts for CH_3OH production. These include working at low (RT) or medium (< 250°C) reaction temperatures, exhibiting short redox cycles, or working in a continuous regime, with catalyst regeneration occurring over a short time, and eliminating the usage of effluent for

oxidation products extraction. In subsections 1.4.1 and 1.4.2, the critical overview from the literature of CH_4 oxidation by N_2O or O_2 over metallozeolites is described in detail.

Table 1. CH_4 oxidation by N_2O or O_2 over metal-containing zeolites: Selected experimental results.

Catalyst	Oxidant	Temperature	Methanol selectivity	Methanol yield	Productivity
		˚C	%	$mmol/g_{cat}$	$mmol/mol_{metal}$
Fe-ZSM-5[83]	N_2O	RT	80	**5.0**	—[a]
Fe-ZSM-5[84]	N_2O	160	76	**160**	—
Fe-ZSM-5[85]	N_2O	25	94	**23**	—
Fe-SSZ-13[86]	N_2O	RT	—	**26.8**	661
Cu-ZSM-5[81]	N_2O	175	98	**8.2**	—
Cu-ZSM-5[81]	N_2O	RT	—	**0.81**	—
Cu-MOR[81]	N_2O	175	—	**11.3**	—
Cu-MOR[87]	N_2O	150	—	**97**	≤300
Cu-SSZ-13[88]	N_2O	260	27	**19(1h)**	—
Fe-FER[71]	O_2	RT	—	**75**	—
Cu-ZSM-5[81]	O_2	175	98	**8.2**	—
Cu-ZSM-5[81]	O_2	RT	—	**0.81**	—
Cu-ZSM-5[89]	O_2	200	—	**16**	30
Cu-ZSM-5[90]	O_2	200	—	**9**	14.3
Cu-ZSM-5[91]	O_2	210	71	**1.81(1h)**	5.2
Co-MOR[81]	O_2	175	—	**11.3**	—
Co-MOR[89]	O_2	200	—	**31.0**	40
Co-MOR[90]	O_2	200	—	**31.2**	43.8
Co-MOR[87]	O_2	150	—	**67**	≤250
Co-MOR[92]	O_2	200	80	**160**	—
Co-MOR[93]	O_2	200	90	**170**	470
Co-MOR[94]	O_2	200	95	**118.5**	180
Co-MOR[95]	O_2	200	—	**56.2**	—
Cu-MAZ[96]	O_2	200	—	**200**	—
Cu-SSZ-13[89]	O_2	200	—	**31.0**	60
Cu-SSZ-13[90]	O_2	200	—	**30.0**	42.4
Cu-SSZ-13[97]	O_2	200	—	**125.0**	200
Cu-SSZ-16[89]	O_2	200	—	**39.0**	50
Cu-SSZ-39[89]	O_2	200	—	**36.0**	90
Co-ZSM-5[98]	O_2	150	40 – 100	**0.3 – 0.4**	—
Ni-ZSM-5[99]	O_2	175	40 – 100	**5.1**	—

[a]— the information is missed in the literature.

1.4.1 Activation of N_2O over TMI-modified zeolites

As mentioned above, the Fe-ZSM-5 zeolite has a long history of being used as a catalyst for CH_4 oxidation by N_2O, as evidenced by numerous studies.[72, 103, 104] Panov et al.[72, 73, 83] reported that Fe-ZSM-5, previously activated at 900°C, efficiently decomposed N_2O at temperatures of ≤ 300°C. As a result of this interaction, the highly reactive α-O, presented as FeO^+ bound to the zeolite surface, is formed. In addition, it has been shown that only a small fraction of the Fe species present in the studied Fe-ZSM-5 was catalytically active in the N_2O activation. In order to distinguish the Fe active fraction in Fe-ZSM-5 from the spectators, the authors used in-situ spectroscopic methods and a theoretical approach. It has been previously assumed that the active precursor associated with the decomposition of N_2O was a binuclear Fe species, analogous to those observed in CH_4 monooxygenase (sMMO) enzymes that provide CH_4 oxidation.[117] However, subsequent studies have demonstrated that the Fe site is a mononuclear Fe(II) species formed via the irreversible auto-reduction of impregnated Fe(III) species upon thermal treatment, which is evidenced by Mössbauer spectroscopy.[72] In addition, the oxidation properties of α-O originating from N_2O decomposition and stabilized on Fe-ZSM-5 were confirmed in the CH_4 transformation.[84]

Jisa et al.[100] experimentally confirmed the structure of α-O by splitting N_2O over Fe-FER, Fe-MFI, and Fe-BEA zeolites. Their multi-spectroscopic results and DFT calculations produced structural models in which two cooperating Fe(II) cations, located in two adjacent β cationic sites of FER zeolites, formed the active site responsible for the N_2O decomposition and stabilization of α-O (Fig. 9).

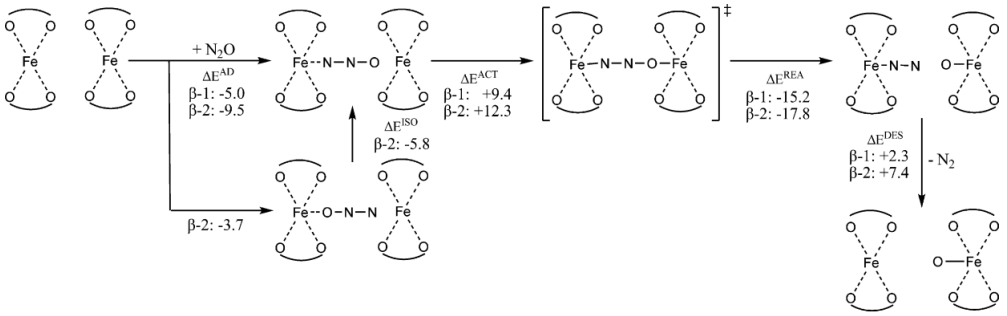

Fig. 9. Energies and barriers in the adsorption of N_2O on Fe(II) accommodated in two adjacent collaborating β sites in a FER zeolite and the reaction steps then leading to FeO(ad) and N_2.

They proposed a local structure with two adjacent β sites, Fe···Fe distanced in 7.5 Å in FER zeolite topology, which cooperated in splitting N_2O to N_2 and forming α-O [Eq. (1)], and which subsequently provided a decomposition of other N_2O molecules [Eq. (3)], obtaining a reduced form of Fe that could start a new redox cycle. Moreover, their findings revealed that Fe-FER exhibited significantly higher catalytic activity (due to the collaboration of two Fe sites) than Fe-*BEA and Fe-MFI despite comparable Fe(II) content in the cationic positions.

$$[Fe(III)\text{-}O^{-}]^{2+} + N_2O \rightarrow Fe(II) + N_2 + O_2 \quad (3)$$

The next experimental study of α-O formation and CH_4 oxidation was performed by Snyder et al.[101] and Bols et al.[86] on Fe-*BEA and Fe-SSZ-13 matrices, respectively (Fig. 10). Snyder et al. reported that the Fe active centers performing α-O from N_2O were a mononuclear, high-spin species within the square planar Fe(II) coordination environment. Further, DFT studies have suggested that the Fe(II) exhibited a square planar environment residing within a β-6MR with two Al atoms. The reactive intermediate α-O formed after N_2O splitting is a mononuclear, high-spin Fe(IV)=O species that contains an Fe(IV)=O center, adopting a square pyramidal geometry within the same β-6MR. Its exceptional reactivity derives from a constrained coordination geometry. The Fe(IV)=O bond has been predicted to be short (1.59 Å) and highly covalent, due to the absence of a trans-axial ligand.

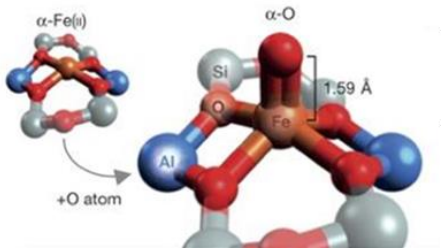

Fig. 10. Structure of the α-O in a *BEA zeolite. Copyright 2016 Nature Publishing Group.[101]

It should be noted that, in the literature, isolated mononuclear[73] and binuclear[72, 102] species have been proposed as Fe-active centers for N_2O activation. Thus, the nature of the Fe active site in N_2O processing is still a subject of debate. However, analysis of the Fe active centers in terms of its stabilization in zeolites with known Al atom organization, in particular zeolite topologies, could significantly extend our understanding of the rules that guide the formation of Fe active centers controlled by the distribution of Al atoms and zeolite topology.

The theoretical approach presented by Göltl et al.[77] included a discussion on the pathway of the mechanism of CH_4 oxidation by α-O (from N_2O splitting), stabilized in Fe-zeolites (Fig. 11). The structure of the α-O has an unusually strong Fe-O bond in $[Fe(IV)=O]^{2+}$, which results from a constrained coordination geometry enforced by the zeolite lattice. These α-O species are responsible for the removal of H from CH_4 to form hydroxy [Fe(III)-O-H] species and the $^{\bullet}CH_3$ radical. It was then suggested that the $^{\bullet}CH_3$ radical reacted with a distant α-O to form Fe(III)-O-CH_3, which can be extracted by hydrolysis or can "rebound" to form related Fe(II)-O(H)-CH_3, which subsequently desorbs as CH_3-OH formation (Fig. 11).[77, 85]

Kinetic isotope experiments have indicated that the initial cleavage of the C-H bond represents the rate-limiting step in this process. Furthermore, FTIR spectroscopy has evidenced the abstraction of the H atom from CH_4 by α-O. The employment of spectroscopic and theoretical

studies, in which the results support each other, has confirmed that the mechanism of CH_4 oxidation occurs by H abstraction by α-O from CH_4. The C-H cleavage is performed via a radical mechanism, with the Fe(IV)=O species elongating and gaining significant radical character in the transition state, becoming closer to the Fe(III)-$O^{\bullet-}$ species. Both Fe(III)-$O^{\bullet-}$ and $[Fe(IV)=O]^{2+}$ have been analyzed by Malykhin et al.[103] and their close electronic structures have been discussed by Rosa et al.[104] based on quantum chemical calculations. Thus, the notations Fe(III)-$O^{\bullet-}$ and $[Fe(IV)=O]^{2+}$ are commonly used to describe the α-O species.

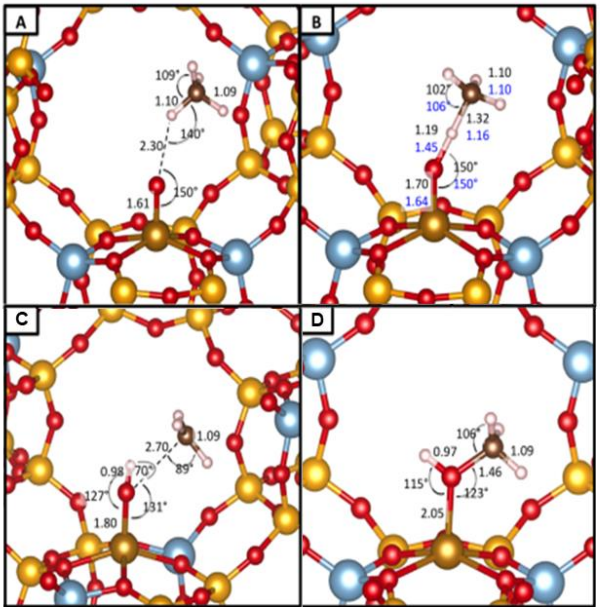

Fig 11. Structures and the most important intermediates during the interaction of α-O stabilized on Fe with CH_4: (A) CH_4 adsorption; (B) transition states (abstraction transition state); (C) rebound transition state along the reaction pathway of selective CH_4 oxidation to CH_3OH over the α-O site; and (D) CH_3OH formation on Fe centers. Si atoms shown in yellow, O atoms in red, Al atoms in blue-grey; Fe atoms in gold, H atoms in white, and C atoms in brown. The black numbers represent distances in Å and angles in degrees. The blue numbers in Panel (B) show the optimized RPA geometry. Adapted from ref. 77. Copyright 2016 American Chemical Society.[77]

Despite several attempts, to date, the production of CH_3OH over Fe-zeolites has occurred only in redox cycles that include the process of oxidation by N_2O, with the formation of α-O, and a reduction step, in which CH_4 is oxidized by α-O, resulting in the formation of oxygenates, such as CH_3OH, and a reduced form of Fe(II) that can perform the next redox cycle (N_2O/CH_4) [Eqs. 1 and 2]. However, the performance of CH_4 to CH_3OH oxidation over Fe-zeolites in a continuous catalytic regime has not yet been successfully developed.[105] Methanol has been observed with very low selectivity (~1%), while CO has been observed as the major product. Furthermore, the selective oxidation of CH_4 by the α-O on Fe-zeolites is terminated after the formation of methoxy groups strongly bound to the catalyst. Subsequently, extraction of the methoxy groups by a water or water-organic medium is necessary to desorb the oxidation products from the Fe-zeolite catalysts.

Materials containing Cu species represent another zeolite-based catalyst for N_2O dissociation and subsequent CH_4-to-CH_3OH oxidation.[106, 107] The reaction pathways for N_2O decomposition over Cu-zeolites have been reported elsewhere. The nature of the studied active Cu sites in zeolites is presented in Fig. 12.[108] It has been reported that isolated Cu(II) sites are inactive in N_2O dissociation over Cu-exchanged zeolites (e.g., MFI, MOR, FER, *BEA, FAU).[109] However, for the high-Cu-loaded MFI zeolite, isolated Cu(I) ions have been reported as active sites for N_2O decomposition. As indicated in the literature, the reaction rate is highly dependent on the distance between the Cu atoms at the sites where the N_2O dissociation occurs.

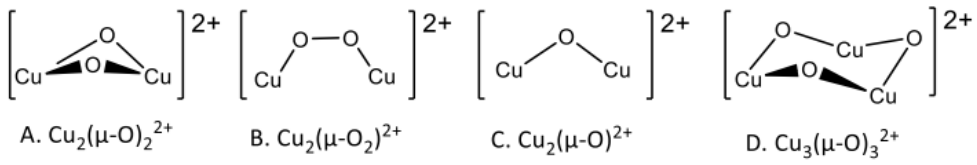

Fig. 12. Cu-oxo complexes have been proposed as the active sites for CH_4 activation in Cu-based zeolites.[108]

Catalytic processes based on Cu-based zeolite catalysts present several challenges. These include the need for high-low temperature cycles and the water or water–organic–medium extraction of methoxy groups strongly bound to the catalyst, the low yields in the catalytic regime, and the catalyst destruction after several catalytic cycles–the main disadvantage.[81, 87]

Besides these, Co-containing zeolites with MFI, MOR, *BEA, ZSM-11, and Zeolite Y (Faujasite type) topologies have exhibited excellent catalytic performance in N_2O decomposition.[110] The studies of catalytic N_2O decomposition have confirmed that Co-ZSM-5, Co-*BEA, and Co-ZSM-11 are the most active structures. By contrast, the Co introduced into Y-zeolites has exhibited very low catalytic activity in N_2O abatement reactions. Data presented in the literature has confirmed that the nature and amount of Co species in the zeolites are crucial factors in determining their catalytic activities. It is understood that Co species can be introduced into the zeolites as various extra-framework Co(II) ions at the exchange sites (α, β, and γ) in Co-oxo clusters in the zeolite channels or as Co_3O_4 nanoparticles outside the zeolite channels. Recent work by Hao et al.[110, 111]has shown that Co atoms present as oxide species contribute little to no N_2O decomposition, while isolated Co(II) ions are more active in this reaction. Isolated Co(II) ions have been identified as the active sites in MOR, ZSM-5, and ZSM-11 topologies.

Zhang et al.[110] observed that Co(II) ions sited in α and β cationic positions in ZSM-5, *BEA, and MOR zeolites were the active centers in N_2O decomposition. It has been shown that Co(II) in the α site in the ZSM-5 structure is the most active site in N_2O decomposition. However, Co(II) in the β site of Co-*BEA and Co-MOR zeolites is responsible for this reaction. The study revealed that the location of the individual Co ions embedded in various structures in ZSM-5, *BEA, and MOR zeolites controlled their chemical coordination, and the distances between the

Co(II) cations had a significant impact on their catalytic activity. Moreover, a special type of active center in Co-MOR was determined as being two distinctive, adjacent β-Co ions (Co-Co pairs) cooperating in N_2O splitting.

Recently, DFT studies[112] dealing with the use of Co-ZSM-5 as a catalyst in selective CH_4 oxidation by N_2O over Co-ZSM-5 have confirmed that a similar reaction mechanism has been observed for Fe(II), as proposed by Göltl et al. (see Fig. 11).[77] Additionally, those authors revealed that the preparation methods for Co-ZSM-5 have an impact on CH_3OH production. It was shown that Co-ZSM-5 prepared via incipient wetness impregnation contained a large fraction of surface Co oxide species that were responsible for an increase in the selectivity to CH_3OH. Conversely, Co-ZSM-5, prepared via ion exchange and containing a higher concentration of Co(II) species within the zeolite channel system, led to formaldehyde formation. Furthermore, the addition of dioxygen to the reaction mixture significantly improved the CH_3OH yield (up to 80%) in an N_2O/CH_4 reaction carried out over mesoporous Co-ZSM-5.[113]

In the literature, there is limited information about the behavior of Ni-containing zeolites in the decomposition of N_2O. Li and Armor[114] discovered a reduction in NO_x on Ni-modified ZSM-5, MOR, and FER zeolites with CH_4. The research performed by Mihaylov et al.[115] focused on the reactivity of Ni-ZSM-5 and Ni-Y in CH_4 oxidation by N_2O via monodentate nitrate formation. This study revealed the lower catalytic activity of monodentate nitrates in Ni-Y zeolites compared to Ni-ZSM-5. The authors proposed that the high coordinative unsaturation of the Ni(II) cations was crucial for CH_4 oxidation by N_2O. The selectivity and CH_3OH yield numbers of the studied Ni-zeolites have not been reported.

The Mn-containing zeolites have not been widely studied in terms of N_2O decomposition. Recently, the Weckhuysen group has reported the presence of the α-O site in Mn-ZSM-5 after N_2O interaction.[116] The formation of α-O was confirmed by the presence of an absorption band in the UV-Vis spectrum at 18500 cm^{-1}. However, no reactivity of α-O toward hydrocarbon oxidation has been reported in Mn-ZSM-5.

1.4.2 Activation of O_2 over TMI-containing zeolites

The most extensive studies of O_2 activation and subsequent CH_4 to CH_3OH oxidation have been performed over Cu-zeolite.[90, 89-97] It was assumed that the difference in activity may have been associated with the nature of active sites (Fig. 12) present in Cu-exchanged zeolites of various structural types.[117] The oxidation of CH_4 by O_2 over Cu-zeolites is performed in the cycle, and comprises two steps: i) the activation of Cu-zeolites in an O_2 flow; and ii) the reaction of O_2-activated Cu-zeolite with CH_4. The products of CH_4 oxidation over Cu-zeolites are attached to the zeolite surface, and to remove them, effluent is needed.[118]

Schoonheydt et al. showed that O_2-activated Cu-ZSM-5 and Cu-MOR zeolites can oxidize CH_4 to CH_3OH.[82, 119] They characterized the Cu active centers for CH_4 transformation as structurally similar to activating cores built from binuclear bis(μ-oxo)diCu species present in the methane monooxygenase (pMMO) enzyme. Later, the authors modified the structure of the proposed Cu activating core for CH_4 transformation to a mono(μ-oxo)dicopper(II) species. Other authors, based on theoretical and extended X-ray absorption fine structure (EXAFS) analyses, assigned the catalytic activity to trinuclear Cu-oxo cluster in Cu-ZSM-5.[92] The nature of the exposed bridging O ligands in trinuclear $[Cu_3(\mu\text{-}O)_3]^{2+}$ clusters was similar to that in the peroxo-bridged complex.

In Cu-MOR-based catalysts, Vanelderen et al.[80] identified two distinct $[Cu\text{-}O\text{-}Cu]^{2+}$ sites that were active in the oxidation of CH_4. They reported that MOR zeolite micropores provided a limited environment for the highly selective stabilization of trinuclear Cu-oxo clusters, $[Cu_3(\mu\text{-}O)_3]^{2+}$. They suggested that two different locations of Cu active sites were possible – one at the intersection of the side pocket with the 12-MR channel and another at the intersection of the side pocket with the 8-MR channel. However, Tomkins et al.[95] concluded, based on the in-situ EXAFS study, that, in Cu-MOR zeolites, the active sites were small clusters of Cu oxides that did not necessarily need to be di- or tri-Cu sites.

In the last decade, van Bokhoven et al. have published numerous studies on the selective oxidation of CH_4 by O_2 over Cu-containing zeolites.[94-96, 118] The majority of their investigations were conducted on Cu-MOR and Cu-ZSM-5 zeolites. They confirmed that the use of high-pressure CH_4 (< 40 bar) provided a higher production of CH_3OH over O_2-activated Cu-zeolites. In their study, they proposed that the optimal Cu-containing-zeolite-based catalysts could efficiently work under isothermal conditions and under high CH_4 pressure, and should fulfill the following requirements: (i) oxidation of CH_4 to a surface-bound stable CH_3OH precursor; (ii) be stable in H_2O at the given reaction temperature; (iii) active centers should regenerate under reaction conditions; and (iv) it should have a high concentration of Cu active centers.

The other class of catalysts represents the Co-exchanged zeolites. Beznis et al.,[98] have shown that Co-ZSM-5 zeolite can be used as a catalyst for CH_4 oxidation by O_2 at low temperature. Significantly, by employing distinct preparation techniques, it is possible to modulate the catalytic activity and selectivity of the catalytic system. Thus, in the Co-ZSM-5 prepared by ion exchange at RT, the majority of Co was found to be in ion exchange positions. This sample exhibited the highest selectivity toward formaldehyde formation. In contrast, impregnated Co-ZSM-5, which contain primarily cobalt oxide species (CoO and Co_3O_4), showed greater selectivity toward CH_3OH formation.

The presence of Ni in zeolites can activate O_2 and selectively oxidize CH_4. The Ni-ZSM-5 zeolite, activated in an O_2 flow, has already been used to selectively oxidize CH_4 to CH_3OH at 150°C.[99] However, the oxidation products required product extraction into the liquid from the catalyst. Several Ni-oxo species in ZSM-5 zeolites after O_2 treatment have been proposed by DFT calculations, including $[NiO]^{2+}$, $[Ni_2(\mu O)]^{2+}$, $[Ni_2(\mu O)_2]^{2+}$, and $[Ni_3(\mu O)_3]^{2+}$ (Fig. 13).[58, 120] The $[Ni_2(\mu O)]^{2+}$ center was suggested as the active site for CH_4 oxidation based on the low value of its activation energy (ranging between 15 and 20 kcal/mol abstraction of H atoms from CH_4).

The DFT calculations defined the structure of the $[Ni_2(\mu O)_2]^{2+}$active site in the ground state, as an open-shell singlet state, where the unpaired electrons from one Ni(III) center are antiferromagnetically coupled with those from another Ni(III) center.[120] The CH_4 molecule is adsorbed on the active site ($[Ni_2(\mu O)_2]^{2+}$) with an adsorption energy of -4.9 kcal/mol and is then activated via a radical-like transition state (TS1) where one of the H atoms is abstracted to form an OH moiety and a methyl radical with an activation energy (15.3 kcal/mol) similar to that calculated for $[Cu_2(\mu O)]^{2+}$ in the ZSM-5 zeolite matrix. As a spectroscopic benchmark for Ni-ZSM-5 activated in an O_2 flow, Shan et al. proposed the band at 22 800 cm^{-1} in the UV-Vis spectrum at 600°C.[99] The highest yield and best selectivity for the production of CH_3OH from CH_4 oxidation by Ni-ZSM-5 were achieved at a reaction temperature of 175°C.

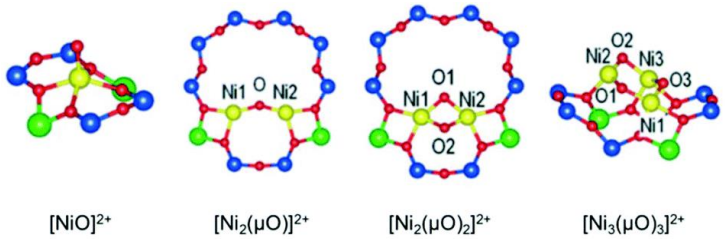

Fig. 13. Optimized ground state structures of $[NiO]^{2+}$, $[Ni_2(\mu O)]^{2+}$, $[Ni_2(\mu O)_2]^{2+}$, and $[Ni_3(\mu O)_3]^{2+}$ in an MFI zeolite. Copyright 2018 Royal Society of Chemistry.[120]

1.5 O_2 activation over binuclear cationic centers in FER zeolites

Recently, Tabor et al.[71] reported a new feature of Fe-zeolites that revealed the cooperation of two (binuclear) Fe(II) centers in O_2 activation. In addition, the stabilized oxygen species (α-O) formed after O_2 splitting selectively oxidized CH_4 to CH_3OH at RT. The binuclear Fe(II) species (Fig. 14A), in contrast to the isolated Fe(II) ions in zeolites, take part in the four-electron reactions process, resulting in O_2 splitting. The binuclear Fe(II) centers are constituted of two Fe(II) cations located in β cationic positions, with two Al atoms in the 6-MR of a FER zeolite, distant at about 7.5 Å. The previous study of Sklenak et al.[28] focused on analyzing the organization of Al atoms in FER (Si/Al 8.6) zeolites, demonstrating that the concentration of Al pairs in the β site was high (50% of the total Al atoms), indicating that approximately 94% of the 6-MRs of the β site could

accommodate bare divalent cations. Therefore, at least 88% of the β sites are capable of forming binuclear Fe(II) structures. Conversely, the investigation demonstrated that the concentration of Al pairs in the α site is relatively low (10% of all the Al atoms), indicating that only a minimal proportion of the α sites can form binuclear Fe(II) structures.

Periodic DFT calculations and spectroscopic studies have confirmed the ability of the binuclear Fe(II) sites in the FER matrix (Fig. 14) to split O_2.[71] The binuclear Fe(II) structures cleaved the O=O double bond and formed a pair of α-O atoms on the two Fe(II) cations (Fig. 14C). Furthermore, the splitting of O_2 over the binuclear Fe(II) centers in the FER zeolite and the formation of α-O has been confirmed by in-situ FTIR and Mössbauer analysis at RT. Both methods provided a spectroscopic fingerprint of the α-O, which is clearly visible in the FTIR spectra as a newly formed band at 890 cm^{-1} after O_2 treatment and in the Mössbauer study as parameters – isomer shift (IS) = 0.29 and quadrupole splitting (QS) = 0.78 mm/s. Additionally, the FTIR spectroscopy confirmed the stability of the previously formed α-O up to 200°C.

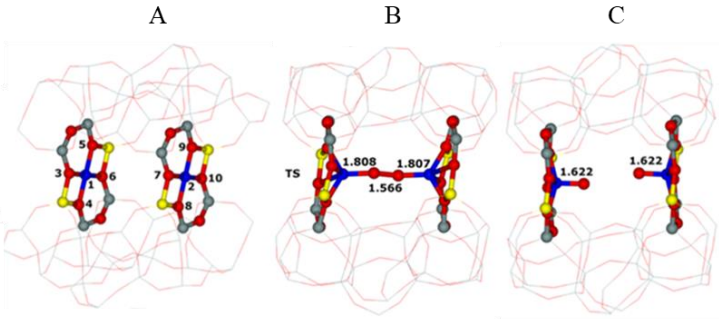

Fig. 14. Model showing O_2 splitting over Fe(II) binuclear centers in FER zeolite after molecular dynamics simulations: (A) Fe(II) binuclear centers; (B) [Fe-O-O-Fe] transition state; and (C) [Fe=O O=Fe] product. The distances are in Å. Si atoms shown in gray, O atoms in red, Al atoms in yellow, and Fe atoms in blue.

In order to check the oxidation properties of α-O stabilized on Fe(II) after O_2 splitting, CH_4 was used as a probe molecule. The mass spectrometry results confirmed the formation of CH_3OH with a significantly higher yield of CH_3OH (75 $\mu mol/g_{cat}$ per cycle) in the gas flow in comparison to the previously reported data over TMI-zeolites.[89-99] It should be noted that no water or any organic solvent was needed here to extract the oxidation products from the zeolite surface.

In general, Fe-FER-containing binuclear Fe(II) sites in FER zeolites performed CH_4 oxidation by molecular O_2, similarly to the previously studied Cu-oxo species in zeolites. Furthermore, Tabor et al.[71] showed that employing Fe-FER catalysts could have a large practical impact as a catalyst for CH_4 utilization due to the reversible Fe(II)/Fe(IV) cycle, the stable active Fe centers under the reaction conditions, and the release of oxidation products to the gas phase without the necessity of water or water-organic medium extraction.

In conclusion, there is still much to be achieved in CH_4-activation research, but zeolites that incorporate TMIs are expected to play a significant role in addressing this challenging issue.

II Aims of the work

This dissertation thesis discusses the determination of the possibility of the formation of distant binuclear structures in zeolite matrices and their reactivity toward small molecules activation.

The following questions were posed:

1. How to analyze the O_2 activation and following CH_4 oxidation over Fe-FER using spectroscopic techniques?
2. Do TMI ions other than Fe(II) ions form binuclear centers in FER for O_2/N_2O cleavage?
3. Could zeolites of topologies other than FER stabilize Fe(II) binuclear active centers for O_2 splitting?
4. Does the α-O originating from N_2O and O_2 splitting stabilized on the binuclear centers of Co(II), Ni(II), Fe(II) and Mn(II) in FER zeolites react with CH_4 at low temperatures?
5. How is the cation speciation in FER and MOR zeolites reflected in the catalytic performance of Fe-zeolites in the CR_{N2O} and SCR_{N2O} of N_2O by CH_4?

To address these queries, the subsequent steps were realized:

1. Developing a methodology based on the spectroscopic methods for analyzing α-O formation over Fe-FER.
2. Potential to form binuclear centers of Co(II), Ni(II), and Mn(II) in FER, their speciation, and the effect of metal loading using FTIR spectroscopy.
3. Study of the possibility of forming binuclear centers in MOR, *BEA, and LTA zeolites, including determining Al distribution in MOR zeolite.
4. Monitoring of the process of N_2O/O_2 splitting toward α-O formation and its stabilization on Co(II), Ni(II), Fe(II), or Mn(II) in FER for the following CH_4 oxidation.
5. Realization of catalytic tests over Fe-FER and Fe-MOR under conditions of CR_{N2O} and SCR_{N2O} of N_2O reduction by CH_4.

The researcher results of this Ph.D. thesis were reported in the six scientific publications, available as **Appendices 7.1 − 7.6** (***Publication I − VI***):

1. **Mariia Lemishka (as a first and corresponding author)**, Jiri Dedecek, Kinga Mlekodaj, Zdenek Sobalik, Stepan Sklenak, Edyta Tabor. Speciation and siting of divalent transition metal ions in silicon-rich zeolites. An FTIR study. *Pure and Applied Chemistry*. **2019**, 91(11), 1721–173.

2. Edyta Tabor, **Mariia Lemishka**, Zdenek Sobalik, Kinga Mlekodaj, Prokopis C. Andrikopoulous, Jiri Dedecek, Stepan Sklenak. Low-temperature selective oxidation of methane over distant binuclear cationic centers in zeolites. *Communications Chemistry*. **2019**, 2, 71.

3. Kinga Mlekodaj, **Mariia Lemishka**, Stepan Sklenak, Jiri Dedecek, Edyta Tabor. Dioxygen splitting at room temperature over distant binuclear transition metal centers in zeolites for direct oxidation of methane to methanol. *Chemical Communication.* **2021**, 57, 3472–3475.

4. Edyta Tabor, **Mariia Lemishka**, Joanna E. Olszowka, Kinga Mlekodaj, Jiri Dedecek, Prokopis C. Andrikopoulos, and Stepan Sklenak. Splitting Dioxygen over Distant Binuclear Fe Sites in Zeolites. Effect of the Local Arrangement and Framework Topology. *ACS Catalysis*. **2021**, 11, 4, 2340–2355.

5. Kinga Mlekodaj, **Mariia Lemishka (as a first author)**, Agnieszka Kornas, Dominik K. Wierzbicki, Joanna E. Olszowka, Hana Jirglová, Jiri Dedecek, and Edyta Tabor. Evolution of Active Oxygen Species Originating from O_2 Cleavage over Fe-FER for Application in Methane Oxidation. *ACS Catalysis*. **2023**, 13, 3345–3355.

6. Maria Cristina Campa, Daniela Pietrogiacomi, Carlotta Catracchia, Simone Morpurgo, Joanna Olszowka, Kinga Mlekodaj, **Mariia Lemishka**, Jiri Dedecek, Agnieszka Kornas, Edyta Tabor. Fe-MOR, and Fe-FER as catalysts for abatement of N_2O with CH_4: in situ UV-vis DRS and operando FTIR study. *Applied Catalysis B: Environmental*. **2024**, 342, 123360.

III Results and discussion

Spectroscopic studies of α-O formation by the dissociation of O_2 and N_2O over metallozeolites were performed, and the reactivity of α-O toward CH_4 oxidation was investigated. As catalysts for O_2 and N_2O activation, the following zeolite topologies were used: FER containing Co(II), Ni(II), Mn(II), Fe(II) cations, and Fe(II)-MOR. The catalytic activity of α-O was tested in a CH_4 to methanol transformation. The experimental data obtained from O_2 and N_2O activation over FER (Co(II), Ni(II), Mn(II), Fe(II)), and Fe(II)-MOR were supported by a theoretical study, including computational modeling, electronic structure calculations, molecular dynamics, and geometry optimizations. The theoretical study was also extended to Fe(II)-*BEA and Fe(II)-LTA zeolites.

As discussed above, TMI zeolite-based catalysts were prepared using commercially available FER and MOR zeolites (Tosoh Corporation, Japan) and Si/Al 8.6 and 9.2, respectively. To determine the framework features of the zeolites and their redox behaviors, a combination of spectroscopic and structural methods was used. The chemical compositions of the parent materials (FER and MOR) and the TMI-containing FER and Fe-MOR zeolites were determined using X-ray fluorescence (XRF). The XRF and low-temperature nitrogen (N_2) adsorption results confirmed that the studied material exhibited FER and MOR topologies and the presence of micropores. The magic-angle spinning nuclear magnetic resonance (MAS-NMR) method was applied to control the location of Al atoms in the framework and as a supporting method for describing the organization of the Al atoms in the parent FER and MOR zeolites. The organization of Al atoms in the MOR zeolite was established using a well-proven method based on Co-ligation in zeolites evaluated by UV-Vis spectroscopy. FTIR spectroscopy was employed to analyze the progress of the cation exchange of the MOR and FER by TMI, referring to the spectra in the region of the OH and T–O–T vibrations. The concentration of divalent cations in the studied metallozeolites was determined by FTIR spectroscopy using nitric oxide (NO) and carbon monoxide (CO) as the probe molecules. To analyze the redox cycle over the metal centers in the zeolites, occurring during O_2 or N_2O oxidation and subsequent CH_4 reduction, the following methods were employed under in-situ conditions: FTIR, UV-Vis, Mössbauer, and X-ray absorption near edge structure (XANES) spectroscopy. The reaction products of CH_4 oxidation by O_2 or N_2O were identified using in-situ FTIR analysis in the gas phase and mass spectrometry techniques. Gas chromatography was applied to analyze the catalytic reduction products of N_2O with CH_4 in the absence or presence of O_2 and H_2O over Fe-MOR and Fe-FER catalysts.

All of the steps involved the preparation of M(II)-FERs and Fe(II)-MORs, optimization of the preparation conditions, and the characterization of the nature of the formed M(II) active sites,

including the coordination and siting of the cation in the zeolite matrix, as well as its accessibility. These were of crucial importance for understanding, predicting, and finally tailoring their properties to the requirements of the catalytic reactions. The spectroscopic studies of α-O formation from N_2O and molecular O_2 dissociation, its reactivity with CH_4 toward CH_3OH production, and the catalytic tests under catalytic reduction of N_2O with CH_4 in the absence or presence of O_2 (CR_{N2O} and SCR_{N2O}) conditions are discussed separately in the following sections (3.1 – 3.5), with each section serving as the answer to a question posed as an aim of the study.

3.1 How to analyze the O_2 activation and following CH_4 oxidation over Fe-FER using spectroscopic techniques? Developing a methodology based on the spectroscopic methods for analyzing α-O formation over Fe-FER

The study of the formation, stabilization, and evolution of α-O from O_2 and N_2O dissociation over metallozeolites, as presented in this thesis, was possible thanks to the careful choice of a combination of several characterization techniques. In order to analyze the activation of molecular O_2 over TMI-containing zeolites, we developed a methodology based on several techniques (gathered together in Table 2), the combined results giving a holistic picture of the behavior of both the nature of the active centers and their structural changes during O_2 activation. The best method for the detection of the binuclear center's ability for splitting O_2 or N_2O to result in α-O formation is the reaction test with CH_4. The main feature of α-O is its high oxidation potential to transform CH_4 into CH_3OH. It should be mentioned that most of the characterization methods employed would have been insufficient used alone to obtain a complete picture of the redox behavior of the TMI centers in the zeolites. However, their combination, along with theoretical predictions, produced credible results for the characterization of the nature of the active centers in zeolite-based catalysts.

Previously, the formation of α-O from O_2 over Fe binuclear centers in FER had been confirmed at RT under ex-situ conditions.[71] The studied Fe-FER had to be activated after the redox cycle (O_2/CH_4) in order to perform the splitting of the O_2 and the CH_4 oxidation. Thus, to extend the application of Fe-FER as a catalyst for CH_4 oxidation by O_2, we focused on performing the study at an elevated temperature under isothermal conditions so as to exclude the catalyst activation step after the redox cycle (O_2/CH_4). To analyze the oxidation properties of the α-O formed by O_2 splitting, we used a combination of in-situ XANES, Mössbauer, FTIR spectroscopy, and mass spectrometry to monitor its interaction with the CH_4. Most of the measurements and examinations of the α-O formation were conducted at 220°C, and this temperature is based on previous results concerning the thermal stability and optimal conditions for O_2 splitting over Fe-FER.[71]

Table 2. Characteristics of α-O obtained using various spectroscopic techniques.

Technique	Type of information	Advantages	Limitations
FTIR spectroscopy	Content and nature (valency and symmetry) of TMI centers in zeolites, monitoring of the behavior of TMI under redox conditions	Simple, rapid, easily available, high selectivity, good sensitivity, fast detection, and convenient operation, working under in-situ and ex-situ conditions	Surface technique
Mössbauer spectroscopy	Information on the oxidation state and symmetry exclusively in the Fe centers in the zeolites, analysis of the formation and reactivity of α-O	Easily available (for our group), working under in-situ and ex-situ conditions, high sensitivity, exclusively for Fe centers	Only for Fe, time-consuming measurement and data evaluation (spectra have to be fitted using dedicated software designed exclusively for Mössbauer spectroscopy)
XANES spectroscopy	Monitoring of changes in the TMI oxidation state, symmetry, and speciation, monitoring of the redox cycle (O_2/N_2O and CH_4)	In-situ detection, rapid, high sensitivity	High cost, not available locally, preparation of proposal needed for measurement, complex and sophisticated equipment, time-demanding and labor-intensive
UV-Vis spectroscopy	Determination of Al distribution in zeolites, reactivity of TMI embedded in zeolites toward N_2O or O_2 dissociation and CH_4 oxidation, stability of the M(III) oxo species under CH_4 treatment	Easily available and convenient operation, in-situ detection	Complex analysis of the results, time-consuming process of sample preparation before measurement
FTIR analysis in the gas phase	Analysis of the oxidation products of CH_4 oxidation by N_2O or O_2	High sensitivity, fast detection, and analysis under in-situ conditions	Difficulties with the spectral analysis due to the overlapping of the bands of the reactants and products
Mass spectrometry	Detection of products of CH_4 oxidation by O_2 or N_2O	Easily available, high sensitivity, and simple product detection	Time-consuming analysis of the products, including the calibration process
DFT calculations	Prediction of possible zeolite topologies, with TMIs performing O_2 splitting and α-O formation, determination of the reaction barriers of the N_2O or O_2 dissociation, and the following CH_4 treatment over M(II)-zeolites	Good support for all experimental methods	Time-consuming, computationally intensive

Below, the choice of the particular methods used for determining the redox properties of Fe(II) active centers in FER are discussed. The Fe-FER was selected as the model catalytic system due to its previously well-documented activity in splitting O_2 and interacting with CH_4.

Mössbauer spectroscopy was used to analyze the oxidation state and the coordination of the Fe species in the ^{57}Fe-FER sample with Fe/Al 0.04, which was prepared intentionally for this study (see **Publication V**). The Mössbauer spectrum of the evacuated ^{57}Fe-FER (Fig. 15A) was deconvoluted into three components (D1–D3), the IS value confirming the exclusive presence of divalent Fe species.[71, 86] Based on data from the literature, the Components D1 (IS = 0.98 and QS = 0.78 mm/s) and D2 (IS = 0.98 and QS = 0.46 mm/s) were both attributed to Fe(II) coordinated to four O atoms in the FER framework in a planar β cationic position.[71, 121] Component D3, with an IS value of 1.03 mm/s, was characteristic of Fe(II), but the higher value of QS (2.07 mm/s) indicated a lower symmetry around the Fe sites. This observation allowed us to assign D3 to Fe(II) in the α cationic position, in which the Fe species were situated above the zeolite ring.[121, 122]

The Mössbauer spectrum of ^{57}Fe-FER, recorded after O_2 interaction, was deconvoluted into three components – D2, D4, and D5 (Fig. 15B). Analysis of the values of the Mössbauer parameters (see **Publication V**) revealed that 41% of the Fe assigned to components D2 and D4 had been not oxidized by O_2. Moreover, in the Mössbauer spectrum of the O_2-oxidized Fe-FER, a new component, D5 (IS = 0.29 and QS = 0.78 mm/s), was formed. The hyperfine parameters of component D5 were similar to those characteristic for the α-O species stabilized on Fe $[Fe(IV)=O]^{2+}$ after interaction with N_2O. This result confirmed the splitting of O_2 over the Fe(II) centers located in the β cationic position and the stabilization of the active O_2 form (α-O).

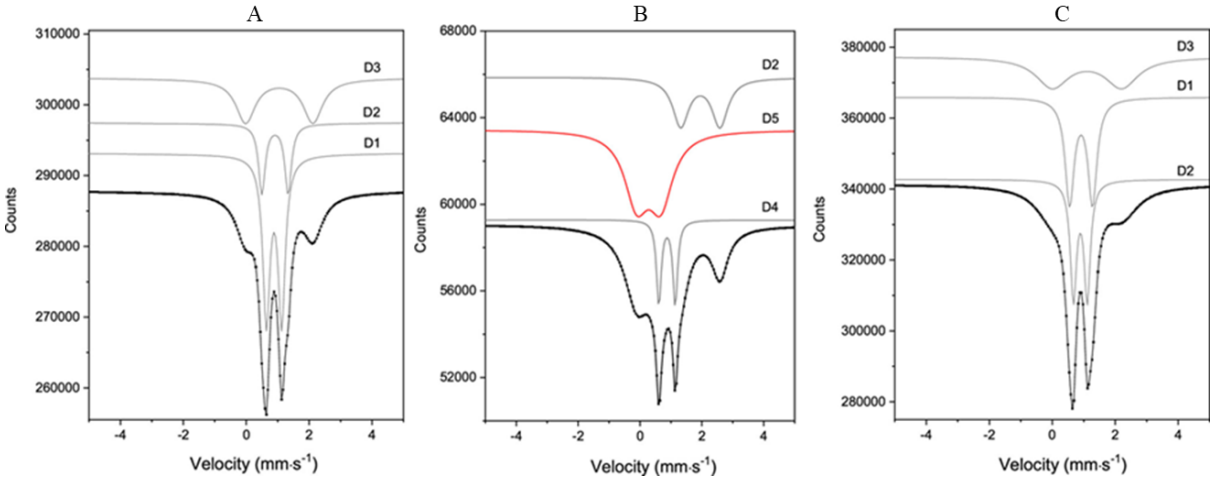

Fig. 15. Mössbauer spectra of ^{57}Fe-FER (recorded under vacuum), together with their fits, collected after the following treatments: (A) 3h evacuation at 450°C under dynamic vacuum; (B) interaction with O_2 for 40 min at 220°C; and (C) interaction with CH_4 for 30 min at 220°C.

To check the oxidation properties of $[Fe(IV)=O]^{2+}$, the Mössbauer spectrum of Fe-FER was recorded after O_2 oxidation and subsequent interaction with CH_4. The spectrum, together with

its deconvolution into three components (D1–D3), is depicted in Fig. 15C. The received Mössbauer hyperfine parameters (see **Publication V**) are close to those observed for evacuated ^{57}Fe-FER, and reveal the presence of exclusively Fe(II) species. Component D5, describing the α-O formed after oxidation, was absent. This observation clearly indicates that the previously formed (α-O) $[Fe(IV)=O]^{2+}$ species was again reduced after CH_4 treatment to Fe(II).[71]

Similarly to the Mössbauer study, an analysis by time-resolved in-situ XANES spectroscopy under the O_2/CH_4 treatment of Fe-FER was performed. Fig. 16 depicts the XANES spectra of Fe-FER (Fe/Al 0.04) collected after activation of the sample in He stream at 450°C (in beige), after O_2 oxidation (in green), and following the interaction with CH_4 (in pink). The XANES spectrum of FeO (Fig. 16, in red) was used to confirm the presence of Fe(II), and the spectra of ferric oxide (Fe_2O_3) (Fig. 16 in black) and nitric oxide (NO)/O_2 (Fig. 16 in blue) were used as a reference for the Fe(III). Importantly, the XANES spectrum recorded after evacuation of the Fe-FER (Fig. 16) indicated that a major fraction of the Fe species in the Fe-FER was present as Fe(II), as reflected by a shift in the absorption edge toward lower energies (see **Publication V**).

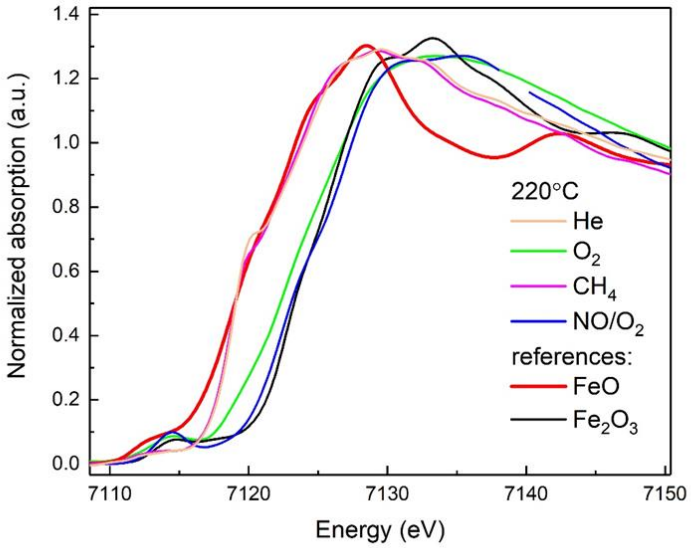

Fig. 16. XANES spectra of Fe-FER recorded under He activation at 450°C (in beige), O_2 at 220°C (in green), and CH_4 at 220°C (in pink) treatments. For reference, FeO (in red), Fe_2O_3 (in black), and NO/O_2 (in blue).

The shoulder arising at the absorption edge at ca. 7120 eV, forming due to a 1s→4p transition, confirmed the square planar symmetry of the Fe(II),[123] typical for Fe(II) in β cationic positions. The interaction of Fe-FER with O_2 (Fig. 16 in green) resulted in the oxidation of the Fe(II) species present in the activated Fe-FER to Fe(III). Moreover, the absorption edge after O_2 treatment was shifted to higher energies, and a pre-edge feature occurred at approximately 7114.4 eV increased this, indicating the formation of a five-fold coordination of the Fe ion.

The XANES spectrum of previously O_2-oxidized Fe-FER treated by CH_4 is presented in Fig. 16 (in pink). The interaction of the CH_4 with the O_2-oxidized sample led to the reduction of

all the Fe(III) to Fe(II), as can be seen in Fig. 16 by the shifting of the spectrum to the position typical for Fe(II) as observed in the activated sample (Fig. 16 in beige). The XANES spectra recorded under NO/O_2 showed a deeper oxidation of the Fe species compared to the O_2, which suggests that some Fe species were resistant to oxidation by O_2, and a stronger oxidizing agent may be required.

In-situ FTIR spectroscopy was used as the third method in developing the complex methodology for monitoring α-O over Fe-FER. To illustrate this approach, the in-situ FTIR spectra (see Fig. 17) of the Fe-FER activated at 450°C (in red) are presented after interaction with O_2 (in blue) and CH_4 (in green). The spectra were analyzed in the region of the OH (Fig. 17A) and T–O–T (Fig. 17B) vibrations.[27, 121] The positions of the silanol groups (3742 cm^{-1}) and Brønsted acid sites (Si-OH-Al) (3588 cm^{-1}) observed in the evacuated samples did not change in either the O_2 or CH_4 treatment.[124] This indicates that the OH groups of the Fe-FER did not participate in the O_2/CH_4 redox cycle. The presence of a band at 907 cm^{-1} (Fig. 17B) confirmed the location of Fe(II) in the β cationic position of the FER structure.[125] Interaction with O_2 led to the formation of a new band at 897 cm^{-1}. Based on data from the literature, this was identified as a spectral fingerprint of α-O $[Fe(IV)=O]^{2+}$.[71, 73, 117]

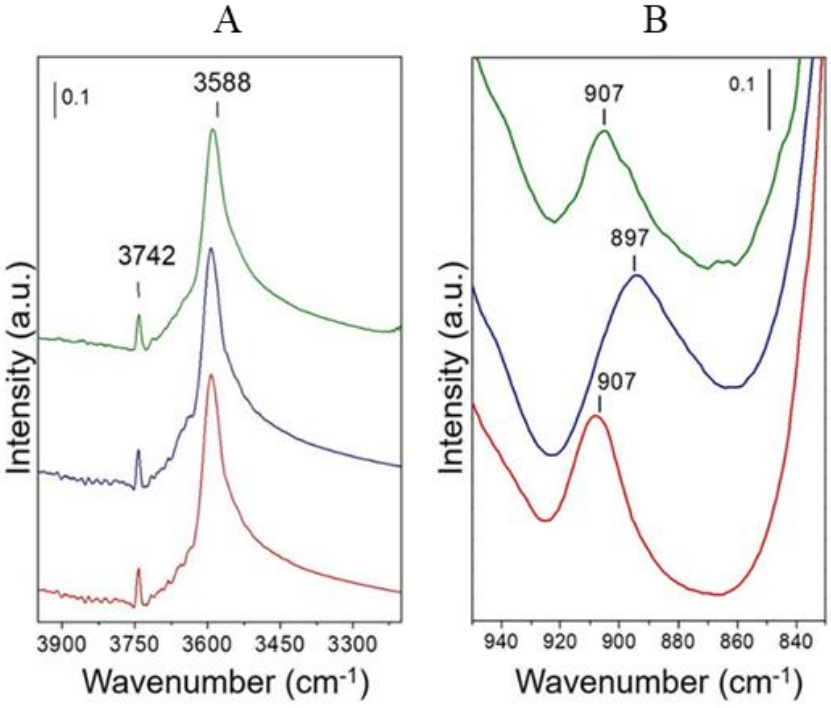

Fig. 17. FTIR spectra of Fe-FER in the range of (A) OH and (B) T–O–T. Activation over 3 h at 450°C in He (in red), 1 h of O_2 interaction at 220°C (in blue), and CH_4 treatment at 220°C (in green).

To investigate the oxidation properties of $[Fe(IV)=O]^{2+}$, the FTIR spectrum was recorded after CH_4 treatment at 220°C (Fig. 17B). Following the interaction of CH_4 with the O_2-pre-oxidized Fe-FER, the intensity of the band at 897 cm^{-1} decreased significantly, and the band at 907 cm^{-1}, which is characteristic of Fe(II) in β sites, reappeared. These results show, for the first

time, that cooperating Fe(II) species are also effective in α-O formation from O_2 at elevated temperatures. Moreover, this indicates that the possible reaction products do not interact with the acid centers of the zeolite. [67, 101, 126]

The results presented above confirm the formation of the α-O over Fe-FER, but they do not describe the kinetics of its formation, which is a crucial point in catalytic studies. For this purpose, FTIR spectroscopy was applied to monitor the behavior of the Fe sites interacting with O_2 under in-situ conditions at 220°C. Analysis of the FTIR spectra (Fig. 18) in the region of the T–O–T vibrations showed that, within an interaction time of 0 – 60 min, the intensity of the band at 907 cm^{-1}, assigned to Fe(II) in the β cationic position, decreased with the increasing intensity of the band characteristic for the α-O at 897 cm^{-1} (Fig. 18A). This correlation between the decreasing concentration of β sites (band at 907 cm^{-1}), estimated from the FTIR spectra, and the formation of the band at 897 cm^{-1} is depicted in Fig. 18B. It was confirmed by an in-situ FTIR study that, to oxidize all the Fe(II) in the β sites and to reach the highest intensity of the band typical for α-O, a time of 60 min was required.

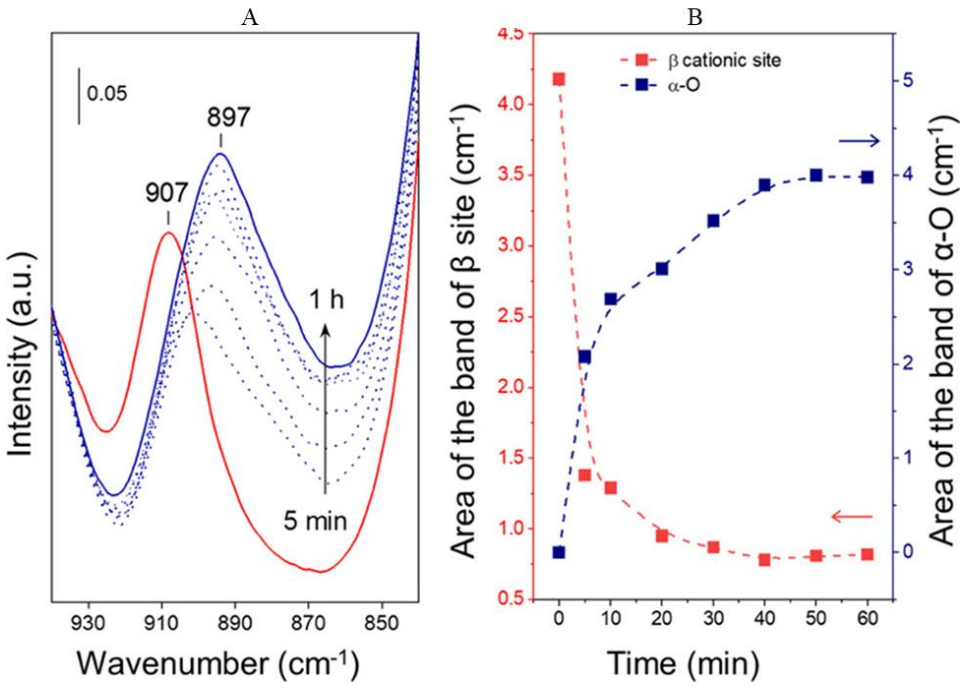

Fig. 18. (A) FTIR spectra of the kinetics of α-O formation over Fe-FER for 1h at 220°C; and (B) temperature dependence of the evolution of the bands characteristic for α-O and Fe(II) in β sites.

In the next step, the thermal stability of the α-O over Fe-FER was investigated using FTIR spectroscopy under in-situ conditions. The α-O previously formed at 220°C after the interaction of Fe-FER with O_2 was monitored every 20°C up to 380°C (Fig. 19). It can be seen that the intensity of the band at 897 cm^{-1}, assigned to the α-O, remained the same up to 260°C, above which, the band intensity decreased in a stepwise manner. Simultaneously, a stepwise reconstruction of the band typical for Fe(II) can be seen (shift in the bands from 897 to 907 cm^{-1},

marked by the gray arrow in Fig. 19A). These findings indicate that the α-O was stable up to 260°C, but decomposed above this temperature, presumably via the recombination of two α-O.[71]

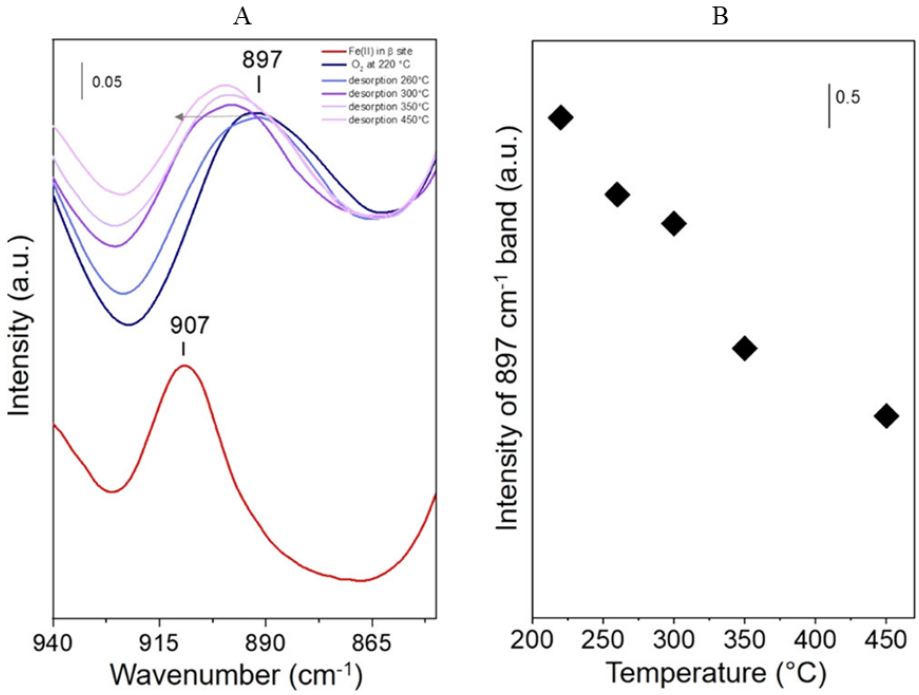

Fig. 19. FTIR spectra of the thermal stability of α-O in the temperature range 220 – 380°C over Fe-FER (A) and temperature dependence of the intensity of the band characterizing α-O (B). The solid violet line indicates a temperature of 280°C.

To determine the oxidation products, an FTIR analysis of the gaseous products of the interaction of the α-O stabilized on the Fe-FER with CH_4 at 220°C (Fig. 20) was performed. The presence of bands with low intensity at 2926 and 2830 cm^{-1}, characteristic of the vibrations of methoxy species, indicated methanol formation.[70] The bands at 2360 and 2338 cm^{-1} corresponded to carbon dioxide (CO_2) stretching vibrations.[127] The appearance of CO_2 among the reaction products, together with the presence of a band in the region of the OH vibrations at 3214 cm^{-1}, typical for OH vibrations in H_2O, suggest the overoxidation of CH_4 and/or the products initially formed during CH_4 oxidation. Similar conclusions have been reported by Sushkevich et al., based on an FTIR product analysis, in which both CO and CO_2 were found after a CH_4 oxidation reaction over Cu-MOR.[127]

Mass spectrometry was used as an additional method to analyze the products of CH_4 oxidation by the α-O previously formed on the Fe(II) species in the FER by O_2 splitting at 220°C (see **Publication V**). The Fe-FER sample was activated at 450°C, cooled down to 220°C, and at this temperature, oxidized by O_2 and subsequently interacted with CH_4. Three consecutive cycles of the interaction of the Fe-FER with O_2 and CH_4 were performed. The mass spectrum exhibited signals with m/z = 31 (methanol) and m/z = 44 (CO_2) (Fig. 21).

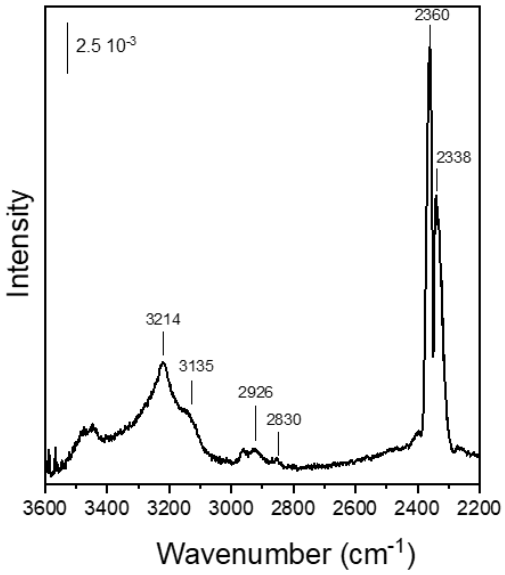

Fig. 20. FTIR spectra of the gas phase acquired during the reaction of the Fe-FER with O_2 and CH_4.

The CH_3OH productivity obtained at 220°C varied over the three subsequent redox cycles between 0.20 and 0.38 μmol/g_{cat}. The obtained results reveal that the oxidation products of CH_4 formed by O_2 were detected in the gas stream, which proves their spontaneous release at 220°C from the active Fe sites and from the zeolite channel system to the gas phase without the need for effluent usage. The FTIR spectroscopy and mass spectrometry results confirmed the formation of the same products of CH_4 oxidation by the α-O stabilized on the Fe-FER.

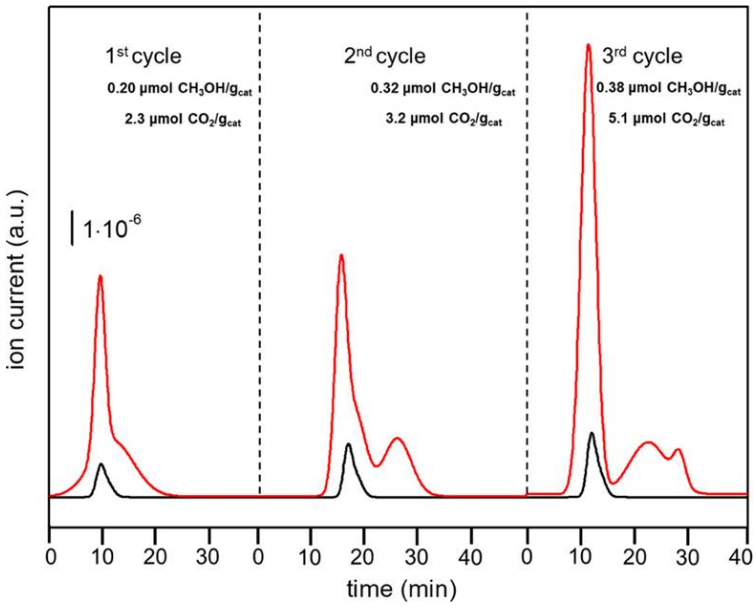

Fig. 21. Time dependence of signal intensity (ion currents) reflecting the products of CH_4 oxidation by the α-O formed on the Fe-FER at 220°C, monitored by mass spectrometry over three consecutive redox cycles. The signals with m/z = 31 and 44 relate to methanol (in black) and CO_2 (in red), respectively. The values in the upper right corner correspond to the productivity of methanol and CO_2.

The spectroscopic results from the in-situ Mössbauer, XANES, and FTIR spectroscopy confirmed that the characterization methodology developed for monitoring the O_2 interaction over the Fe-FER can be successfully used for analysis of the formation, kinetics, and oxidation properties of α-O. By including the results from the mass spectrometry and FTIR analysis in the gas phase, it was also possible to detect the oxidation products. The results indicate that two Fe(II) centers with planar geometry embedded in the FER worked together in the redox cycle. When the Fe-FER interacts with O_2, $[Fe(IV)=O]^{2+}$ is produced, which is then reduced by CH_4 to the Fe(II) centers. It was found that the α-O formed under throughflow conditions was stable up to 260°C and exhibited oxidation properties in CH_4 to methanol oxidation. Methanol production was recorded in the gas phase through the use of FTIR and mass spectrometry. Combining the methodologies of in-situ Mössbauer, XANES, and FTIR spectroscopy, mass spectrometry, and FTIR analysis in the gas phase can be used as a tool for the determination of potential TMI-containing zeolites for O_2 activation and CH_4 oxidation.

3.2 Do TMI ions other than Fe(II) ions form binuclear centers in FER for O_2/N_2O cleavage? Potential to form binuclear centers of Co(II), Ni(II), and Mn(II) in FER, their speciation, and the effect of metal loading using FTIR spectroscopy

In this section, special attention is given to the analysis of the siting and location of bare divalent cations of Co(II), Ni(II), and Mn(II) in the extra-framework cationic sites in the FER matrix (Si/Al 8.6, M/Al 0.04 – 0.33) (see **Publication I**). The introduction of cations of Co, Ni, or Mn to the FER was performed by ion exchange or impregnation methods. The ion-exchange method was used to prepare a whole concentration range of Co-FER (Co/Al 0.04 – 0.33) zeolites and low-loaded samples with Ni and Mn/Al (0.04 – 0.16 M/Al). For the Ni- and Mn-FER samples (0.16 – 0.38 M/Al), it was necessary to use the impregnation method. These two preparation methods were used because of difficulties associated with the preparation of high-loaded samples in the ion exchange procedure. The study required samples with high TMI loading, as this guarantees the formation of high-fraction catalytically active binuclear centers in the zeolite framework. The sizes of the metal atom radii, types of precursors, preparation conditions, pH of the solution, the concentration of TMIs, temperature, and contact time between the zeolite and the precursor were all considered to be the most probable factors influencing the introduction of cations into the FER structure.

Analysis of the FTIR spectra of the Co-, Ni-, and Mn-FER[27] with M/Al 0.16 in the region of the T–O–T vibrations (Fig. 22) revealed the presence of M(II) bare cations in α, β, and γ cationic positions.[27] In all the studied samples, the majority (70% – 75%) of M(II) cations were located in

β positions, which is regarded as a precondition for the formation of binuclear centers. The rest of the M(II) cations were in the α (15% – 20%) and γ (10%) sites (see **Publication I**).

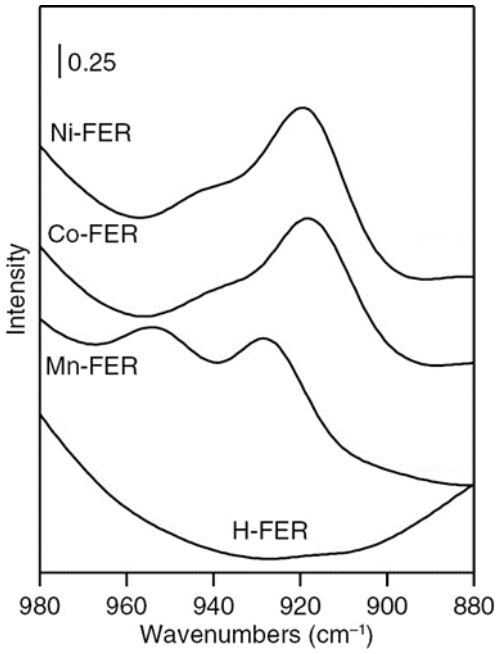

Fig. 22. FTIR spectra of the perturbed T–O–T antisymmetric mode of dehydrated H-, Mn-, Co-, and Ni-FER.

In order to analyze the M(II) siting in the zeolite, FTIR and XRF data were used, with a quantitative evaluation based on the extinction coefficients for Co, Ni, and Mn in the FER. The liner function of the integrated area of M(II) bands in the FTIR spectra in the T–O–T region as a dependence of M/Al provided the values of the extinction coefficient for particular cations (Table 3). These extinction coefficients for the individual cations (Co, Ni, and Mn) embedded in the FER structure were used to evaluate the fraction of M(II) species in cationic positions in the studied zeolites.[128] As previously shown, due to the specific Al distribution in the FER sample, the upper limit for the accommodation of any bare divalent cation was about M/Al 0.33.[26] By employing the FTIR and XRF data, and the values of the established extinction coefficients for Co, Ni, and Mn in the FER, it was found that, in all the M(II)-FERs with M/Al < 0.16, the bare cations were highly prevalent.

Table 3. Wavenumbers of the T–O–T vibrations reflecting cations in the α, β, and γ sites for Mn-, Co-, and Ni-FERs. The extinction coefficient of Mn-, Co-, and Ni-FERs.

	α	**β**	**γ**	**Extinction coefficient**
		(cm^{-1})		**(cm µmol^{-1})**
Mn	953	928	902	30.4
Co	942	918	885	38.5
Ni	940	918	879	35.8

Contrastingly, in more concentrated samples (M-FERs with M/Al > 0.16 up to a limit of M/Al 0.33), the occupation of cationic positions by bare cations depended on the specific cation and was approximately as follows: Mn(II) – 80%, Ni(II) – 55%, and Co(II) – 98%. As also shown, the share of occupation of the α and β positions strongly depended on the individual cations.

In general, all the prepared Co-, Ni-, and Mn-FERs were close to the maximum loading of bare divalent cations (M/Al 0.33). Analysis of the obtained data indicated that, for the M-FER samples with M/Al > 0.22, at least 50% of the M(II) cations were located in β cationic positions that could form the binuclear centers that can perform O_2/N_2O activation. The results showed that the TMIs (Co, Ni, and Mn) had been introduced and had stabilized as M(II) species over the FER topology, as confirmed by in-situ FTIR spectroscopy of the region of the perturbed T–O–T vibrations. By using a series of M-FERs with different metal loadings (M/Al 0.04 – 0.16), it was possible to establish an extinction coefficient of bare M(II) (Co, Ni, and Mn) located in the FER matrix. This data allowed us to determine the fraction of bare cations located in the β cationic position, which is crucial for the formation of binuclear centers. Those M-FERs with high loadings of bare M(II) in cationic sites were successfully prepared, and a unique type of active site – binuclear structure was formed.

3.3 Could zeolites of topologies other than FER stabilize Fe(II) binuclear active centers for O_2 splitting? Study of the possibility of forming binuclear centers in MOR, *BEA, and LTA zeolites, including determining Al distribution in MOR zeolite

The DFT method was used to understand the role of zeolitic matrices for the stabilization of Fe(II) sites forming binuclear centers in FERs that are active in O_2 splitting. It has been confirmed that the FER structure offers two arrangements of Al atoms in 6-MR, which results in the stabilization of Fe(II) binuclear centers. As previously shown, the major share of the binuclear centers in FERs in one of the possible locations of the two Al atoms in the 6-MR performed O_2 splitting.[71] In this study, it was showed another arrangement of Al atoms in the 6-MR in the FER was participating in O_2 cleavage. This confirmed that the position of the two Al atoms in the 6-MR did not have an effect on the ability of the Fe(II) binuclear sites in the FER to split molecular O_2. This opened up the possibility of studying the reactivity of the binuclear sites in other zeolite matrices and the relationship between the arrangement of the binuclear site and its reactivity toward O_2 splitting. Thus, DFT calculations were used to analyze the possibility of O_2 splitting over Fe(II) embedded in MOR, *BEA, and LTA zeolites (see **Publication IV**). In this study, we focused on evaluating the potential of zeolites with topologies other than that of FER to find an arrangement suitable for the formation of an optimal distance between two Fe(II) ions so it could

cooperate in O_2 dissociation. For this purpose, ^{27}Al MAS-NMR and UV-Vis spectroscopy were employed to determine the organization of Al atoms in MOR zeolites used as catalysts for CR_{N2O} and SCR_{N2O} reactions (the catalytic study is discussed in Section 3.5) (see **Publication VI**).

As previously established, the formation of binuclear Fe(II) centers in FER with the potential for splitting O_2 is controlled by certain structural and geometrical requirements, including: i) the presence of Al atoms in pairs that stabilize the Fe(II) ions; ii) a parallel arrangement of the two zeolite rings containing the Fe(II) cations; and iii) an optimal distance between two Fe ions of about 7 – 9 Å.[71]

Accordingly, the DFT calculations (see **Publication IV**) were employed to interrogate the structural properties of MOR, *BEA, and LTA zeolites in fulfillment of these structural demands (i.e., having Fe(II) in their binuclear centers and their potential for splitting O_2). The calculated geometrical positions of the two cationic sites and the resulting Fe···Fe distance in MOR, *BEA, and LTA zeolite frameworks with actual Al distribution are summarized in Table 4, along with the calculated barriers for O_2 splitting.

Table 4. Selected mutual geometrical positions of the two cationic sites.

Fe-zeolite	Fe…Fe distance	Facing	Parallel	Ring–ring distances [a]	E_{ACT1} [b] (kcal/mol)
FER	7.41	yes	yes	7.4	24.9
*BEA	7.61	yes	yes	9.5	31.2
LTA	7.33	yes	no	7.6	61.6
MOR	7.26	yes	yes	7.5	15.0

[a] Distance between two rings in the empty zeolite.

[b] Calculated barrier of the cleaved O_2.

The calculation predicted variation in the potentials of the studied *BEA, LTA, and MOR zeolites for the formation of an optimal arrangement of binuclear Fe(II) centers and their O_2 splitting abilities. This opened the possibility for the development of highly active and selective catalytic systems based on alternative zeolite structures and their utilization in the direct oxidation of CH_4 to methanol, and/or other organic compounds to valuable oxidation products.

The DFT calculation predicted the geometrical distance between the two β cationic sites in the *BEA zeolite without a divalent cation as 9.5 Å. After the introduction of Fe(II) cations, the Fe···Fe distance in the binuclear center was significantly shortened to 7.6 Å (Table 4). Furthermore, theoretical calculations have shown that O_2 can be split over binuclear Fe centers in

*BEA with the energy barrier of O_2 splitting (see **Publication IV**). Thus, this result confirmed that the splitting of O_2 is not unique to FER topology. It has been pointed out that, recently, the ability of binuclear Fe(II) sites in FER in O_2 splitting has been confirmed experimentally.

The DFT analysis of the LTA zeolite matrix showed that the Fe(II) cations were ligated to three O atoms of two AlO_4^- tetrahedra and one O atom of a SiO_4 tetrahedron. The two closest 6-MRs across the LTA super cage could create two adjacent rings with cationic sites facing each other, albeit they would not be in an optimal parallel arrangement. The distance between the Fe···Fe in such binuclear centers is 7.33 Å, but the location of the two Fe centers is not parallel. DFT calculations clearly showed that such an arrangement of Fe sites in LTA zeolite is far from optimal and thus incapable of O_2 splitting. Accordingly, the corresponding barrier for O_2 splitting was calculated to be 61.6 kcal/mol (Table 4). In comparison with other studied zeolite structures, this value is very high. The presented result clearly shows that for O_2 splitting over the binuclear center, the curtail is their parallel arrangement.

The periodic DFT calculation (see **Publication IV**) indicated that the structure of the MOR zeolite was suitable for the accommodation of Fe(II) cations and the formation of binuclear centers across the zeolite channel with a distance of 7.63 Å. It was also shown that the Fe(II) ions in β cationic positions are located at the bottom of the MOR pockets, and thus they are accessible through the 8-MRs main channels. The calculated energy barrier of the O_2 splitting is 15.0 kcal/mol (Table 4), indicating that a MOR with Fe(II) binuclear centers could split O_2 via a mechanism similar to that observed for the Fe in the FER matrix.

Accordingly, the study focused on the evaluation of Fe-active centers in MOR for the CR_{N2O} and SCR_{N2O} reactions (see **Publication VI**). As previously shown, the organization of Al atoms in the zeolite matrix plays a crucial role in the stabilization of the Fe active sites.[9] Thus, we started our study by determining the distribution of the Al atoms in the commercially available MOR (Si/Al 9.2). It is worth noting that, until our study, there had been no investigation of Al atom organization in MOR. The Al atom organization in the MOR zeolite was investigated using a combination of ^{27}Al MAS-NMR and UV-Vis spectroscopy. The ^{27}Al MAS-NMR spectrum of hydrated MOR confirmed that the Al atoms were exclusively located in the framework positions of the MOR. The determination of the distribution of Al atoms in the MOR matrix was based on the application of Co(II) ions as probes monitored by UV-Vis spectroscopy supported by quantitative data from chemical analysis. The results obtained from the UV-Vis and XRF methods showed that the MOR matrix contained the majority (72%) of the Al atoms forming Al pairs. This type of Al distribution is crucial for stabilizing divalent cations. The rest (28%) of the Al atoms in the MOR zeolite were present as single atoms (see **Publications VI**).

The results of the DFT calculations presented above suggested that the binuclear Fe(II) sites with suitable parameters could be accommodated in topologies other than the FER topology in MOR, *BEA, and LTA zeolites. The calculations showed that the potential for the splitting of O_2 over Fe-zeolites strongly depended not only on cation distance but also on their mutual orientation. It has been found that the axial arrangement of the Fe(II) centers in MOR and *BEA zeolites enabled the splitting of O_2 and the formation of α-O. Conversely, the non-parallel orientation of Fe(II) binuclear centers in the LTA zeolite precludes O_2 activation. The results of this study have revealed that the ability for O_2 cleavage represents a general property of distant binuclear Fe(II) centers optimally stabilized in zeolites, thus suggesting the possibility of developing various Fe zeolite-based systems for O_2 activation for direct hydrocarbon oxidations.

3.4 Does the α-O originating from N_2O and O_2 splitting stabilized on the binuclear centers of Co(II), Ni(II), Fe(II) and Mn(II) in FER zeolites react with CH_4 at low temperatures? Monitoring of the process of N_2O/O_2 splitting toward α-O formation and its stabilization on Co(II), Ni(II), Fe(II), or Mn(II) in FER for the following CH_4 oxidation

The exceptional activity of Fe(II) binuclear centers embedded in Fe-FER in the formation of α-O from O_2 has been presented in previous sections. This section contains a report on the study of the potential for O_2 activation and the following CH_4 selective oxidation over ions other than Fe(II) binuclear ions – that is, the use of Co, Ni, or Mn in the FER matrix (see Section 3.4.1). The formation of α-O obtained by N_2O decomposition and its activity toward CH_4 to methanol oxidation was studied over the binuclear centers of Fe-, Co-, and Ni-FERs (see Section 3.4.2).

3.4.1 O_2 splitting and subsequent CH_4 interaction at low temperature

Herein, the investigations of the dissociation of O_2 over binuclear centers formed by Ni(II), Co(II), and Mn(II) in FERs (see **Publication III**) will be shown. The interaction of O_2 with Ni(II)-, Co(II)-, and Mn(II)-FERs at RT was monitored by FTIR spectroscopy. Analysis of the FTIR spectra of the M-FERs (where M = Ni, Co or Mn) in the T–O–T vibration region revealed that, for all the studied zeolites, after exposure to O_2, the band in the region attributed to the accommodation of bare M(II) cations located in the β cationic position (see Fig. 23) disappeared, a new band being formed at around 870 cm^{-1} (see Fig. 23).[71] This new band remained stable after the gas-phase O_2 had desorbed at RT. As previously indicated, the vanishing of the band at about 920 cm^{-1}, characteristic for bare M(II) cations accommodated in the β site in M(II)-FERs, and the simultaneous formation of the new band at lower frequencies (870 cm^{-1}) due to stronger perturbation in the zeolite ring, indicates that the M(II) was oxidized by the O_2 to $[M(IV)=O]^{2+}$

(α-O). The band at around 870 cm^{-1} was established as an FTIR characteristic of the α-O.[71, 73] These results indicated that, over all three FER samples, the O_2 molecule was cleaved over the distant binuclear Ni(II), Co(II), and Mn(II) centers present in the FERs, and a pair of distant α-O atoms were formed, (i.e., analogous to the Fe-FER).[71] These findings are the first evidence of the splitting of O_2 and the formation of the α-O on binuclear sites other than Fe in FERs at RT.

All three M(II)-FER samples, featuring pairs of the distant α-O atoms originating from the O_2 cleavage, subsequently interacted with CH_4 (Fig. 23). This interaction led to the disappearance of the band at 870 cm^{-1} and the appearance of the band at 920 cm^{-1}, corresponding to the bare M(II) cations accommodated in the β cationic sites. The regeneration of the band at 920 cm^{-1} indicates that the CH_4 interacted with the $[M(IV)=O]^{2+}$ (formed after O_2 treatment) to form volatile products.

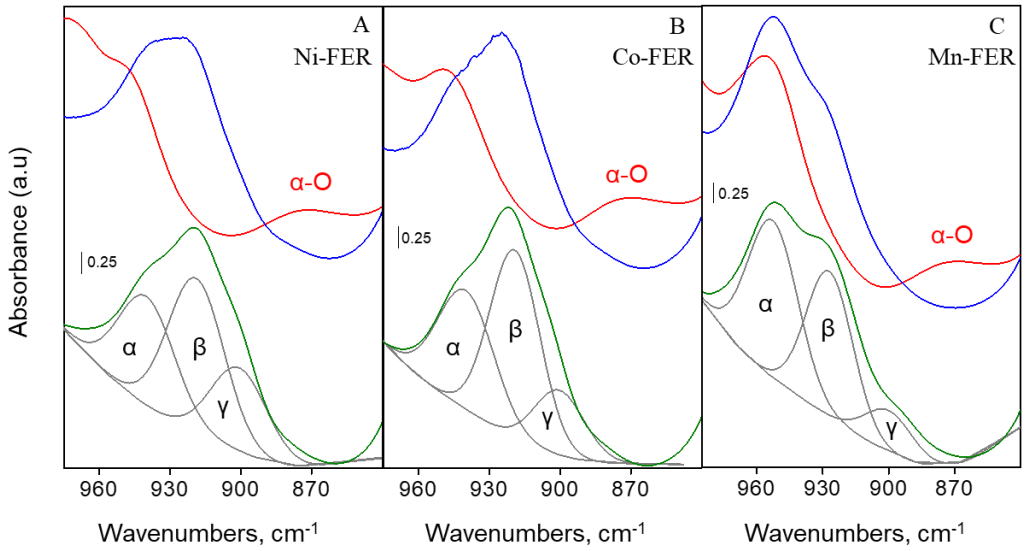

Fig. 23. FTIR spectra of (A) Ni-FER, (B) Co-FER, and (C) Mn-FER samples in the T–O–T vibration region recorded at RT after the following treatments: evacuation at 450°C for 3 h (in green), with the α, β, and γ cationic positions marked (grey lines); (B) 1 h of interaction with O_2 at RT (in red); and (C) consecutive interaction with CH_4 for1 h at RT (in blue).

To detect the volatile products of CH_4 oxidation by $[M(IV)=O]^{2+}$, mass spectrometry was applied (see **Publication III**). The M(II)-FER samples were oxidized by O_2 and subsequently interacted with CH_4 at RT, respectively. The mass spectrum revealed the presence of a signal with m/z = 31 that confirmed the formation of methanol in the gas phase. These results proved that the α-O atoms from the O_2 splitting over all the studied M(II)-FER samples could directly oxidize CH_4 to methanol. The yields of methanol produced per gram of zeolite were 20 $\mu mol/g_{cat}$ for Co-FER, 42 $\mu mol/g_{cat}$ for Mn-FER, and 116 $\mu mol/g_{cat}$ for Ni-FER per cycle. These methanol yields indicate that the Ni-FER had the best performance in the direct oxidation of CH_4 to methanol. Because the methanol was detected in the gas stream, it can obviously be released from the active sites and zeolite channel system to the gas stream without the need for an effluent.

In summary, α-O species are formed by O_2 cleavage over distant binuclear (Ni(II), Mn(II), and Co(II)) cationic centers stabilized in the FER matrix. The presence of methanol in the gas stream after the interaction of the M(II)-FERs with the O_2/CH_4 is clear evidence of the engagement of α-O in CH_4 oxidation. In contrast to other zeolitic systems, the methanol produced over the distant binuclear cationic structures can be released to the gas phase from the M(II)-FER samples without using an effluent. The stability of cationic active centers makes systems based on Ni(II), Mn(II), or Co(II)-FER attractive for use as potential catalysts in CH_4 to methanol oxidation at the industrial level.

3.4.2 N_2O decomposition and subsequent CH_4 treatment at low temperature

The DFT study was used to determine the ability of binuclear M(II) (where M = Co or Fe) cations to cleave N_2O and stabilize α-O over binuclear centers of Co(II) and Fe(II) cations in FER (see **Publication II**). The calculations were performed for a theoretical model, in which two M(II) cations formed binuclear centers across a FER channel and cooperated in N_2O splitting. Here, the DFT results from the N_2O activation of Co(II)-FER are discussed. (The DFT study on Fe-FER interacting with N_2O has been presented previously).

The reaction pathway for N_2O decomposition over binuclear centers in a Co(II)-FER (Fig. 24A) occurs via N_2O adsorption on the Co(II) by the terminal N atom (calculated adsorption energy = -15.4 kcal/mol), forming a [Co…NNO Co] complex (Fig. 24B). The O atom in N_2O is well positioned to attack the second Co(II) cation in the binuclear centers located across FER channels.

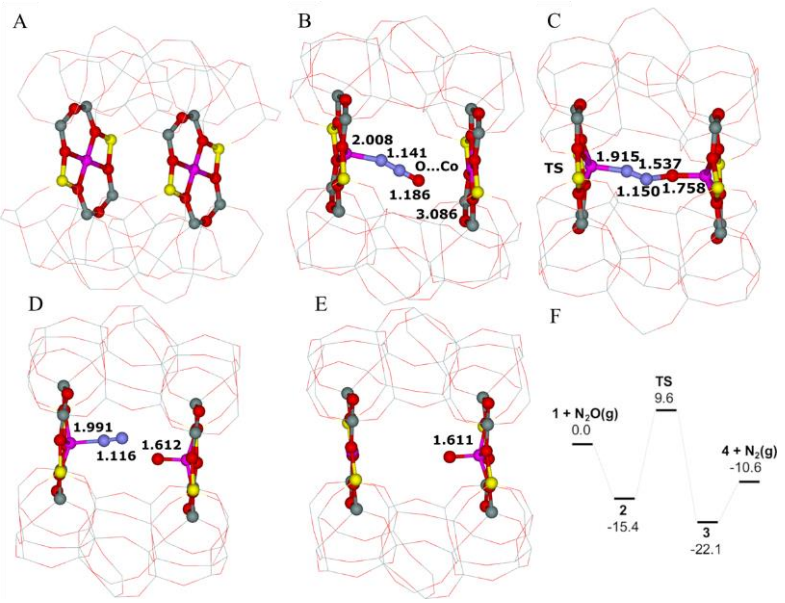

Fig. 24. DFT model of binuclear Co centers in a FER and their interaction with N_2O: (A) binuclear centers in Co-FER; (B) Co…NNO Co complex; (C) transition state formed over binuclear centers; (D) Co…NN O=Co intermediate formed over the binuclear centers; (E) the Co O=Co product (formation of the α-O); and (F) schematic energy profile during N_2O activation over the Co(II) binuclear centers. Si atoms in gray, O atoms in red, Al atoms in yellow, Co atoms in violet, and N atoms in blue. Schematic energy profile (in kcal/mol).

Consequently, the N-O bond is cleaved, and the bare Co(II) cation in the β site is oxidized to yield a [Co…NN O=Co] intermediate (Fig. 24D) via the [Co-NNO-Co] transition state (energy barrier = 9.6 kcal/mol) (Fig. 24C). Subsequently, the N_2 desorbs (energy cost = 11.5 kcal/mol) and the [Co O=Co] product (Fig. 24E), featuring the α-O, is formed. Our calculations also revealed that N_2O does not adsorb on Co(II) via the O atom, as had previously been suggested for isolated Co(II) cations. These results confirm that α-O can be created on binuclear Co(II) centers. The schematic energy profile during N_2O activation over the binuclear centers is presented in Fig. 24F.

In order to assess the redox behavior of binuclear Fe, Ni, and Co in FERs (Fig. 25), the interaction of N_2O (Fig. 26) and CH_4 was analyzed by FTIR (Fig. 27) and mass spectrometry (Fig. 28). The FTIR results from the interaction of N_2O with the M-FERs (M = Fe(II), Ni(II) or Co(II)) (Fig. 26) at RT clearly showed that the bands of the M(II) cations located in the β cationic positions disappeared, with two new bands being formed at approximately 950 and 880 cm^{-1} (Fig. 26). The band at 880 cm^{-1} was attributed to the $[M(IV)=O]^{2+}$ complex, featuring the α-O, similarly to in the Fe-FER.[71] The weak band at 950 cm^{-1} was assigned to the ligand complex M(II) with N_2O (see **Publication II**).

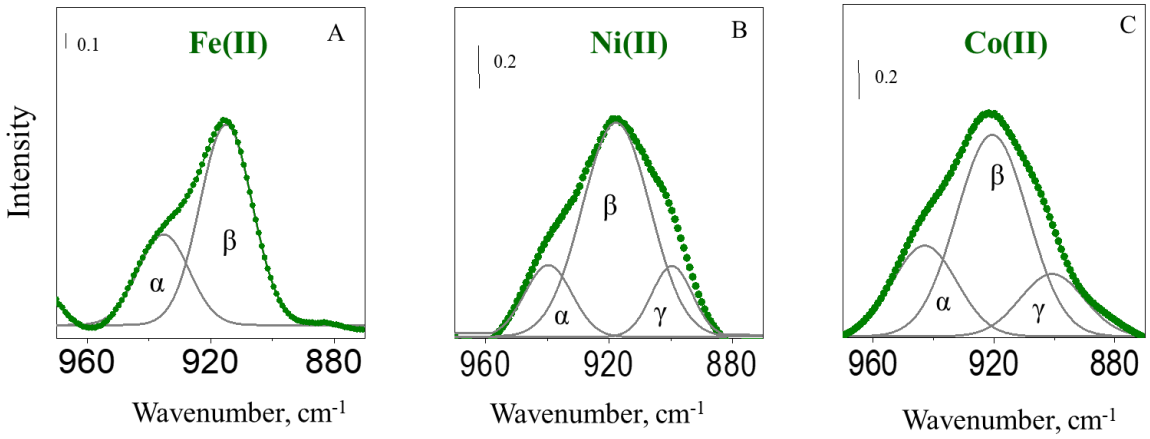

Fig. 25. FTIR spectra of (A) Fe-FER, (B) Ni-FER, and (C) Co-FER samples in the T–O–T vibration region, recorded at RT after evacuation at 450°C for 3 h, with the α, β, and γ cationic positions marked (grey lines).

The oxidation properties of the α-O formed on the Co-, Ni-, and Fe-FER samples were investigated through the selective oxidation of CH_4, monitored by in-situ FTIR spectroscopy. The FTIR spectra of the M-FERs recorded after interaction with the previously N_2O-oxidized M-FERs with CH_4 (Fig. 27) indicated that the band at 880 cm^{-1}, which corresponded to the α-O, had disappeared completely, while the band at around 920 cm^{-1}, characterizing the bare M(II) cations accommodated in the β site, had reappeared (Fig. 27).[27, 71] The emergence of the band at about 920 cm^{-1}, which characterized the bare divalent cations located in the β site, suggests the protonation of methoxy groups.

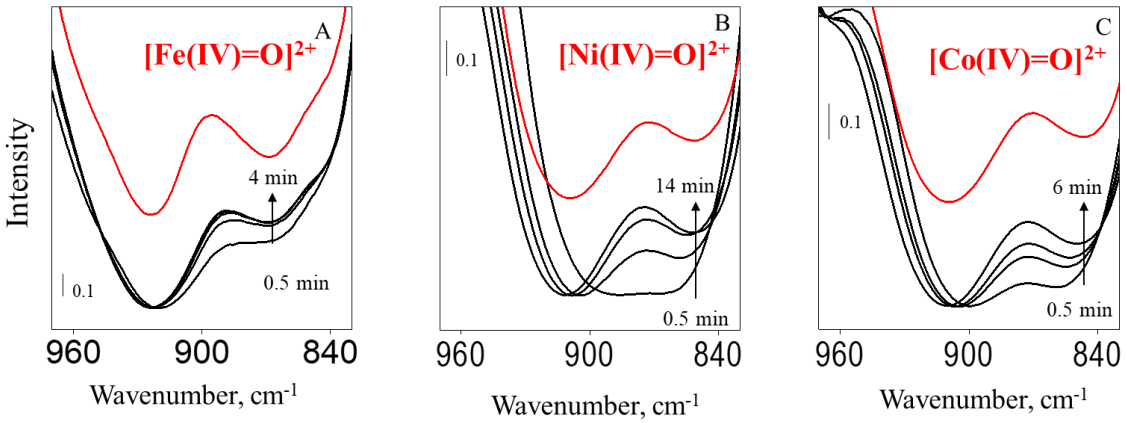

Fig. 26. FTIR spectra of (A) Fe-FER, (B) Ni-FER, and (C) Co-FER samples in the T–O–T vibration region, recorded at RT after evacuation at 450°C for 3 h and subsequent interaction with N_2O for 4 – 14 min (in black). FTIR spectra after desorption of N_2O for 5 min at 200°C (in red).

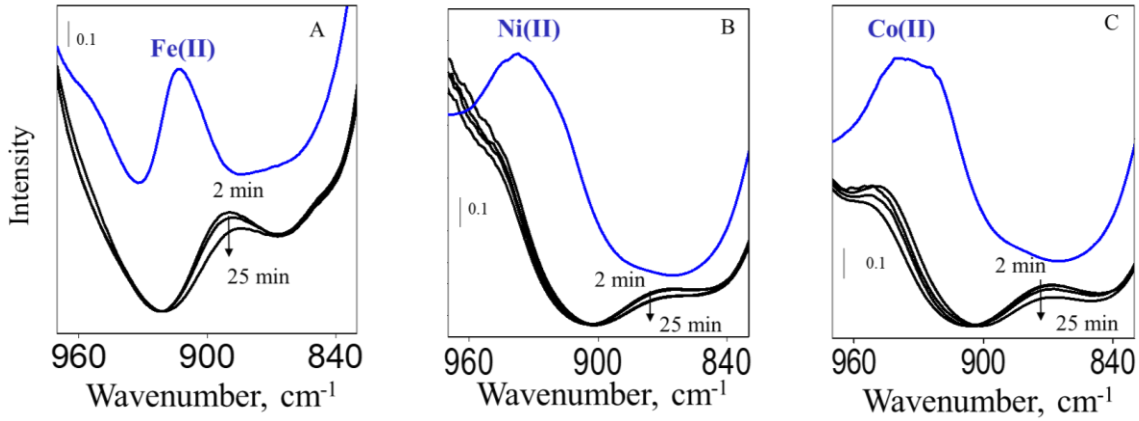

Fig. 27. FTIR spectra of (A) Fe-FER, (B) Ni-FER, and (C) Co-FER samples in the T–O–T vibration region, recorded at RT after the following treatments: evacuation at 450°C for 3 h, 14 min interaction with N_2O; and consecutive interaction with CH_4 for 25 min at 200°C (in black). FTIR spectra after desorption of CH_4 for 5 min at 200°C (in blue).

Analysis of the FTIR spectra (Fig. 28) in the region of the C-H stretching vibrations (3000 – 2830 cm^{-1}) revealed the presence of a band at 2960 cm^{-1} corresponding to formate species bound to the Fe cation, a band at 2853 cm^{-1} attributed to CH_3-OH, and a band at 2920 cm^{-1}, which was assigned to the methoxy group bound to the Fe cation. Bands in the region of methyl group (δCH_3), carboxyl group (δCOH), and νCO vibrations (1800 – 1290 cm^{-1}) appeared at 1666 and 1355 cm^{-1} and were assigned to formate anions bound to the Fe cation, and at 1642 cm^{-1}, attributed to formaldehyde adsorbed on the Fe cation.[66, 129] The presence of bands characterizing methanol, formaldehyde, and formate suggests the protonation of methoxy groups in the M(II)-FERs with binuclear M(II) species. The higher protonation activity of all three M-FER samples resulted in the creation of protonated oxidation products that is, methanol, formaldehyde, and formic acid.

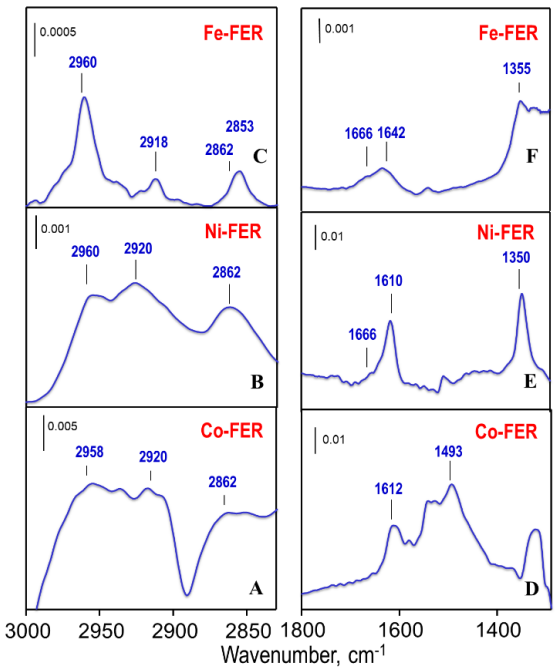

Fig. 28. FTIR spectra of the M-FER samples: (A) Co-FER; (B) Ni-FER; (C) Fe-FER; (D) Co-FER; (E) Ni-FER; and (F) Fe-FER. The spectra were recorded after the interaction of the M-FER samples with N_2O for 14 min and the subsequent interaction with CH_4 for 25 min at 200°C, respectively.

The oxidation products of CH_4 over N_2O-oxidized M-FER (M = Co, Ni or Fe) were also monitored using mass spectrometry in order to confirm the protonation of the methoxy groups and to determine the composition of the oxidation products (Fig. 29).

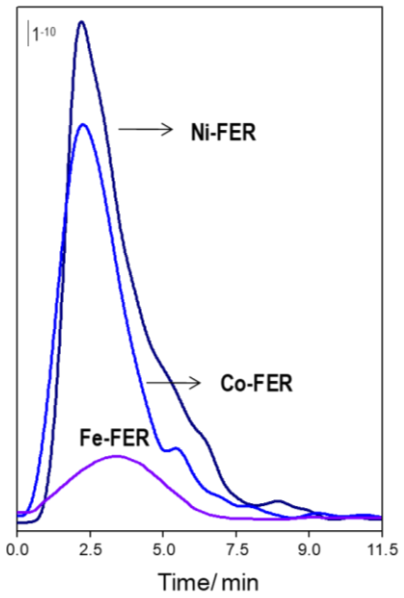

Fig. 29. Mass spectrometry results of methanol formation (m/z = 31) over the Ni-FER, Co-FER, and Fe-FER. Methanol was detected after oxidation of the samples by N_2O at 200°C, and then the formed α-O was titrated by CH_4 at the same temperature.

The previously N_2O-oxidized M-FERs interacted with CH_4, and the products of the oxidation were detected by mass spectrometry. The mass spectrometry results confirmed the formation of methanol (m/z = 31) and small amounts of other oxidation products, such as

formaldehyde, formic acid, dimethyl ether, and CO_2. The yields of methanol produced per gram of zeolite were 200 μmol/g_{cat} for Co-FER, 290 μmol/g_{cat} for Ni-FER, and 32 μmol/g_{cat} for Fe-FER per cycle. These results confirm that the active sites for the formation of the α-O and methane oxidation involved two cooperating M(II) cations.

In all three M(II)-FER samples, the α-O was generated by pairs of M(II) cations abstracting the O atom from the N_2O. The α-O already selectively oxidized CH_4 to methanol at RT. Notably, the methoxy groups were protonated to methanol and other oxidation products without the use of water vapor, which distinguishes this system from previously reported zeolite-based systems. Additionally, it should be mentioned that the formation of the α-O only occurred in binuclear Co(II)...Co(II) and Ni(II)...Ni(II) centers, and not in isolated Co(II) or Ni(II) cations.

3.5 How is the cation speciation in FER and MOR zeolites reflected in the catalytic performance of Fe-zeolites in the CR_{N2O} and SCR_{N2O} of N_2O by CH_4? Realization of catalytic tests over Fe-FER and Fe-MOR under conditions of CR_{N2O} and SCR_{N2O} of N_2O reduction by CH_4

In order to analyze the influence of zeolite topology on the catalytic performance in CR_{N2O} and SCR_{N2O} reactions, Fe-FER and Fe-MOR with similar Fe loadings were used (see **Publication VI**). The Fe was introduced to both the FER (Si/Al 8.6) and MOR (Si/Al 9.2) matrices via impregnation in acetylacetone. The compositions of the four samples are presented in Table 1 (see **Publication VI**). To determine the role of various Fe species in the CR_{N2O} and SCR_{N2O} processes, we intentionally prepared the samples to contain low (below 0.8 wt.%) and high (above 1.5 wt.%) Fe loadings that differed in the type of Fe sites. The studied samples were marked Fe-FER-32, Fe-FER-70, Fe-MOR-23, and Fe-MOR-95, where the number represented the $3Fe^{3+}$/Al ratio.

3.5.1 Detections of Fe(II) in studied Fe-zeolites

Carbon monoxide and NO were used as probe molecules for the detection of Fe(II) in Samples Fe-FER-32, Fe-FER-70, Fe-MOR-23, and Fe-MOR-95 (Fig. 30).

Analysis of the FTIR spectra after CO adsorption verified that, in all the samples, a band at 2200 cm^{-1} typical for Fe(II)-CO was formed (Fig. 31A and C).[130] This confirmed the presence of the Fe(II) species in all the studied Fe-zeolites. The adsorption of CO on the evacuated Fe-FERs confirmed the formation of a carbonyl band at 2196 cm^{-1}, which corresponded to the Fe(II)-CO species. A comparison of the spectra for Fe-FER-32 and Fe-FER-70 showed that the intensity of the Fe(II)-CO band did not increase with Fe loading. This suggests that, in the FER matrix, the saturation of specific cationic positions by Fe(II) was reached at a low Fe loading.

In the Fe-MOR samples, the intensity of the Fe(II)-CO bands significantly increased with increasing Fe loading, indicating that, in the MOR matrix, the specific cationic positions accessible to Fe(II) were gradually populated at increasing Fe concentrations.

The NO adsorption was used to better evaluate the speciation of Fe(II) due to the strong NO affinity toward Fe(II), which results in the formation of stable nitrosyl species.[131] In Fe-zeolites, several types of active Fe(II) species can be identified - the intense band at 1877 cm^{-1} was assigned to an Fe(II)-NO species, the band at 1760 cm^{-1} corresponded to the low-frequency mode of the Fe(II)-$(NO)_2$ species, and the bands at 1825 and 1805 cm^{-1} coupled with the shoulder at 1920 cm^{-1} to represent an Fe(II)-$(NO)_3$ species.

In the studied Fe-FERs, only one type of Fe(II)-NO species was revealed at around 1820 cm^{-1}, as indicated by the symmetrical shape of the corresponding band. This indicates that the active Fe(II) species capable of adsorbing only one NO molecule was introduced into the FER matrix at low Fe loading, while the active Fe(II) species adsorbing two or three NO molecules were introduced at higher Fe loading. This evidence confirmed that the FER matrix strongly stabilizes peculiar Fe(II) sites (i.e., able to adsorb only one NO molecule) that were already highly populated at low Fe loadings.

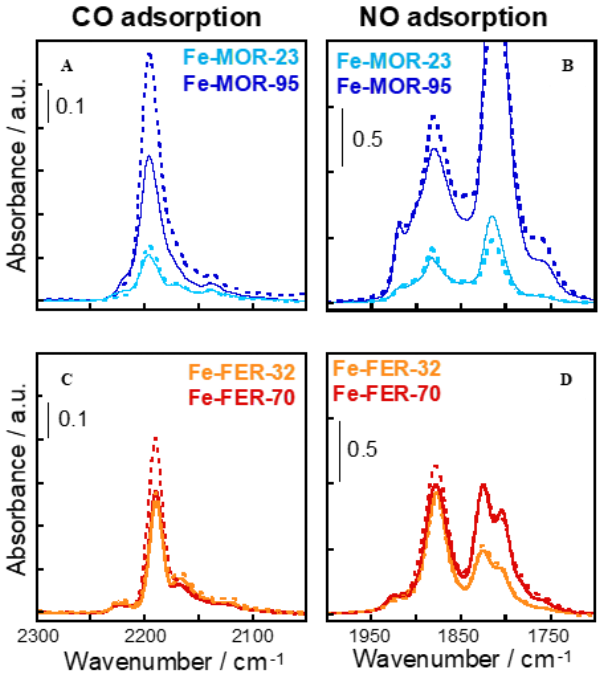

Fig. 30. In-situ FTIR spectra of (A and C) CO and (B and D) NO adsorbed at RT on activated (A and B) Fe-MOR and (C and D) Fe-FER catalysts at different Fe loadings. Experiments on samples pre-reduced by CO at 320°C are also reported (dotted-lines). The samples were heated in CO from RT up to 320°C, kept for 5 min at 320°C, then cooled back to RT before recording the spectra in the presence of CO or NO. In (B), the band at about 1800 cm^{-1} is not to scale.

In the NO adsorption over the Fe-MOR samples, the nitrosyl region showed an intense band at 1880 cm^{-1} with a shoulder at about 1910 cm^{-1}, indicating two types of Fe(II)-NO mono nitrosyl species. A weak band at 1760 cm^{-1} was ascribed to Fe-$(NO)_2$ dinitrosyls, and bands at

1820 and 1925 cm^{-1} were typical for Fe-$(NO)_3$ trinitrosyl species.[132] Based on this, at least three types of Fe(II) species were inferred, in different positions of MOR cavities - two species able to adsorb a maximum of one molecule of NO, and a third species filling its coordination sphere with two or three NO molecules. At increasing Fe loading in the MOR matrix, the intensity of all the nitrosyl bands increased, indicating that the amount of active Fe(II) species increased (in agreement with the CO adsorption results). Therefore, a comparison of the NO adsorption results obtained from the Fe-FER and Fe-MOR samples with similar Fe loadings highlighted the role of the matrix topology in controlling the active Fe(II) speciation in terms of the coordinative unsaturation and symmetry of the stabilized Fe(II) sites.

3.5.2 Role of zeolite topology in CR_{N2O} and SCR_{N2O} reactions over Fe-FER and Fe-MOR: Catalytic and operando study

All the studied Fe-FER and Fe-MOR catalysts were highly active in the reduction of N_2O by CH_4 (CR_{N2O}) (Fig. 31A and 31C). Under laboratory conditions, the N_2O conversion reached 100% in the range 350 – 400°C, during which the CH_4 conversion reached its maximum value (about 30%), remaining constant at higher temperatures (Fig. 31A and 31C). With increasing Fe content in the zeolite, the activity increased nearly proportionally over the Fe-FER catalysts, but was less over the Fe-MOR catalysts.

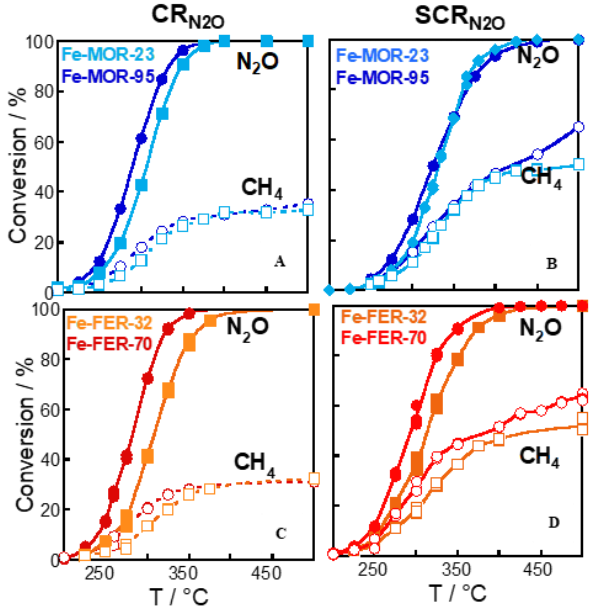

Fig. 31. (A and C) CR_{N2O} and (B and D) SCR_{N2O} reactions on (A and B) Fe-MOR and (C and D) Fe-FER catalysts at different Fe loadings. The %N_2O and %CH_4 conversion are presented as a function of temperature. Reactant concentrations: [N_2O]=[CH_4] = 0.4% and [O_2] = 0% or 2% (total flow rate = 50 cm^3 STP/min, with He as balance).

When excess O_2 was added to the N_2O+CH_4 mixture (SCR_{N2O}), both the Fe-MOR and Fe-FER systems were still highly active for N_2O reduction with CH_4 (Fig. 31B and D). Again, by

increasing the Fe loading, the N_2O conversion increased over the Fe-FER catalysts but was less over the Fe-MOR catalysts.

A comparison between the catalytic activity of the Fe-MOR and Fe-FER catalysts showed that N_2O abatement under conditions of CR_{N2O} action only negligibly depended on the zeolite matrix used (see **Publication VI**), suggesting the presence of similar amounts of Fe(II) working sites in both zeolites at similar Fe loading. Contrastingly, the N_2O abatement in the SCR_{N2O} process was higher on the Fe-FER than on the Fe-MOR catalyst.

To verify if the Fe-MOR and Fe-FER systems were stable under real feeds, the activity, stability, and reversibility of the catalytic activity for SCR_{N2O} after the addition of H_2O vapor were investigated. After the addition of H_2O, the activity slightly decreased in both the Fe-MOR-95 and Fe-FER-70 catalysts across the whole temperature range (Fig. 32A and C). In particular, at the temperature at which the N_2O conversion in the dry feed was about 70% (350°C for Fe-MOR-95 and 315°C for Fe-FER-70), the conversion decreased to about 50% after the addition of H_2O, but it remained stable for both zeolites as a function of time on stream (Fig. 32B and D).

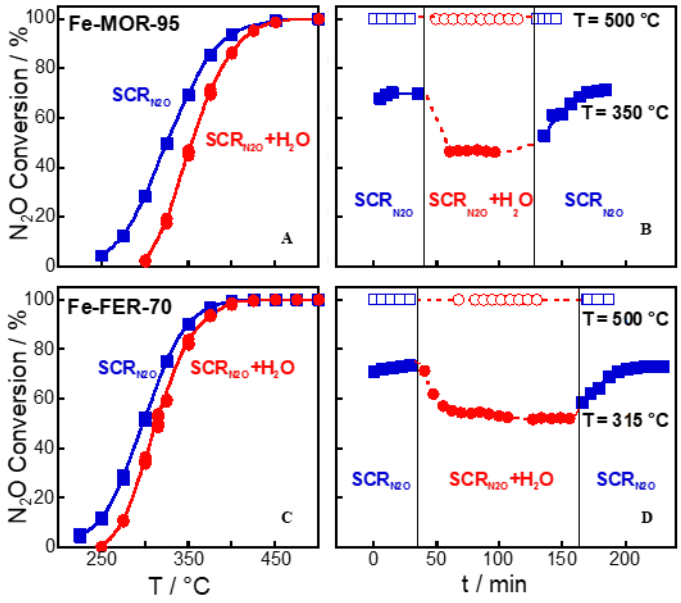

Fig. 32. (A and B) SCR_{N2O} reaction on Fe-MOR-95 and (C and D) Fe-FER-70 in the presence or absence of H_2O vapor in the reactant mixture. (A and C) $\%N_2O$ conversion as a function of temperature and (B and D) of time on stream at set temperatures, as indicated. Reactant concentration: $[N_2O]=[CH_4] = 0.4\%$, $[O_2] = 2\%$, and $[H_2O] = 0\%$ or 2% (total flow rate = 50 cm^3 STP/min, with He as balance).

These results suggested that only a fraction of the Fe active sites were poisoned. On both catalysts, the activity was fully restored when the H_2O was switched off from the feed, suggesting that the deactivation by H_2O was probably due to reversible poisoning (H_2O adsorption /desorption).

Operando FTIR experiments were performed to obtain information on the pathways of the CR_{N2O} and SCR_{N2O} and the key intermediates stabilized on the active Fe centers involved in these

processes. To analyze the FTIR operando study, low-loaded Fe-zeolites (Fe-MOR-32 and Fe-FER-23) were selected (see **Publication VI**). It should be stressed that, regardless of the concentration of the Fe in the studied MOR or FER, the general trend in the interaction with the CR_{N2O} and SCR_{N2O} detected under operando conditions was the same. The spectra of the Fe-MOR and Fe-FER catalysts under a N_2O+CH_4 feed (Fig. 33), recorded at increasing temperatures in the range 250 – 400°C, showed absorption bands in the range 1700 – 1300 cm^{-1} that were typical for the presence of the reaction products (i.e., CH_xO_y species). The newly formed bands were assigned to formaldehyde (1620 cm^{-1}), formate (1590 – 1560 and 1390 cm^{-1}), and methoxy (1475 – 1435 cm^{-1}) species.[66, 129, 133] The CH_xO_y species were better defined in the experiments over Fe-FER, which probably indicates the lower heterogeneity of these surface species. This finding clearly suggests that the topology influenced the type of intermediate species. However, over Fe-MOR-23, the CHxOy species were more abundant than over Fe-FER-32, although both Fe-MOR-23 and Fe-FER-32 exhibited rather similar catalytic activity. These differences in the population of CH_xO_y and the catalytic activity of the studied Fe-zeolites can be tentatively assigned to the presence of a higher fraction of spectator species in the case of Fe-MOR-23 compared to Fe-FER-32.

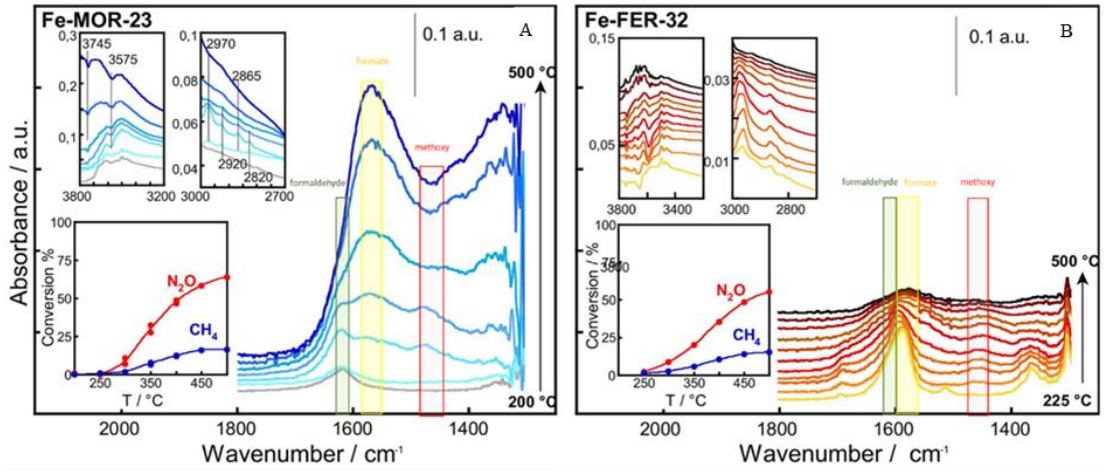

Fig. 33. Operando FTIR spectra of surface species during CR_{N2O} reaction at temperatures increasing up to 500°C on: (A) Fe-MOR-23; and (B) Fe-FER-32 catalysts. The insets show the corresponding reactant conversions as a function of temperature and magnifications of the O-H and C-H stretching regions.

Analysis of the operando FTIR results during SCR_{N2O} revealed the formation of formaldehyde and formate species (Fig. 34). Compared with the CR conditions, the FTIR spectra for Fe-FER-32 and Fe-MOR-23 under SCR_{N2O} conditions were free from methoxy species. These findings indicate that the addition of O_2 to the reaction mixture blocked the formation (or accumulation) of methoxy species on the surface. A similar amount of CH_xO_y (formaldehyde and formate species) was observed on the Fe-FER-32 sample in both the CR_{N2O} and SCR_{N2O} reactions. However, in the Fe-MOR-23 sample, the fraction of CH_xO_y that appeared in the SCR_{N2O} was lower

than in the CR_{N2O}. These results confirmed that the addition of O_2 to the reaction mixture prevented the formation (accumulation) of C-containing species, including spectators, on the catalyst surface.

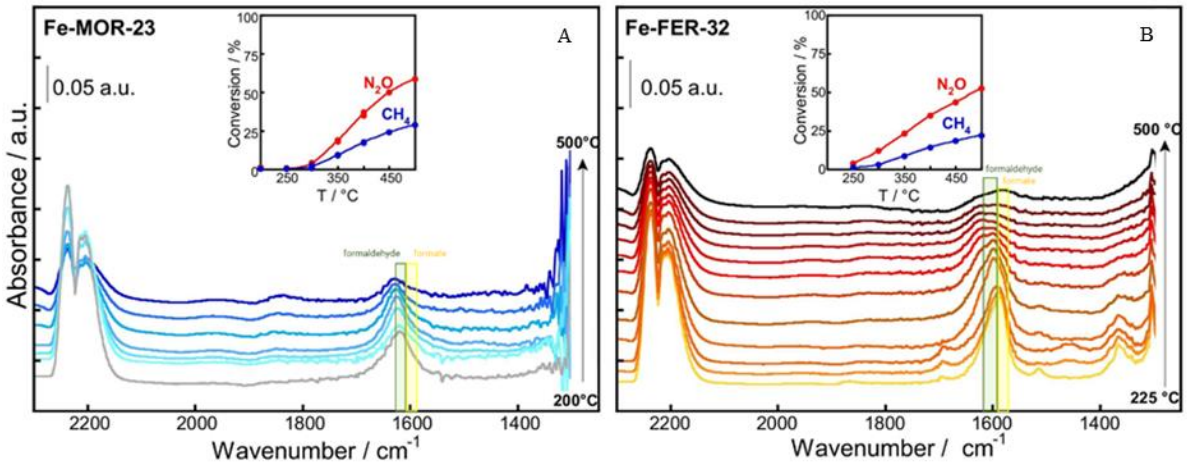

Fig. 34. Operando FTIR spectra of surface species during SCR_{N2O} reaction at temperatures increasing up to 500°C on: (A) Fe-MOR-23; and (B) Fe-FER-32 catalysts. The insets show the corresponding reactant conversions as a function of temperature and magnifications of the O-H and C-H stretching regions.

The results presented above clearly show that the FER and MOR matrices, with comparable amounts of Al pairs, influenced the formation of individual Fe(II) sites with different redox properties. Accordingly, the differences in zeolite topology affected the formation of various types of Fe species with different valencies. The Fe-FER zeolite contained a higher fraction of well-defined Fe(II) than its Fe-MOR analog, with similar Fe loading. It was confirmed that the Fe-FER was more active than the Fe-MOR in the reduction of N_2O in the presence of O_2 (SCR_{N2O}), whereas both systems were similarly active for CR_{N2O}. It was also shown that the conditions of the catalytic reactions were strongly influenced by the redox properties of the studied zeolites. A combination of structural characteristics of the Fe-MOR and Fe-FER samples, with their catalytic performance, revealed that, in the CR_{N2O} reaction, the active centers were Fe(II) located in cationic positions. In the case of SCR_{N2O}, the reaction conditions influenced the redox properties of the Fe species present in the Fe-FER and Fe-MOR samples. However, a higher fraction of Fe(II) species performing the redox cycle was observed in Fe-FER, as reflected in its higher catalytic activity.

In both systems, the addition of H_2O to the SCR_{N2O} feed caused a slight and reversible deactivation due to adsorption/desorption phenomena. However, the limited extent of the interaction with H_2O allowed both the Fe-FER and Fe-MOR systems to be potentially effective catalysts for N_2O abatement with CH_4 under real conditions (i.e., with O_2 and H_2O vapor present in the feed) Fe-FER being more efficient due to its better resistance to the presence of O_2 in the reaction feed.

IV General conclusions

The conclusions of the study are presented as answers to the questions posed in the aims of the thesis.

1. How to analyze the O_2 activation and following CH_4 oxidation over Fe-FER using spectroscopic techniques? The methodology used to explore the formation of α-O from O_2 splitting over Fe-FER was developed using in-situ Mössbauer, XANES, and FTIR spectroscopy. The structural and valence changes in Fe(II)→Fe(III) occurring over the β site in the Fe-FER were revealed by in-situ Mössbauer and XANES spectroscopy before and after O_2 interaction. Thus, the in-situ Mössbauer spectral benchmark of the α-O originating from O_2 stabilized on Fe in the FER was established. It was shown that the formation, kinetics, and oxidation properties of α-O can be analyzed using the in-situ FTIR technique in the region of the OH and T–O–T vibrations. The FTIR spectral characteristic for α-O was also established. Methane was used as a probe molecule to analyze the oxidation properties of α-O, and it was confirmed that the CH_4 was oxidized by α-O to methanol. The products of the interaction of O_2/CH_4 with Fe-FER monitored by FTIR and mass spectrometry confirmed methanol formation. The application of the developed methodology (combined in-situ Mössbauer, XANES, and FTIR spectroscopy, mass spectrometry, and FTIR analysis in the gas phase) could be used as a tool for determining the potential of TMI-containing zeolites for O_2 activation and CH_4 oxidation.

2. Do other than Fe(II) TMI ions form binuclear centers in FER for O_2/N_2O cleavage? The outcomes of FTIR spectroscopy investigations, as well as the DFT modeling, confirmed that the FER topology is an optimal candidate for stabilizing a significant fraction of divalent TMI cations in β cationic positions, which can form binuclear centers. It was further demonstrated that preparing Co-, Ni-, and Mn-FERs with the high level of loading of bare divalent cations is feasible for all of these cations. Moreover, for the first time, the values of the FTIR extinction coefficients of the individual bare M(II) cations (M = Co, Ni, and Mn) located in the FER matrix were established. This data allows us to determine the fraction of bare cations located in particular cationic positions, which is crucial for forming binuclear centers.

3. Could zeolites of topologies other than FER stabilize Fe binuclear active centers for O_2 splitting? The results of the DFT calculations indicated that the binuclear Fe(II) sites could be accommodated in topologies other than FER (e.g., MOR, *BEA, and LTA). However, the DFT calculations also showed that the splitting of O_2 over Fe(II) zeolites was significantly influenced by the location of the Fe centers and their mutual orientations. The optimal parallel orientation of Fe(II) centers in the MOR and *BEA zeolites enabled the splitting of O_2 and the formation of α-O, whereas the non-parallel orientation of Fe binuclear centers in the LTA zeolite precluded O_2

cleavage. The results of this study have confirmed that the capability for O_2 splitting represents a general property of the binuclear Fe(II) centers stabilized in zeolites. This suggests the possibility of developing further optimizing the O_2 activation in direct hydrocarbon oxidations based on Fe cations in other zeolites.

4. Does the α-O originating from N_2O and O_2 splitting stabilized on the binuclear centers of Co(II), Ni(II), Fe(II), and Mn(II) in FER zeolites react with CH_4 at low temperatures? The findings obtained from FTIR and mass spectrometry analysis confirmed that the α-O species was formed by O_2/N_2O cleavage over the binuclear Ni(II), Mn(II), Fe(II), and Co(II) in the FER reacting with CH_4, oxidizing it to methanol at RT. In contrast to other zeolitic systems, the methanol produced over distant binuclear cationic structures in FER zeolites was released to the gas phase without using an effluent. The yields of methanol produced by N_2O dissociation over M-FERs were twice as high as the yields of methanol produced by O_2 splitting. In comparison to the Fe-FER, other cations [Ni(II), Mn(II), and Co(II)] exhibited higher chemical stability, thus making these systems more attractive for use as potential catalysts in CH_4 to methanol oxidation at the industrial level.

5. How is the cation speciation in FER and MOR zeolites reflected in the catalytic performance of Fe-zeolites in the CR_{N2O} and SCR_{N2O} of N_2O by CH_4? Our findings showed that FER and MOR matrices with a comparable amount of Al pairs (for the MOR zeolites, the Al distribution was determined in this work) stabilized the Fe sites with different redox properties. In addition, we confirmed that the topology of the zeolites affected the formation of various types of Fe species with different valencies. Namely, Fe-FER zeolite contained a higher fraction of well-defined Fe(II) than its Fe-MOR analog with similar Fe loading. The Fe-FER zeolite was also a more active catalyst than the Fe-MOR in the selective catalytic reduction of N_2O by CH_4 (SCR_{N2O}), whereas both systems were similarly active for CR_{N2O}. It further confirmed that the conditions of the catalytic reactions strongly influenced the redox properties of the studied zeolites. A combination of the structural characteristics of the Fe-MOR and Fe-FER zeolites with their catalytic performance revealed that, in the CR_{N2O} reaction, the active centers were Fe(II) located in cationic positions. In the case of the SCR_{N2O}, the reaction conditions influenced the redox properties of the Fe species present in both the Fe-FER and Fe-MOR zeolites. Nevertheless, a higher fraction of Fe species performing the redox cycle was observed in the Fe-FER zeolite, as reflected in its higher catalytic activity. In Fe-FER and Fe-MOR systems, adding H_2O to the SCR_{N2O} feed caused a slight and reversible deactivation due to adsorption/desorption phenomena. However, the limited extent of the interaction with H_2O allowed both the Fe-FER and Fe-MOR catalysts to be potentially effective for N_2O abatement with CH_4 under real conditions.

V Outlook

The scientific future plan is mainly focused on the study of the ability of zeolite frameworks to stabilize active centers for the activation of small molecules and oxidation of hydrocarbons. Below the list of the main topics is presented:

- ✓ Employing various zeolite topologies, e.g., CHA, MOR, or *BEA, and ensuring an optimal distribution of Al atoms in zeolite structure for stabilization of cation active centers performing activation of O_2.
- ✓ Check the potential of CHA, MOR, or *BEA with optimal Al distribution for stabilization of various binuclear centers formed, e.g., by Fe, Ni, or Mn cations, and their performance in O_2/CH_4 activation.
- ✓ Employment of the α-O stabilized on TMI-containing zeolites for oxidation of other molecules than CH_4, e.g., cyclohexane or propane.
- ✓ Consideration of the possibility of TMI binuclear centers in zeolites for activation of various small molecules, e.g., CO_2, CO, or N_2, and analyze their potential in environmentally important catalytic reactions.

VI References

(1) Corma, A. Inorganic solid acids and their use in acid-catalyzed hydrocarbon reactions. *Chem. Rev.* **1995**, 95(3), 559–614.

(2) Zhang, Q.; Yu, J. H.; Corma, A. Applications of Zeolites to C1 Chemistry: Recent Advances, Challenges, and Opportunities. *Adv. Mater.* **2020**, 32(44), 2002927.

(3) Tabor, E.; Bernauer, M.; Wichterlova, B.; Dedecek, J. Enhancement of propene oligomerization and aromatization by proximate protons in zeolites; FTIR study of the reaction pathway in ZSM-5. *Catal. Sci. Technol.* **2019**, 9(16), 4262–4275.

(4) http://www.iza-structure.org/databases/.

(5) Smith, J. V. Definition of a zeolite. *Zeolites.* **1984**, 4, 309–310.

(6) Li, C. G.; Vidal-Moya, A.; Miguel, P. J.; Dedecek, J.; Boronat, M.; Corma, A. Selective Introduction of Acid Sites in Different Confined Positions in ZSM-5 and Its Catalytic Implications. *ACS Catal.* **2018**, 8(8), 7688–7697.

(7) Findley, J. M.; Ravikovitch, P. I.; Sholl, D. S. The Effect of Aluminum Short-Range Ordering on Carbon Dioxide Adsorption in Zeolites. *J. Phys.Chem.C.* **2018**, 122(23), 12332–12340.

(8) Dinh, K. T.; Sullivan, M. M.; Serna, P.; Meyer, R. J.; Dinca, M.; Roman-Leshkov, Y. Viewpoint on the Partial Oxidation of Methane to Methanol Using Cu- and Fe-Exchanged Zeolites. *ACS Catal.* **2018**, 8(9), 8306–8313.

(9) Dedecek, J.; Sobalik, Z.; Wichterlova, B. Siting and Distribution of Framework Aluminium Atoms in Silicon-Rich Zeolites and Impact on Catalysis. *Catal. Rev.* **2012**, 54(2), 135–223.

(10) Dedecek, J.; Tabor, E.; Sklenak, S. Tuning the Aluminum Distribution in Zeolites to Increase their Performance in Acid-Catalyzed Reactions. *ChemSusChem.* **2019**, 12(3), 556–576.

(11) Palomino, M.; Corma, A.; Rey, F.; and Valencia, S. New Insights on CO_2-Methane Separation Using LTA Zeolites with Different Si/Al Ratios and a First Comparison with MOFs. *Langmuir.* **2010**, 26(3), 1910–1917.

(12) Kuznicki, K. A. T. Characterization of chabazite and chabazite-like zeolites of unusual composition. *J. Chem. Soc., Faraday Trans.* **1991**, 87, 1031–1035.

(13) Sazama, P.; Tabor, E.; Klein, P.; Wichterlova, B.; Sklenak, S.; Mokrzycki, L.; Pashkkova, V.; Ogura, M.; Dedecek, J. Al-rich beta zeolites. Distribution of Al atoms in the framework and related protonic and metal-ion species. *J. Catal.* **2016**, 333, 102–114.

(14) Sazama, P.; Mokrzycki, L.; Wichterlova, B.; Vondrova, A.; Pilar, R.; Dedecek, J.; Sklenak, S.; Tabor, E. Unprecedented propane-SCR-NOx activity over template-free synthesized Al-rich Co-BEA* zeolite. *J. Catal.* **2015**, 332, 201–211.

(15) Bekkum, H. V.; Flanigen, E. M.; Jansen, J. C. Introduction to zeolite science and practice. *In Studies in Surface Science and Catalysis*. **1991**, 58.

(16) Derouane, E. G.; Vedrine, J. C.; Pinto, R. R.; Borges, P. M.; Costa, L.; Lemos, M.; Lemos, F.; Ribeiro, F. R. The Acidity of Zeolites: Concepts, Measurements and Relation to Catalysis: A Review on Experimental and Theoretical Methods for the Study of Zeolite Acidity. *Catal. Rev.* **2013**, 55(4), 454–515.

(17) Serrano, D. P.; Melero, J. A.; Morales, G.; Iglesias, J.; Pizarro, P. Progress in the design of zeolite catalysts for biomass conversion into biofuels and bio-based chemicals. *Catal. Rev.* **2018**, 60(1), 1–70.

(18) Loewenstein, W. The distribution of aluminum in the tetrahedra of silicates and aluminates. *Am. Mineral.* **1954**, 39(1–2), 92–96.

(19) Sazama, P.; Wichterlova, B.; Tabor, E.; Stastny, P.; Sathu, N. K.; Sobalik, Z.; Dedecek, J.; Sklenak, S.; Klein, P.; Vondrova, A. Tailoring of the structure of Fe-cationic species in Fe-ZSM-5 by distribution of Al atoms in the framework for N_2O decomposition and NH_3-SCR-NOx. *J. Catal.* **2014**, 312, 123–138.

(20) Barrer, R. M. *Hydrothermal Chemistry of Zeolites*. Academic press. **1982**.

(21) Sobalik, Z.; Dedecek, J.; Ikonnikov, I.; Wichterlova, B. State and coordination of metal ions in high silica zeolites. Incorporation, development and rearrangement during preparation and catalysis. *Micropor. Mesopor. Mater.* **1998**, 21(4-6), 525–532.

(22) Gamliel, D. P.; Augustine, E.; Hall, J.; Bollas, G. M.; Valla, J. A. Nickel impregnated mesoporous USY zeolites for hydrodeoxygenation of anisole. *Micropor. Mesopor. Mater.* **2018**, 261(18).

(23) Townsend, E. N. C. *Studies in surface science and catalysis*. **2001**, 137.

(24) Dedecek, J.; Wichterlova, B. Co^{2+} ion siting in pentasil-containing zeolites I. Co^{2+} ion sites and their occupation in mordenite. A Vis-NIR diffuse reflectance spectroscopy study. *J. Phys. Chem. B.* **1999**, 103(9), 1462–1476.

(25) Dalconi, M.C.; Gruciani, C.; Alberti, A.; Ciambelli, P.; Rapacciuolo, M.T. Ni^{2+} ion sites in hydrated and dehydrated forms of Ni-exchanged zeolite ferrierite. *Micropor. Mesopor. Mater.* **2000**, 39(3), 423–430.

(26) Sklenak, S.; Andrikopoulos, P. C.; Boekfa, B.; Jansang, B.; Novakova, J.; Benco, L.; Bucko, T.; Hafner, J.; Dedecek, J.; Sobalik, Z. N_2O decomposition over Fe-zeolites: Structure of the active sites and the origin of the distinct reactivity of Fe-ferrierite, Fe-ZSM-5, and Fe-beta. A combined periodic DFT and multispectral study. *J. Catal.* **2010**, 272(2), 262–274.

(27) Sobalik, Z.; Tvarůžková, Z.; Wichterlova, B. Skeletal T-O-T vibrations as a tool for characterization of divalent cation complexation in ferrierite. *J. Phys. Chem. B.* **1998**, 102, 1077.

(28) Sklenak, S.; Andrikopoulos, P. C.; Whittleton, S. R.; Jirglova, H.; Sazama, P.; Benco, L.; Bucko, T.; Hafner, J.; Sobalik, Z. Effect of the Al Siting on the Structure of Co(II) and Cu(II) Cationic Sites in Ferrierite. A Periodic DFT Molecular Dynamics and FTIR Study. *J. Phys. Chem. C.* **2013**, 117(8), 3958–3968.

(29) Kaucky, D.; Dedecek, J. I.; Wichterlova, B. Co^{2+} ion siting in pentasil-containing zeolites II. Co^{2+} ion sites and their occupation in ferrierite. A VIS diffuse reflectance spectroscopy study. *Micropor. Mesopor. Mater.* **1999**, 31(1-2), 75–87.

(30) Benco, L.; Bucko, T.; Grybos, R.; Hafner, J.; Sobalik, Z.; Dedecek, J.; Sklenak, S.; Hrusak, J. Multiple Adsorption of NO on Fe^{2+} Cations in the α- and β-Positions of Ferrierite: An Experimental and Density Functional Study. *J. Phys. Chem. C.* **2007**, 111(26), 9393–39402.

(31) Fernandes, L.D.; Monteiro, J.L.F.; Sousa-Aguiar, E.F.; Martinez, A.; Corma, A. Ethylbenzene hydroisomerization over bifunctional zeolite-based catalysts: The influence of framework and extraframework composition and zeolite structure. *J. Catal.* **1998**, 177, 363.

(32) Campa, M. C.; Pietrogiacomi, D.; Occhiuzzi, M. The simultaneous selective catalytic reduction of N_2O and NO_X with CH_4 on Co- and Ni-exchanged mordenite. *Appl. Catal. B: Environmental.* **2015**, 168–169, 293–302.

(33) Bulánek, R.; Novoveská, K.; Wichterlová, B. Oxidative dehydrogenation and ammoxidation of ethane and propane over pentasil ring Co-zeolites. *Appl. Catal. A: General.* **2002**, 235(1–2), 181–191.

(34) Pietrogiacomi, D.; Campa, M. C.; Carbone, L. R.; Occhiuzzi, M. N_2O decomposition and reduction on Co-MOR, Fe-MOR and Ni-MOR catalysts: in situ UV-vis DRS and operando FTIR investigation. An insight on the reaction pathways. *Appl. Catal. B.* **2019**, 240, 19–29.

(35) Nakao, R.; Katada, N.; Nishiyama, N.; Kunimori, K.; Tomishige, K. Performance and characterization of BEA catalysts for catalytic cracking. *App. Catal. A: General.* **2004**, 273(1–2), 63–73.

(36) Kaucký, D.; Pilař, R.; Kukula, P.; Bartáček, J.; Morávková, J.; Sazama, P. Low-temperature selective transformation of diethylbenzene to isobutane and cyclohexanes via the interplay of Pt and acid centres in Pt/H-*BEA zeolites. *J. Catal.* **2022**, 407, 186–197.

(37) Nivarthy, G. S.; Seshan, K.; Lercher, J. A. The influence of acidity on zeolite H-BEA catalyzed isobutane/n-butene alkylation. *Micropor. Mesopor. Mater.* **1998**, 22(1–3), 379–388.

(38) Beers, A. E. W.; Nijhuis, T. A.; Aalders, N.; Kapteijn, F.; Moulijn, J.A. BEA coating of structured supports – performance in acylation. *Appl. Catal. A: General.* **2003**, 243(2), 237–250.

(39) Lima, P. M.; Garetto, T.; Cavalcante Jr., C. L.; Cardoso, D. Isomerization of n-hexane on Pt–Ni catalysts supported on nanocrystalline H-BEA zeolite. *Catal. Today.* **2011**, 172(1), 195–202.

(40) Capek, L.; Dedecek, J.; Wichterlova, B. Co-beta zeolite highly active in propane-SCR-NOx in the presence of water vapor: effect of zeolite preparation and Al distribution in the framework. *J. Catal.* **2004**, 227(2), 352–366.

(41) Lu, T.; Yan, W.; and Xu, R. Chiral zeolite beta: structure, synthesis, and application. *Inorg. Chem. Front.* **2019**, 6, 1938.

(42) Centi, G.; Genovese, C.; Giordano, G.; Katovic, A.; Perathoner, S. Performance of Fe-BEA catalysts for the selective hydroxylation of benzene with N_2O. *Catal. Today.* **2004**, 91–2, 17-26.

(43) Ogura, M.; Itabashi, K.; Dedecek, J.; Onkawa, T.; Shimada, Y.; Kawakami, K.; Onodera, K.; Nakamura, S.; Okubo, T. Stabilization of bare divalent Fe(II) cations in Al-rich beta zeolites for superior NO adsorption. *J. Catal.* **2014**, 315, 1–5.

(44) Dedecek, J.; Capek, L.; Kaucky, D.; Sobalik, Z.; Wichterlova, B. Siting and distribution of the Co ions in beta zeolite: A UV-Vis-NIR and FTIR study. *J. Catal.* **2002**, 211(1), 198–207.

(45) Sazama, P.; Wichterlová, B.; Sklenák, S.; Parvulescu, V. I.; Candu, N.; Sádovská, G.; Dědeček, G.; Klein, P.; Pashkova, V.; Šťastný, P. Acid and redox activity of template-free Al-rich H-BEA* and Fe-BEA* zeolites. *J. Catal.* **2014**, 318, 22.

(46) Breck, D. W.; Eversole, W. G.; Milton R. M. New synthetic crystalline zeolites. *J. Am. Chem. Soc.* **1956**, 78(10), 2338–2339.

(47) Loiola, A. R.; Andrade, J. C. R. A.; Sasaki, J. M.; da Silva, L. R. D. Structural analysis of zeolite NaA synthesized by a cost-effective hydrothermal method using kaolin and its use as water softener. *Colloid Interface Sci.* **2012**, 367, 34–39.

(48) Montanari, T.; Salla, I.; Busca, G. Adsorption of CO on LTA zeolite adsorbents: An IR investigation. *Micropor. Mesopor. Mater.* **2008**, 109, 216–222.

(49) Guo, X.; Wu, L.; Navrotsky, A. Thermodynamic evidence of flexibility in H_2O and CO_2 absorption of transition metal ion-exchanged zeolite LTA. *Phys. Chem.* **2018**, 20, 3970.

(50) Zhao, G.; Drewery, M.; Mackie, J.; Oliver, T.; Kennedy, E. M.; Stockenhuber, M. The Catalyzed Conversion of Methane to Value-Added Products. *Energy Technol.* **2020**, 8(8), 1900665.

(51) https://www.epa.gov/gmi/importance-methane.

(52) Sun, L. L.; Wang, Y.; Guan, N. J.; Li, L. D. Methane Activation and Utilization: Current Status and Future Challenges. *Energy Technol.* **2020**, 8(8).

(53) Schorn, F.; Breuer, L.; Samsun, R. C.; Schnorbus, T.; Heuser, B.; Peters, R.; Stolten, D. Methanol as a renewable energy carrier: An assessment of production and transportation costs for selected global locations. *Adv. Appl. Energy.* **2021**, 3, 100050.

(54) Wheeler, W. A. B. *J. Chem. Soc., Dalton Trans.* **1903**, 83, 1074–1087.

(55) Grant, J. T.; Venegas, J. M.; McDermott, W. P.; and Hermans, I. Aerobic Oxidations of Light Alkanes over Solid Metal Oxide Catalysts. *Chem. Rev.* **2018**, 118, 2769–2815.

(56) Gol'dshleger, N. F.; Shilov, A. E.; Shteinman, A. A. Activation of saturated hydrocarbons. Deuterium-hydrogen exchange in solutions of transition metal complexes. **1969**, 18, 2174–2175.

(57) Periana, R. A.; Taube, D. J.; Gamble, S.; Taube, H.; Satoh, T.; Fujii, H. Platinum catalysts for the high-yield oxidation of methane to a methanol derivative. *Science.* **1998**, 280, 560–564.

(58) Mahyuddin, M. H.; Staykov, A.; Shiota, Y.; Yoshizawa, K. Direct Conversion of Methane to Methanol by Metal-Exchanged ZSM-5 Zeolite (Metal = Fe, Co, Ni, Cu). *ACS Catal.* **2016**, 6, 8321–8331.

(59) Weng, T.; Wolf, E. E. Partial oxidation of methane on mo/sn/p silica supported catalysts. *Applied Catalysis A: General.* **1993**, 96(2), 383–396.

(60) Han, S.; Kaufman, E. A.; Martenak, D. J.; Palermo, R. E.; Pearson, J. A.; Walsh, D. E. Direct partial oxidation of methane over ZSM-5 catalyst: Zn-ZSM-5 catalyst studies. *Catal. Lett.* **1994**, 29, 27–32.

(61) Durante, V. A.; Walker, D. W.; Gussow, S. M; and Lyons, J. E. Sillicometallate molecular sieves and their use as catalyst in oxidation in alkanes. *US4918249A.* **1990**.

(62) Olivos-Suarez, A. I.; Szécsényi, A.; Hensen, E. J. M.; Ruiz-Martinez, J.; Pidko, E. A.; Gascon, J. Strategies for the Direct Catalytic Valorization of Methane Using Heterogeneous Catalysis: Challenges and Opportunities. *ACS Catal.* **2016**, 6, 2965−2981.

(63) Ovanesyan, N. S.; Dubkov, K. A.; Pyalling, A. A.; Shteinman, A. A. The Fe active sites in FeZSM-5 catalyst for selective oxidation of CH_4 to CH_3OH at room temperature. *J. Radioanal. Nucl. Chem.* **2000**, 246(1), 149–152.

(64) Jovanovic, Z. R.; Lange, J. P.; Ravi, M.; Knorpp, A. J.; Sushkevich, V. L.; Newton, M. A.; Palagin, D.; van Bokhoven, J. A. Oxidation of methane to methanol over Cu-exchanged zeolites: Scientia gratia scientiae or paradigm shift in natural gas valorization? *J. Catal.* **2020**, 385, 238–245.

(65) Armstrong, R. D.; Freakley, S. J.; Forde, M. M.; Peneau, V.; Jenkins, R. L.; Taylor, S. H.; Moulijn, J. A.; Morgan, D. J.; Hutchings, G. J. Low temperature catalytic partial oxidation of ethane to oxygenates by Fe- and Cu-ZSM-5 in a continuous flow reactor. *J. Catal.* **2015**, 330, 84–92.

(66) Nobukawa, T.; Yoshida, M.; Kameoka, S.; Tomishige, K.; Kunimori, K. In-Situ Observation of Reaction Intermediate in the Selective Catalytic Reduction of N_2O with CH_4 over Fe Ion-Exchanged BEA Zeolite Catalyst for the Elucidation of Its Reaction Mechanism Using FTIR. *The Journal of Physical Chemistry B.* **2004**, 108(13), 4071–4079.

(67) Lange, J. P.; Sushkevich, V. L.; Knorpp, A. J.; van Bokhoven, J. A. Methane-to-Methanol via Chemical Looping: Economic Potential and Guidance for Future Research. *Ind. Eng. Chem. Res.* **2019**, 58(20), 8674–8680.

(68) Knorpp, A. J.; Newton, M. A.; Mizuno, S. C. M.; Zhu, J.; Mebrate, H.; Pinar, A. B.; van Bokhoven, J. A. Comparative performance of Cu-zeolites in the isothermal conversion of methane to methanol. *Chem. Commun.* **2019**, 55(78), 11794–11797.

(69) Raynes, S.; Shah, M. A.; Taylor, R. A. Direct conversion of methane to methanol with zeolites: towards understanding the role of extra-framework d-block metal and zeolite framework type. *Dalton Trans.* **2019**, 48(28), 10364–10384.

(70) Sushkevich, V. L.; Verel, R.; van Bokhoven, J. A. Pathways of Methane Transformation over Copper-Exchanged Mordenite as Revealed by In Situ NMR and IR Spectroscopy. *Angew. Chem. Int. Ed.* **2020**, 59(2), 910–918.

(71) Tabor, E.; Dedecek, J.; Mlekodaj, K.; Sobalik, Z.; Andrikopoulos, P. C.; Sklenak, S. Dioxygen dissociation over man-made system at room temperature to form the active α-oxygen for methane oxidation. *Sci. Adv.* **2020**, 6(20), eaaz9776.

(72) Dubkov, K. A.; Ovanesyan, N. S.; Shteinman, A. A.; Starokon, E. V.; Panov, G. I. Evolution of iron states and formation of alpha-sites upon activation of FeZSM-5 zeolites. *J. Catal.* **2002**, 207(2), 341–352.

(73) Panov, G. I.; Sobolev, V. I.; Kharitonov, A. S. The role of iron in N_2O decomposition on ZSM-5 zeolite and reactivity of the surface oxygen formed. *J. Mol. Catal.* **1990**, 61(1), 85–97.

(74) Pirutko, L. V.; Chernyavsky, V. S.; Starokon, E. V.; Ivanov, A. A.; Kharitonov, A. S.; Panov, G. I. The role of α-sites in N_2O decomposition over Fe-ZSM-5. Comparison with the oxidation of benzene to phenol. *Appl. Catal. B.* **2009**, 91(1-2), 174–179.

(75) Ivanov, D. P.; Sobolev, V. I.; Panov, G. I. Deactivation by coking and regeneration of zeolite catalysts for benzene-to-phenol oxidation. *Appl. Catal. A.* **2003**, 241(1–2), 113–121.

(76) Wood, B. R.; Reimer, J. A.; Bell, A. T.; Janicke, M. T.; Ott, K. C. Methanol formation on Fe/Al-MFI via the oxidation of methane by nitrous oxide. *J. Catal.* **2004**, 225(2), 300–306.

(77) Göltl, F.; Michel, C.; Andrikopoulos, P. C.; Love, A. M.; Hafner, J.; Hermans, I.; Sautet, P. Computationally Exploring Confinement Effects in the Methane-to-Methanol Conversion Over Iron-Oxo Centers in Zeolites. *ACS Catal.* **2016**, 6(12), 8404–8409.

(78) Jackson, R. B.; Solomon, E. I.; Canadell, J. G.; Cargnello, M.; Field, C. B. Methane removal and atmospheric restoration. *Nat. Sustain.* **2019**, 2(6), 436–438.

(79) Newton, M. A.; Knorpp, A. J.; Sushkevich, V. L.; Palagin, D.; van Bokhoven, J. A. Active sites and mechanisms in the direct conversion of methane to methanol using Cu in zeolitic hosts: a critical examination. *Chem. Soc. Rev.* **2020**, 49(5), 1449–1486.

(80) Vanelderen, P.; Snyder, B. E. R.; Tsai, M. L.; Hadt, R. G.; Vancauwenbergh, J.; Coussens, O.; Schoonheydt, R. A.; Sels, B. F.; Solomon, E. I. Spectroscopic Definition of the Copper Active Sites in Mordenite: Selective Methane Oxidation. *J. Am. Chem. Soc.* **2015**, 137(19), 6383–6392.

(81) Groothaert, M. H.; Smeets, P. J.; Sels, B. F.; Jacobs, P. A.; Schoonheydt, R. A. Selective oxidation of methane by the bis(mu-oxo)dicopper core stabilized on ZSM-5 and mordenite zeolites. *J. Am. Chem. Soc.* **2005**, 127(5), 1394–1395.

(82) Woertink, J. S.; Smeets, P. J.; Groothaert, M. H.; Vance, M. A.; Sels, B. F.; Schoonheydt, R. A.; Solomon, E. I. A $[Cu_2O]^{2+}$ core in Cu-ZSM-5, the active site in the oxidation of methane to methanol. *PNAS.* **2009**, 106(45), 18908-18913.

(83) Sobolev, V. I.; Panna, O. V.; Panov, G. I. Selective oxidation of methane to methanol on a FeZSM-5 surface. *Catal. Today.* **1995**, 24, 251–252.

(84) Starokon, E. V.; Parfenov, M. V.; Arzumanov, S. S.; Pirutko, L. V.; Stepanov, A. G.; Panov, G. I. Oxidation of methane to methanol on the surface of Fe-ZSM-5 zeolite. *J. Catal.* **2013**, 300, 47–54.

(85) Starokon, E. V.; Parfenov, M. V.; Pirutko, L. V.; Abornev, S. I.; Panov, G. I. Room-Temperature Oxidation of Methane by α-Oxygen and Extraction of Products from the Fe-ZSM-5 Surface. *J. Phys. Chem. C.* **2011**, 115, 2155–2161.

(86) Bols, M. L.; Hallaert, S. D.; Snyder, B. E. R.; Devos, J.; Plessers, D.; Rhoda, H. M.; Dusselier, M.; Schoonheydt, R. A.; Pierloot, K.; Solomon, E. I.; Sels, B. F. Spectroscopic Identification of the alpha-Fe/alpha-O Active Site in Fe-CHA Zeolite for the Low-Temperature Activation of the Methane C-H Bond. *J. Am. Chem. Soc.* **2018**, 140(38), 12021–12032.

(87) Kim, Y.; Kim, T. Y.; Lee, H.; Yi, J. Distinct activation of Cu-MOR for direct oxidation of methane to methanol. *Chem. Commun.* **2017**, 53(29), 4116–4119.

(88) Ipek, B. I.; Lobo, B. I. Catalytic conversion of methane to methanol on Cu-SSZ-13 using N_2O as oxidant. *Chem. Commun.* **2016**, 52, 13401–13404.

(89) Wulfers, M. J.; Teketel, S.; Ipek, B.; Lobo, R. F. Conversion of methane to methanol on copper-containing small-pore zeolites and zeotypes. *Chem. Commun.* **2015**, 51, 4447–4450.

(90) Park, M. B.; Ahn, S. H.; Mansouri, A.; Ranocchiari, M.; van Bokhoven, J. A. Comparative Study of Diverse Copper Zeolites for the Conversion of Methane into Methanol. *ChemCatChem.* **2017**, 9, 3705–3713.

(91) Narsimhan, K.; Iyoki, K.; Dinh, K.; Roman-Leshkov, Y. Catalytic Oxidation of Methane into Methanol over Copper-Exchanged Zeolites with Oxygen at Low Temperature. *ACS Central Science.* **2016**, 2(6), 424–429.

(92) Grundner, S.; Markovits, M. A. C.; Li, G.; Tromp, M.; Pidko, E. A.; Hensen, E. J. M.; Jentys, A.; Sanchez-Sanchez, M.; Lercher, J. A. Single-site trinuclear copper oxygen clusters in mordenite for selective conversion of methane to methanol. *Nat. Commun.* **2015**, 6, 7546.

(93) Pappas, D. K.; Martini, A.; Dyballa, M.; Kvande, K.; Teketel, S.; Lomachenko, K. A.; Baran, R.; Glatzel, P.; Arstad, B.; Berlier, G.; Lamberti, C.; Bordiga, S.; Olsbye, U.; Svelle, S.; Beato, P.; and Borfecchia, E. The Nuclearity of the Active Site for Methane to Methanol Conversion in Cu-Mordenite: A Quantitative Assessment. *J. Am. Chem. Soc.* **2018**, 140, 15270–15278.

(94) Sushkevich, V. L.; and van Bokhoven, J. A. Effect of Brønsted acid sites on the direct conversion of methane into methanol over copper-exchanged mordenite. *Catal. Sci. Technol.* **2018**, 8, 4141–4150.

(95) Tomkins, P.; Mansouri, A.; Bozbag, S. E.; Krumeich, F.; Park, M. B.; Alayon, E. M. C.; Ranocchiari, M.; and van Bokhoven, J. A. Isothermal Cyclic Conversion of Methane into Methanol over Copper-Exchanged Zeolite at Low Temperature. *Angew. Chem.* **2016**, 128, 5557–5561.

(96) Knorpp, A. J.; Newton, M. A.; Sushkevich, V. L.; Zimmermann, P. P.; Pinar, A. B.; van Bokhoven, J. A. The influence of zeolite morphology on the conversion of methane to methanol on copper-exchanged omega zeolite (MAZ). *Catal. Sci. Technol.* **2019**, 9(11), 2806–2811.

(97) Pappas, D. K.; Borfecchia, E.; Dyballa, M.; Pankin, I.; Lomachenko, K. A.; Martini, A.; Signorile, M.; Teketel, S.; Arstad, B.; Berlier, G.; Lamberti, C.; Bordiga, S.; Olsbye, U.; Lillerud, K. P.; Svelle, S.; and Beato, P. Methane to Methanol: Structure-Activity Relationships for Cu-CHA. *J. Am. Chem. Soc.* **2017**, 139, 14961–14975.

(98) Beznis, N. V.; Weckhuysen, B. M.; Bitter, J. H. Partial Oxidation of Methane Over Co-ZSM-5: Tuning the Oxygenate Selectivity by Altering the Preparation Route. *Catal. Lett.* **2010**, 136, 52–56.

(99) Shan, J.; Huang, W.; Nguyen, L.; Yu, Y.; Zhang, S.; Li, Y.; Frenkel, A. I.; and Tao, F. Conversion of Methane to Methanol with a Bent Mono(μ-oxo)dinickel Anchored on the Internal Surfaces of Micropores. *Langmuir.* **2014**, 30, 8558–8569.

(100) Jisa, K.; Novakova, J.; Schwarze, M.; Vondrova, A.; Sklenak, S.; Sobalik, Z. Role of the Fe-zeolite structure and iron state in the N_2O decomposition: Comparison of Fe-FER, Fe-BEA, and Fe-MFI catalysts. *J. Catal.* **2009**, 262(1), 27–34.

(101) Snyder, B. E. R.; Vanelderen, P.; Bols, M. L.; Hallaert, S. D.; Bottger, L. H.; Ungur, L.; Pierloot, K.; Schoonheydt, R. A.; Sels, B. F.; Solomon, E. I. The active site of low-temperature methane hydroxylation in iron-containing zeolites. *Nature.* **2016**, 536(7616), 317.

(102) Szécsényi, A. S., Khramenkova, E.; Chernyshov, I. Y.; Li, G.; Gascon, J.; and Pidko, E. A. Breaking Linear Scaling Relationships with Secondary Interactions in Confined Space: A Case Study of Methane Oxidation by Fe/ZSM-5 Zeolite. *ACS Catal.* **2019**, 9, 9276−9284.

(103) Malykhin, S. Hydrogen abstraction reactions of the $[FeO]^{2+}$ moiety: The role of the electronic state. *Chem. Phys. Lett.* **2015**, 622, 69–74.

(104) Rosa, A.; Ricciardi, G.; and Baerends, E. J. Is $[FeO]^{2+}$ the Active Center Also in Iron Containing Zeolites? A Density Functional Theory Study of Methane Hydroxylation Catalysis by Fe-ZSM-5 Zeolite. *Inorg. Chem.* **2010**, 49, 3866–3880.

(105) Chow, Y. K.; Dummer, N. F.; Carter, J. H.; Meyer, R. J.; Armstrong, R. D.; Williams, C.; Shaw, G.; Yacob, S.; Bhasin, M. M.; Willock, D. J.; Taylor, S. H.; and Hutchings, G. J. A Kinetic Study of Methane Partial Oxidation over Fe-ZSM-5 Using N_2O as an Oxidant. *ChemPhysChem.* **2018**, 19, 402–411.

(106) Tsai, M. L.; Hadt, R. G.; Vanelderen, P.; Sels, B. F.; Schoonheydt, R. A.; and Solomon, E. I. $[Cu_2O]^{2+}$ active site formation in Cu-ZSM-5: geometric and electronic structure requirements for N_2O activation. *J. Am. Chem. Soc.* **2014**, 136, 3522–3529.

(107) Lin, F.; Andana, T.; Wu, Y. Q.; Szanyi, J.; Wang, Y.; Gao, F. Catalytic site requirements for N_2O decomposition on Cu-, Co-, and Fe-SSZ-13 zeolites. *J. Catal.* **2021**, 401, 70–80.

(108) Markovits, M. A. C.; Jentys, A.; Tromp, M.; Sanchez-Sanchez, M.; and Lercher, J. A. Effect of Location and Distribution of Al Sites in ZSM-5 on the Formation of Cu-Oxo Clusters Active for Direct Conversion of Methane to Methanol. *Top. Catal.* **2016**, 59, 1554–1563.

(109) Smeets, P. J.; Groothaert, M. H.; van Teeffelen, R. M.; Leeman, H.; Hensen, E. J. M.; Schoonheydt, R. A. Direct NO and N_2O decomposition and NO-assisted N_2O decomposition over Cu-zeolites: Elucidating the influence of the Cu–Cu distance on oxygen migration. *J. Catal.* **2021**, 401, 70–80.

(110) Zhang, X.; Shen, Q.; He, C.; Ma, C.; Cheng, J.; Liu, Z.; and Hao, Z. Decomposition of nitrous oxide over Co-zeolite catalysts: role of zeolite structure and active site. *Catal. Sci. Technol.* **2012**, 2, 1249–1258.

(111) Zhang, X. S., Q.; He, C.; Wang, Y.; Cheng, J.; Hao, Z. Co-MOR zeolite catalyst prepared by buffered ion exchange for effective decomposition of nitrous oxide. *J. Hazard. Mater.* **2011**, 192(3), 1756–1765.

(112) Ryder, J. A.; Chakraborty, A. K.; and Bell, A. T. Density Functional Theory Study of Nitrous Oxide Decomposition over Fe- and Co-ZSM-5. *J. Phys. Chem. B.* **2002**, 106, 7059–7064.

(113) Krisnandi, Y. K.; Samodro, B. A.; Sihombing, R.; and Howe, R. F. Direct synthesis of methanol by partial oxidation of methane with oxygen over cobalt-modified mesoporous H-ZSM-5 catalyst. *J. Chem.* **2015**, 15, 263–268.

(114) Li, Y.; Armor, J. N. Catalytic decomposition of nitrous oxide on metal exchanged zeolites. *Appl. Catal. B.* **1992**, 1(3), 21–29.

(115) Mihaylov, M. H., K.; and Panayotov, D. . FTIR mechanistic studies on the selective catalytic reduction of NOx with methane over Ni-containing zeolites: comparison between Ni-Y and Ni-ZSM-5. *Appl. Catal. B: Environmental.* **2004**, 51, 33–42.

(116) Radu, P. G., Gloter, A.; Stephan, O.; Weckhuysen, B. M.; and de Groot, F. M. F. Geometric and Electronic Structure of α-Oxygen Sites in Mn-ZSM-5 Zeolites. *J. Phys. Chem. C* **2008**, 112(32), 12409–12416.

(117) Artiglia, L.; Sushkevich, V. L.; Palagin, D.; Knorpp, A. J.; Roy, K.; van Bokhoven, J. A. In Situ X-ray Photoelectron Spectroscopy Detects Multiple Active Sites Involved in the Selective

Anaerobic Oxidation of Methane in Copper-Exchanged Zeolites. *ACS Catal.* **2019**, 9(8), 6728–6737.

(118) Ravi, M.; Ranocchiari, M.; van Bokhoven, J. A. The Direct Catalytic Oxidation of Methane to Methanol-A Critical Assessment. *Angew. Chem. Int. Ed.* **2017**, 56(52), 16464–16483.

(119) Smeets, P. J.; Woertink, J. S.; Sels, B. F.; Solomon, E. I.; Schoonheydt, R. A. Transition-Metal Ions in Zeolites: Coordination and Activation of Oxygen. *Inorg. Chem.* **2010**, 49(8), 3573–3583.

(120) Mahyuddin, M. H.; Yoshizawa, K. DFT exploration of active site motifs in methane hydroxylation by Ni-ZSM-5 zeolite. *Catal. Sci. Technol.* **2018**, 8, 5875–5885.

(121) Tabor, E.; Sádovská, G.; Bernauer, M.; Sazama, P.; Nováková, J.; Píla, V.; Kmječ, T.; Kohout, J.; Závěta, K.; Sobalík, Z. Feasibility of application of iron zeolites for high-temperature decomposition of N_2O under real conditions of the technology for nitric acid production. *Appl. Catal. B.* **2019**, 240, 358–366.

(122) Sobalik, Z.; Novakova, J.; Dedecek, J.; Sathu, N. K.; Tabor, E.; Sazama, P.; Stastny, P.; Wichterlova, B. Tailoring of Fe-ferrierite for N_2O decomposition: On the decisive role of framework Al distribution for catalytic activity of Fe species in Fe-ferrierite. *Micropor. Mesopor. Mat.* **2011**, 146(1-3), 172–183.

(123) Wilke, M.; Farges, F. O.; Petit, P. E.; Brown, G. E. J.; Martin, F. O. Oxidation state and coordination of Fe in minerals: An Fe K-XANES spectroscopic study. *Am. Mineral.* **2001**, 86(5-6), 714–730.

(124) Bordiga, S.; Lamberti, C.; Bonino, F.; Travert, A.; Thibault-Starzyk, F. Probing zeolites by vibrational spectroscopies. *Chem. Soc. Rev.* **2015**, 44(20), 7262–7341.

(125) Tabor, E.; Zaveta, K.; Sathu, N. K.; Tvaruzkova, Z.; Sobalik, Z. Characterization of iron cationic sites in ferrierite using Mossbauer spectroscopy. *Catal. Today* **2011**, 169(1), 16–23.

(126) Snyder, B. E. R.; Bols, M. L.; Schoonheydt, R. A.; Sels, B. F.; Solomon, E. I. Iron and Copper Active Sites in Zeolites and Their Correlation to Metalloenzymes. *Chem. Rev.* **2018**, 118(5), 2718–2768.

(127) Sushkevich, V. L.; van Bokhoven, J. A. . Kinetic study and effect of water on methane oxidation to methanol over copper-exchanged mordenite. *Catal. Sci.Technol.* **2020**, 10, 382−390.

(128) Benco, L.; Bucko, T.; Grybos, R.; Hafner, J.; Sobalik, Z.; Dedecek, J.; Hrusak, J. Adsorption of NO in Fe^{2+}-exchanged ferrierite. A density functional theory study. *J. Phys.Chem.C.* **2007**, 111(2), 586–595.

(129) Wang, C.-T.; Willey, R. J. Mechanistic Aspects of Methanol Partial Oxidation over Supported Iron Oxide Aerogels. *J. Catal.* **2001**, 202(2), 211–219.

(130) Busca, G.; Elmi, A. S.; Forzatti, P. Mechanism of selective methanol oxidation over vanadium oxide-titanium oxide catalysts: a FT-IR and flow reactor study. *The Journal of Physical Chemistry.* **1987**, 91(20), 5263–5269.

(131) Berlier, G.; Zecchina, A.; Spoto, G.; Ricchiardi, G.; Bordiga, S.; Lamberti, C. The role of Al in the structure and reactivity of iron centers in Fe-ZSM-5-based catalysts: a statistically based infrared study. *J. Catal.* **2003**, 215(2), 264–270.

(132) Zecchina, A.; Bordiga, S.; Salvalaggio, M.; Spoto, G.; Scarano, D.; Lamberti, C. Formation of Nonplanar $CuI(CO)_3$Tricarbonyls on CuI–ZSM-5:An FTIR Study at 80 K. *J. Catal.* **1998**, 173(2), 540–542.

(133) Busca, G.; Elmi, A. S.; Forzatti, P. Mechanism of selective methanol oxidation over vanadium oxide-titanium oxide catalysts: a FT-IR and flow reactor study. *J. Phys. Chem.* **1987**, 91(20), 5263–5269.